To the Graduate Council:

I am submitting herewith a thesis written by Javier de la Vega entitled "Mechanical Properties and Residual Stresses in Non-equilibrium Glasses." I have examined the final copy of this thesis for form and content and recomend that it be accepted in partial fulfillment of the requirements for the degree of Master of Science, with a major in Polymer Engineering.

Donald C. Bogue, Major Professor

We have read this thesis
and recommend its acceptance:

J. E. Spruiell

John F. Fellers

Accepted for the Council:

The Graduate School

MECHANICAL PROPERTIES AND RESIDUAL STRESSES IN NON-EQUILIBRIUM GLASSES

A Thesis

Presented for the

Master of Science

Degree

The University of Tennessee, Knoxville

Javier de la Vega

December 1983

ABSTRACT

The effect of thermal history on the glassy state properties of amorphous polystyrene was investigated, giving separate consideration to homogeneous and non-homogeneous samples. The work on homogeneous samples dealt with how the degree of non-equilibrium (free volume) frozen into the quenched material affects the tensile properties of small, fiber-like samples. Some exploratory work was also done on the tensile properties of standard dumbbell specimens (1/8" thick) cooled under identical conditions as the small samples. The work in non-homogeneous samples was a continuation of recent work at the University of Tennessee on the measurement and prediction of residual birefringences related to residual stresses frozen into large slab-like samples.

The extent of non-equilibrium (i.e., the severity of the quench) was found to affect the ductility and other mechanical properties of the final, presumably homogeneous, fiber-like samples. Dramatic changes in ductility (elongations-to-break as high as 100% in some cases) were observed in quenched polystyrene specimens at a testing temperature as low as 70°C, whereas the literature indicates the brittle-to-ductile transition for this polymer to occur at about 90°C. The ductility measurements scattered considerably, however, (from a low of about 10% up to 140%) , presumably due to random irregularities in the test pieces. In contrast, quenching larger dumbbell specimens resulted in no appreciable changes in ductility.

Residual birefringence profiles were measured on slab-like

samples quenched from 120°C and 160°C into ice water. In agreement with the existing literature both quenching cases exhibited positive birefringences at the surface, and negative birefringences in the center of the slab. Although similar in shape, these profiles were nonetheless significantly different in detail. Quenching from a relatively low temperature (120°C) produced an approximate balancing of the positive and negative, birefringences, whereas a high initial temperature resulted in highly negative, unbalanced profiles. The simplified theory of Aggarwala and Saibel (2) used in earlier work at the University of Tennessee, was not succesful in explaining this difference. Therefore, the more general theory of Lee, Rogers, and Woo (47) was brought into the analysis. Lacking basic data on a number of functions and parameters (relaxation functions for both the mechanical and optical behavior and a function for the thermal coefficient of expansion), certain arbitrary decisions were necessary. This more general theory was able to predict the observed result qualitatively, and also quantitatively, if a certain (although arbitrary) choice of parameters was made.

TABLE OF CONTENTS

CHAPTER PAGE

LIST OF FIGURES

FIGURE PAGE

FIGURE PAGE

CHAPTER I

INTRODUCTION

The polymeric glassy state as actually encountered in practice is virtually never in thermodynamic equilibrium. As one fabricates plastic parts from a melted polymer, various properties of the molten (or rubbery) state are trapped in the material as it is cooled quickly into the glassy state. An important example is the so-called frozen in "free volume" which, as will be described in detail in the next chapter, has been used as an organizing variable for characterizing the behavior of the non-equilibrium glass. Stated in simple, and perhaps oversimplified, terms, a glass with a high level of frozen in free volume can be expected to show properties which are less glassy (less brittle) than an equilibrium glass.

Although there is a considerable literature on the non-equilibrium glassy state, the mechanical properties of that state appear not to have been studied systematically. A difficulty is that there is always some degreee of non-homogeneity in the sample, due to the differing thermal histories of the surface and the core. It appears that one must use quite small (fiber-like) samples to achieve satisfactory degrees of homogeneity for mechanical testing. Thus a major objective of the present work was to produce a series of carefully prepared, nearly homogeneous samples of an amorphous polymer (polystyrene) and to measure the mechanical properties (modulus, yield strength,....) at various temperatures in the glassy range.

It was further planned to continue those studies to include large, intentionally non-homogeneous samples as well. Some work on such samples, which have frozen-in "residual stresses," has already been done at the University of Tennessee by C. J. Wust Jr., as will be reviewed in subsequent chapters. While some work was done on mechanical properties, the complexity of the residual stress problem is such that it was decided to continue detailed studies of that problem in lieu of continuing to look at mechanical properties at this time. The residual stress problem is made complicated by the fact that while the non-uniform cooling produces a stress gradient through the cross-sections, that gradient is quite difficult to measure experimentally. Rather, most researchers have chosen to measure the gradient of birefringence, as an indirect indicator of stress. Thus, any theoretical analysis must grapple with both the mechanical and optical response of the material. The literature in these various areas will now be reviewed in detail, followed by a summary of the new work of mechanical properties of homogeneous samples and on residual stresses (birefringences) in non-homogeneous ones.

CHAPTER II

LITERATURE REVIEW

The present work focuses on the properties of the glassy state of amorphous polymers with separate consideration to both homogeneous and non-homogeneous samples. The work on homogeneous materials specifically considers the effect of thermal history on the mechanical properties of small fiber-like samples. Studies on residual stresses and residual birefringence, on the other hand, constitute the research topic in the area of non-homogeneous samples. A survey of the most relevant literature on these topics will now be presented.

A. MECHANICAL AND OPTICAL PROPERTIES OF GLASSY POLYMERS

The literature on mechanical properties in the glassy amorphous state is extensive and quite complicated; but little attention has been paid to the matter of homogeneity through the cross-section. An homogeneous sample is one in which properties are not position dependent. Matsumoto and Bogue (54) stated that fiber-like samples no larger than about 250 micrometers in diameter are required to obtain homogeneous specimens for cooling rates up to $2^{\circ}C$/sec. However, most of the data in the literature involve considerably larger samples and therefore their degree of homogeneity is questionable. For this reason a more general survey of the literature dealing with mechanical properties of glassy polymers is presented.

Mechanical Properties of Glassy Polymers

Rigid, glassy polymers show a diversity of mechanical behavior, ranging from apparently brittle to ductile. Several factors are recognized to influence this behavior: firstly, the nature of the polymer itself, i.e., its constitution, configuration, molecular weight...; secondly, the thermal and/or mechanical history experienced by the material during the shaping process, which may affect the degree of homogeneity and/or isotropy, i.e., molecular orientation, of the final part ; and finally, the conditions under which testing is performed such as temperature, pressure, and deformation rate.

The chemical structure-properties relationship of polymers has been reviewed in detail, for instance, by Van Krevelen (89). Molecular weight and molecular weight distribution also have a significant effect on the stress-strain behavior of rigid polymers (51,56,79,80,100).

More important to the scope of this research is, however, the effect that thermal and mechanical histories have on the performance of the fabricated part. Thermal treatments can modify the mechanical properties of glassy polymers by creating changes in the structure of the material. Rapid cooling from the melt, as opposed to slow cooling or annealing processes, creates a great deal of free volume in the material (45,71,77,82,97,98). Another effect of rapid cooling, of course, may be the creation of non-uniformities across the cross-section of the sample, which are known to substantially enhance its impact properties (12,14,15,78); but the literature concerning such non-uniformities will be reviewed in the next section.

A great deal of the literature relates the yield behavior of glassy polymers to the free volume frozen into the material during vitrification from the melt (48,49,50,70,71). In a series of publications Litt, with Koch and Tobolsky (48,49,50) proposed that yielding is due to the increase in unoccupied volume under applied stress by a Poisson ratio effect. They postulated that glassy polymers showing ductile failure have the same unoccupied volume at the yield strain as in the unstrained state at some temperature T^* close to the glass transition temperature. T^* is that temperature at which the slightly strained polymer can relax at the same rate as the test specimen (at T) is being strained. Brittle polymers, on the other hand, do not sustain enough force to reach the yield strain and they break before yielding can take place.

Rusch and Beck (71) argued that the model developed by Litt et al. could not account completely for the strain rate dependence of the yield strain. Based on previous work by Rusch (70), Rusch and Beck (71) refined the free volume approach by introducing the so-called "effective temperature" concept. This is a time dependent parameter which describes the state of the glass. T_e is defined as the hypothetical temperature at which the glass would have an equilibrium free volume equal to the total free volume of the non-equilibrium glass at temperature T, keeping the pressure constant. This improved free volume model was shown to describe more satisfactorily the temperature and strain rate dependences of the initial yield strain of polymethyl-methacrylate (PMMA).

Other investigators have focused on how the "degree of order" in the glassy state affects the properties there. Tensile experiments conducted in the past by Golden, Hammat and Hazel (27) showed the effect of annealing at temperatures close to T_g (142°C) on the yield strength of polycarbonate. They found that keeping the testing conditions constant (T = 20°C and elongation rate = 0.1 inch/min), the tensile yield strength increased significantly with annealing time and temperature, while the extension to yield and energy to yield decreased. Golden et al. proposed that the increased strength observed after annealing in polycarbonate is due to further ordering of the amorphous region.

Bowden and Raha (10) and later on Brady and Yeh (11) conducted systematic compressive experiments on PS, PMMA and other glassy polymers with samples of various thermal histories and under varying testing temperatures and strain rates. Like Golden et al., Brady and Yeh (11) found that holding the strain rate and temperature constant, the yield stress of reannealed samples was higher than that of as-quenched samples; furthermore, slowly cooled specimens and reannealed ice-quenched ones showed nearly identical behavior, all other conditions constant. They showed that regardless of the thermal history, increasing strain rates induce higher yield stresses, which grow more rapidly in the case of as-quenched samples as compared with reannealed specimens. Brady and Yeh noted fibrillar structure, at the 200 A level when PMMA was pulled to the yield point. They showed that

annealing treatments affect this kind of microstructure, which in turn affects the density and yield strength.

The long term gradual free volume decay (aging) in amorphous glasses and its effect on the mechanical behavior, has been studied in some detail by Struik and co-workers (82). He was able to correlate PS creep data in the glassy state in terms of an "aging shift factor", in some ways analogous to the one derived by Williams Landel and Ferry (97) for stress relaxation studies in the rubbery state.

Another important variable in connection to the properties of these materials is molecular orientation. If the sample is deformed, (either during flow or by pulling), while still in the rubbery state (usually just above T_g), a high degree of orientation can be created and frozen-in during subsequent quenching (22,32,38,64). As a result the modulus in the direction of orientation increases noticeably; but the tensile strength and elongation to break properties are much more dramatically enhanced. Orientation can alter the mechanical behavior of rigid glassy polymers such as PS and PMMA from brittle to ductile (16,17,18,63). Matsumoto and Bogue (48), and Carey, Wust and Bogue (16) achieved large degrees of orientation in polystyrene by spinning just above T_g. The latter reported ultimate elongations as high as 90% in tensile experiments with just a small amount of orientation. Property changes in biaxially stretched polystyrene films have been investigated by Thomas and Cleereman (85), and Matsumoto, Fellers and White (55).

Such a dramatic enhacement of the mechanical properties is, of

course, of great interest when using polymers as structural materials. When considering the long-range behavior of these materials, one must take into account the subsequent relaxation (aging) of such orientation. This not only is detrimental to the properties noted above, but also can result in significant shrinkage of the part in service.

The literature includes a few studies dealing with orientation relaxation in purely amorphous polymers (37,39,40,67,84). A general observation is that relatively high temperatures are needed for shrinkage to occur. Particularly, Ito, Horie and Kobayashi (37) reported that at temperatures above 80°C a decrease of birefringence was accompanied by shrinkage, whereas at lower temperatures birefringence relaxation proceeds with no observable dimensional change. Also, when shrinkage occurs it often lags sligthly behind the birefringence decay (37,67).

Test conditions constitute another major factor greatly influencing the mechanical response of polymers.

Generally speaking, a decrease in temperature is accompanied by an increase of modulus and tensile strength. On the contrary, the ultimate elongation usually decreases with temperature for rigid polymers. When considering the temperature dependence on the stress-strain behavior of glassy amorphous polymers, the following trends are often observed (see, for example, 52). As the temperature increases, the modulus remains fairily constant until T_g is approached. At this point the modulus may decrease by a factor of about a thousand with a slightly further temperature increase. Opposed to this, the

elongation-to-break is generally small below T_g ; however, as this temperature is approached the elongation suddenly becomes very large. In the case of polystyrene, Matsushige, Radciffe and Baer (52), (see Figure II-1), showed this sudden drastic change in ultimate elongation to occur at a temperature between 80°C and 90°C.

The influence of pressure and temperature on the yield behavior of polymers has been the major concern of several researchers. Ainbinder, Laka and Maiors (3), experimenting with PS, PMMA and other polymers noted increases in modulus and yield strength with increasing hydrostatic pressure. In a later investigation Biglione, Baer and Radcliffe (9) studied the tensile behavior of PS for a wide range of hydrostatic pressure, from atmospheric pressure to 6 kilobars. At the former this polymer behaved in a brittle manner, while at pressures of 3 kilobar or greater it became ductile and necked. In the region of ductile behavior the yield stress was found to increase linearly with increasing applied pressure.

More recently Matsushige, Radcliffe and Baer (52) conducted systematic tensile experiments on PS and PMMA over a wide range of pressure and temperature. They showed that a brittle-to-ductile transition was induced in both polymers by the superposition of hydrostatic pressure as well as by the increase of the experimental temperature. Brittle fracture of a glassy polymer is considered to be caused by the propagation of existing crazes. For crazing to occur, however, a "critical stress" having a tensile component must be reached (8,24,31,101). Fellers and Kee (24) showed that this critical crazing

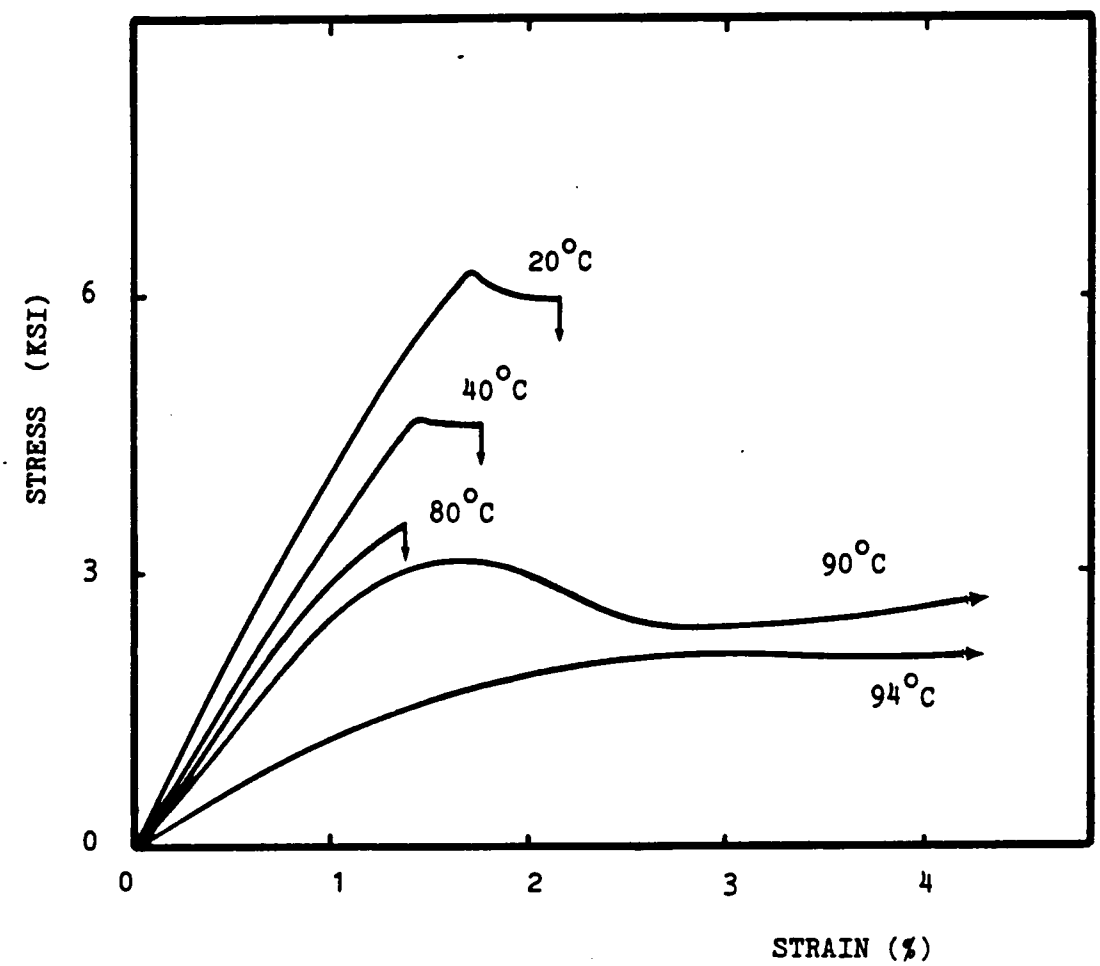

Figure II-1. Temperature dependence of the stress-strain behavior of polystyrene (from Matsushige et al.(52)).

stress does not depend on molecular weight. When a glassy polymer fails in a ductile fashion, the onset of plastic deformation is in the form of shear bands (5,42,53). It has been proposed (52) that a glassy polymers behaves in a brittle manner if the stress level for craze initiation (critical stress) is lower than that of shear band initiation. Matsushige et al. (52) showed that in the case of polystyrene the craze and shear band initiation stresses exhibit quite different temperature dependences; both decrease monotonically with temperature, the latter being much steeper than the former. In the low temperature region the critical crazing stress level is considerably lower than that of shear band initiation. Crazes can develop and propagate and thus brittle fracture occurs. At relatively high temperatures, however, this situation is reversed. Matsushige et al. found that in the temperature region in which these two curves intersect a brittle-to-ductile transition is observed. At such temperatures crazing lags behind shear banding. The propagation of crazes is inhibited by the already formed shear bands causing the specimen to fail in a ductile fashion. For annealed polystyrene specimens tested at atmospheric pressure this brittle-to-ductile transition temperature was found to be about 90^{o}C. When considering both temperature and pressure changes, the brittle-to-ductile transition pressure decreases with increasing temperature.

The factors influencing the brittle-to-ductile transition in polymers have been studied quite extensively. Vincent (90,91) investigated the effects of strain rate, molecular weight,

crystallinity, additives, crosslinking, side groups, and molecular orientation on the brittle-to-ductile transition temperature.

The effect of the speed of testing (strain rate) on the yield behavior of PS and PMMA has already been cited when describing the work of Brady and Yeh (11). Typically, as the elongation rate increases, the modulus, yield strength and tensile (ultimate) strength of the material also increase. On the other hand, increasing testing speed generally produces low elongations to break (4,21,23,43).

Smith (76) has shown the applicability of the "time-temperature superposition principle", as formulated by Williams, Landel and Ferry (97), to correlate tensile data of rigid polymers, obtained at a diversity of strain rates. He obtained separate master curves to describe the tensile strength, ultimate elongation, and modulus of these materials. This indicates that, for all practical purposes, an increase in the strain rate is equivalent to decreasing the testing temperature.

The above paragraphs constitute only but a brief review of the extensive literature on the mechanical behavior of glassy amorphous polymers. The aspects considered above and other topics regarding the mechanics of polymers in general have been reviewed in detail in books edited by Nielsen (60) and Ward (94). A separate review dealing specifically with the mechanics of the glassy state is that of Haward (30).

Optical Properties of Glassy Polymers

In this section the concern will be with some of the aspects of

anisotropic optical behavior of glassy polymers. When considering an isolated polymer molecule, it can be intuitively appreciated that different polarizabilities may exist in the directions parallel and perpendicular to the chain backbone. If there is a preferential orientation of the polymer molecules constituting a sample, these directionally dependent polarizabilities will give rise to birefringence, when inspecting the sample between crossed polarizers. Birefringence measurements have been widely used as a tool for obtaining information about the average orientation of molecules in a fabricated polymer part (see, for example, 20,81,95).

Since the present research deals with glassy polymers, particularly polystyrene, the proposed mechanisms causing birefringence in this material will now be reviewed. Homogeneous PS samples exhibit negative birefringence at temperatures above its glass transition temperature. Below T_g, however, the observed birefringence is positive.

Two mechanisms attempting to explain this behavior have been generally acknowledged in the literature (34,44,69), although the exact origin of negative and positive birefringences has not been agreed upon.

The negative birefringences associated with the rubbery state are explained in terms of chain orientation in the direction of applied stress and the alignment of the phenyl rings perpendicularly to that direction. Positive birefringences, on the other hand, are believed to be the consequence of elastically straining the phenyl rings in the

direction of applied stress (Jones (39)), or arise when these phenyl rings become oriented parallely to that direction (Rudd and Gurnee (69)). A third investigator, Kolsky (44), associates the positive birefringence of the glassy state with molecular orientation, whereas the negative birefringence is thought to stem from the orientation of the phenyl rings.

The relationship between the tensional state of a body and the observed birefringence has been well established in photoelasticity theory (86). It takes mathematical form in the so-called stress-optical law

$$\Delta n = n_I - n_{II} = C_s (\sigma_I - \sigma_{II}) \qquad \text{(II.1)}$$

which simply assumes direct proportionality between the differences of principal stresses σ_I and σ_{II} and principal refractive indices n_I and n_{II}. The proportionality constant is C_s, the stress optical coefficient.

The above expression can be recast in terms of the difference of principal strains ε_I and ε_{II}, if assuming Hookean behavior, i.e., stress-strain proportionality

$$\Delta n = n_I - n_{II} = C_\varepsilon (\varepsilon_I - \varepsilon_{II}) \qquad \text{(II.2)}$$

Here the proportionality constant is C_ε, the strain optical coefficient.

The optical coefficients involved in these expressions depend on the chemical structure as it affects the polarizabilities, and on the temperature. The temperature dependence of the optical coefficients is of utmost importance in non-isothermal processes. Particularly, the optical behavior of PS has been quite extensively investigated at two extremes: room temperature and well above its glass transition temperature. A typical room temperature value for the stress optical coefficient in this polymer is that of about +9 to +10 Br (1Br = 10^{-13} cm^2/dyne) (28,39,44,68,96). At the high temperature extreme, values ranging from -4100 to -6100 Br have been reported. Nielsen and Buchdahl (61,62), Wilkes and Stein (96), and Jones (39), all agree on a value of about -5200 Br for polysterene in the rubbery state. The former group of investigators emphasize that the stress optical coefficient does not depend on the stress or deformation levels, on molecular weight or on temperature. Values of -4100 Br and -4950 Br have been observed at high temperatures (about 190^{o}C) by Wales (92) and Han and Drexler (29), respectively, while Matsumoto and Bogue (54) reported a value of -6100 Br.

In studies concerning vitrification of polymers while in a stress field, Oda, White and Clark (64) showed that the final part could be characterized by the state of the melt at the moment of vitrification. They reported an observed value of -4500 Br for shear and elongational flow fields at relatively high temperatures.

At least one study has been done at low temperatures. Rudd and Gurnee (68) investigated the stress and strain optical coefficients of

polystyrene in the -195°C to 24°C temperature range. Their experiments show practically temperature independent results with the stress optical coefficient ranging from +17 Br at -195°C to +10 Br at 24°C.

Very little stress optical coefficient data have been obtained at intermediate temperatures between the two extremes already mentioned. The work of Tsvetkov and Krym (88) on laboratory synthesized polystyrene covered the range from room temperature to about 140°C. Their results show a relatively mild temperature dependence up to about 100°C. At this point the stress optical coefficient drastically drops from an approximate value of -200 Br down to about -4000 Br, staying constant at this level with further temperature increase. They obtained the cross-over point from positive to negative birefringences at the relatively low temperature of about 50°C.

Very recently Wust (98) (see also Wust and Bogue (99)) conducted tensile-compressive experiments on homogeneous samples of commercial polystyrene, obtaining qualitatively speaking similar results. Small, unexplained differences, however, were observed between tensile and compressive determinations, the latter being consistently more negative.

The most significant discrepancies between the work of Tsvetkov and Krym (88), and that of Wust (98) are the temperatures at which the transition from positive to negative birefringences, and the sudden drop from low to high negative values take place. In Wust's data, both these features are observed at a temperature of about 92°C in tensile

experiments and at about 75°C and 87°C, respectively, for compressive experiments.

Wust (98) also investigated to a certain extent the time dependency (relaxation) of the stress optical coefficient in stress relaxation experiments at constant strain, for a variety of temperatures. The results are shown in Figure II-2, along with the stress relaxation data.

Rudd and Gurnee (68) in their work on the optical coefficients at very low temperatures already mentioned, calculated the strain optical coefficient C_ε, by multiplying C_s and the tensile modulus. This procedure is justified since

$$\Delta n = C_s \, \Delta\sigma \tag{II.3}$$

and assuming proportionality between stress and strain, i.e.,

$$\sigma = E \, \varepsilon \tag{II.4}$$

the above can be written as

$$\Delta n = C_s \, E \, \Delta\varepsilon = C_\varepsilon \, \Delta\varepsilon \tag{II.5}$$

and therefore

$$C_\varepsilon = C_s \, E \tag{II.6}$$

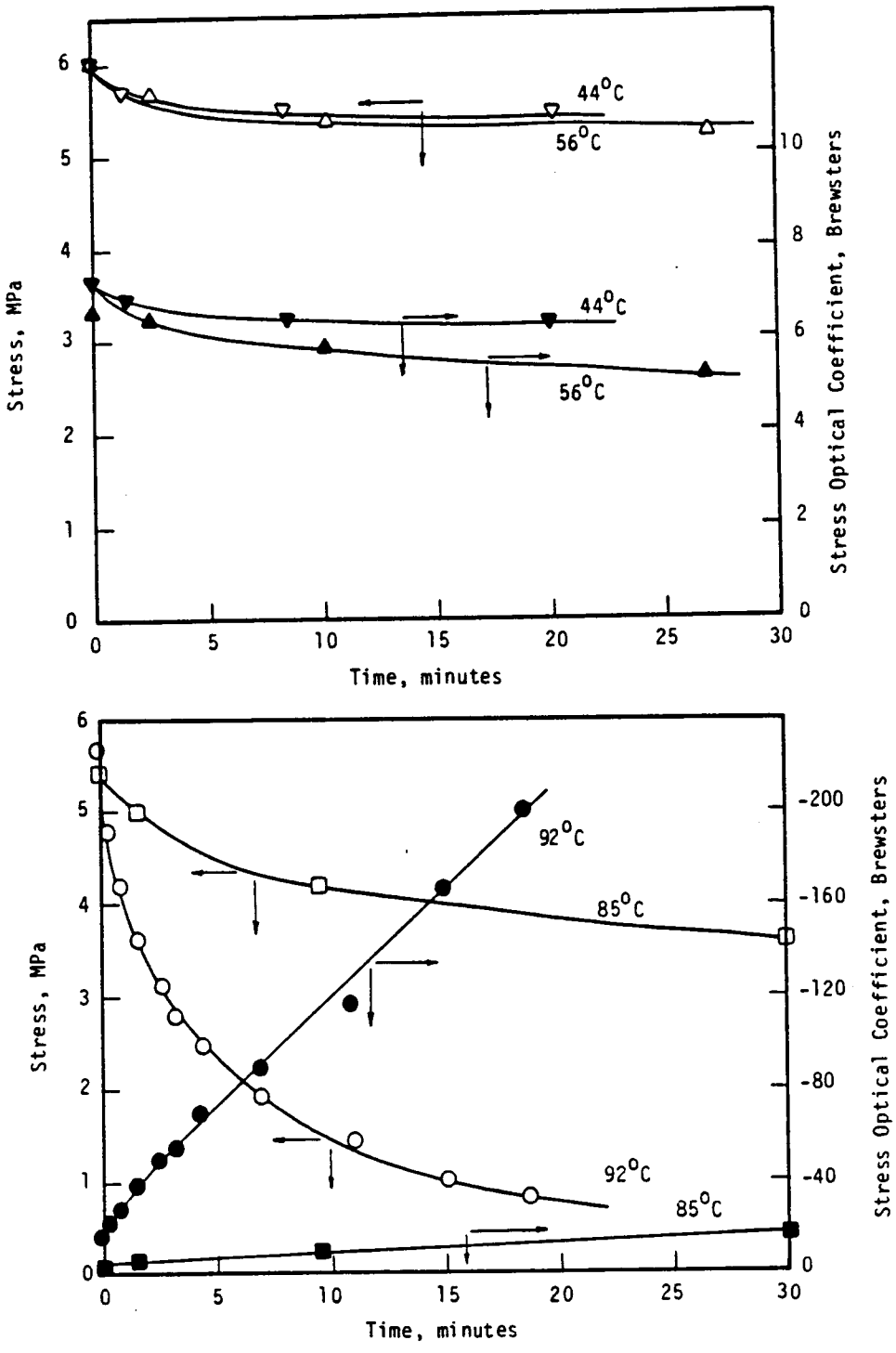

Figure II-2. Time dependence (relaxation) of the stress and stress optical coefficient of polystyrene at constant strain (from Wust (98)).

Rudd and Gurnee obtained values for C ranging from +0.03 at 24°C to +0.072 at -195°C. More recently, Wust (98) has performed similar calculations to obtain strain optical coefficient data from his C_s determinations. The temperature dependence of the modulus in the range of interest was obtained from Wust's own tensile modulus data and a quite extensive number of determinations found in the literature, many of which come from dynamic experiments. To minimize the effects of machine compliance, Wust followed the suggestions of Patel and Bogue (65), using various gauge lengths (L) in his determininations of the modulus. The reciprocal of the apparent (measured) modulus was plotted against 1/L and extrapolated to infinite L to obtain the true modulus. The final result of the C calculation is shown on Figure II-3 in which the 0 °C determination of Rudd and Gurnee (68) has been included. Figure II-3 also includes the expression for the least squares fit of the optical coefficient tension data in the 0°C to 100°C temperature range.

B. RESIDUAL STRESSES AND RESIDUAL BIREFRINGENCES IN NON-HOMOGENEOUS SAMPLES

The term non-homogeneous refers to those samples having position dependent properties. The origins of this non-homogeneity may be diverse. It may be caused by structural heterogeneity of the material, arising as a consequence of mechanical deformation, thermal history, or both, during the fabrication process. This shaping process may involve deformation (flow) of the molten material under an applied stress field

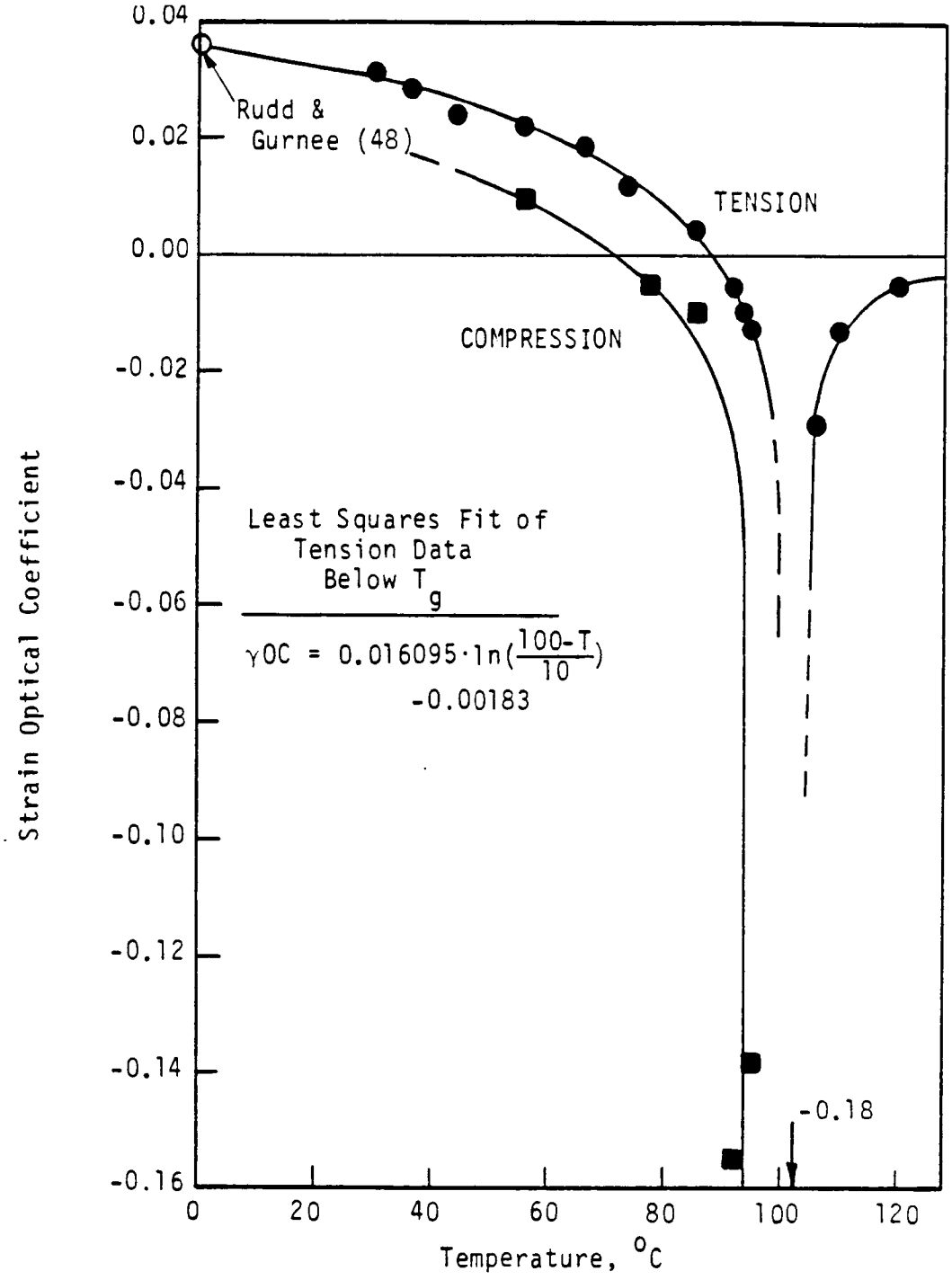

Figure II-3. Temperature dependence of the strain optical coefficient of polystyrene (from Wust (98)).

and subsequent cooling to ambient temperature. This deformation often results in molecular orientation that manifests itself in the form of birefringence.

If the shaping process consists of homogeneous deformation followed by homogeneous cooling to temperatures below the glass transition, this molecular orientation may be trapped-in, and the resulting sample will be anisotropic in nature but free of property gradients, i.e., homogeneous. However, in the more likely case of non-homogeneous deformation and/or cooling, particularly during fabrication of large parts, a gradient of properties through the cross-section of the sample may be originated.

During non-homogeneous cooling of oriented amorphous samples the flow-induced orientation may partially relax. Due to the differing thermal histories experienced by the inner and outer regions of the sample, different degrees of orientation relaxation will occur, resulting in structural heterogeneity through the thickness of the sample that give rise to residual stresses.

Non-homogeneities arising solely by inhomogeneous cooling of initially isotropic samples are of concern here.

Residual Stresses

As a consequence of many processing operations, residual stresses are created within the fabricated part. These residual stresses are a consequence of non-homogeneities trapped in the material during its shaping and subsequent cooling. The origin of these stresses, like the non-homogeneities that cause them, may be due to a

variety of reasons. They may be the consequence of structural heterogeneity of the material due to the presence of various phases, as in a crystalline material, or be the result of mechanical (e.g., cold rolling) and/or thermal (e.g., inhomogeneous cooling) histories of the fabricated part. The residual stresses of interest to us in the present study are those that originate in non-uniform cooling of large samples at finite rates.

During inhomogeneous cooling an instantaneous temperature gradient in both time and space is induced. The various parts of the body undergo different thermal histories and, therefore, experience differential contractions between surface and internal layers. This mismatching causes strains in the body that give rise to stresses. These stresses that are a direct consequence of the existence of temperature gradients throughout the body are generally referred to as "thermal stresses". During the first stage of cooling the surface cools much more rapidly than the central regions; the thermal contraction of the surface layers is thus greater than that of the still hot material of the midplane, which opposes this contraction. This tends to result in tensile stresses on the surface and compressive stresses in the core. After the first few seconds of cooling, however, the temperature difference between the surface and the midplane goes through a maximum. From this moment on as cooling continues, this situation is reversed. With the central regions cooling more rapidly than the surface layers, the former now experience a greater thermal contraction which is opposed by the already hard surface.

In a perfectly elastic (ideal) body the thermal stresses that arise during the first stage of quenching are compensated (cancelled out) by same magnitude and opposite sign stresses that originate during the final cooling stage. The quenching of a perfectly elastic solid, therefore, does not produce residual stresses.

Most materials, and certainly this is the case of polymeric glasses, do not behave elastically at high temperatures. During the quenching process of these systems, the thermal stress field present will relax to an extent that depends on the temperature of the material; the higher the temperature, the higher the rate of relaxation. Most of the thermal stresses induced during the first stage of quenching, when the material is still hot, will relax, whereas the extent of relaxation of the stresses originated in the final stage of cooling , when the material is colder, is rather small.

The decay of the temperature gradient during inhomogeneous cooling of a viscoelastic body thus results in temporary thermal stresses. As a consequence of differential relaxation processes between the inner and outer regions of the body, these "otherwise temporary" stresses turn into residual stresses, which persist when the cooling process has been completed. The various steps involved in the generation of residual stresses are illustrated in Figure II-4. The state of residual stresses thus originated is characterized by tensile stresses in the midplane, balanced by compressive stresses on the surface.

The importance of residual stresses as a factor influencing the

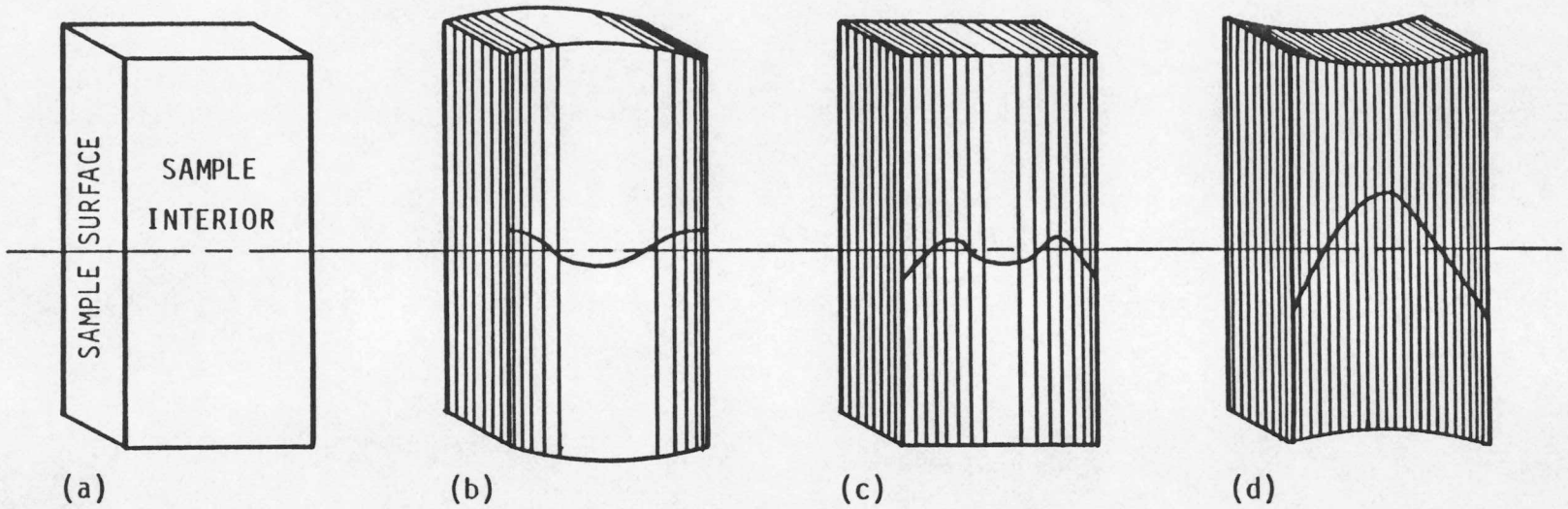

Figure II-4. Development of residual stresses in a quenched body (from Wust (98)).

mechanical behavior of metals and inorganic glasses has long been recognized. For this reason the literature dealing with the prediction (modelling) and measurement of residual stresses in these materials is quite prolific (see, for example, 1,25,66). Of it, only the most relevant aspects to this particular research will be briefly reviewed here.

Residual Stress Theories

Most of the existing theories dealing with residual stresses were motivated by the necessity to predict and control the generation of tempering stresses in structural inorganic glasses.

Since 1920 when Adams and Williamson (1) first calculated tempering residual stresses in glass plates, obtaining a parabolic law of stress distribution, several theories involving various degrees of complexity have been developed.

Mathematical analysis of the tempering process involves the coupling of the thermal history of the material and its mechanical response. The former can be dealt with, in a relatively straightforward manner, by means of standard heat transfer theory, especially if radiation is neglected. Similarly, with the aid of thermoelasticity theory, the determination of the thermal stresses involved in the process can be achieved. The major difficulty, however, arises when the temperature dependent relaxation of the varying thermal stress field, i.e., the viscoelastic response of the material, needs to be accounted for.

Bartenev (6,7) assumed that at temperatures above its glass

transition temperature T_g, the material behaves like an inviscid fluid, with instantly produced strains and no stress generation (total relaxation of thermal stresses). As the material cools through T_g, however, it freezes instantly. Thus, below T_g the glass behaves thermoelastically and no further relaxation of the thermal stresses generated in the rest of the cooling process occurs. With reference to the coordinate system shown in Figure II-5, Bartenev's final expression is

$$\sigma(x_1) = \frac{\beta E}{1 - \nu} [\bar{\Phi} - \Phi(x_1)] \qquad \text{(II.7)}$$

where β is the linear coefficient of thermal expansion, E is Young's modulus, ν is Poisson's ratio, ϕ is a specific temperature defined by

$$\frac{d\Phi(x_1,t)}{dx_1} = \frac{dT(x_1,t \mid T_{x_1} = T_g)}{dx_1} \qquad \text{(II.8)}$$

and Φ which is given by

$$\bar{\Phi} = \frac{1}{b} \int_0^b \Phi(x_1', t \mid T_{x_1} = T_g) \, dx_1' \qquad \text{(II.9)}$$

is the average value of Φ through the thickness of the plate, 2b.

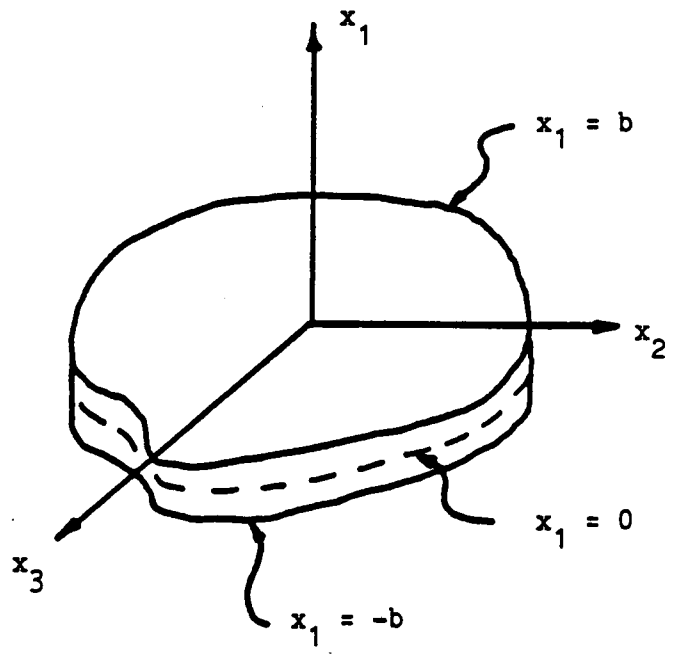

Figure II-5. Reference axes for residual stress analysis.

Bartenev's theory provided a good fit to experimental results in cases where the cooling rate was rather low. However, an increasingly marked disagreement between theory and experiment results as the cooling rate is increased (25).

Subsequently, this theory was modified by Indenbom (33,34). On the basis of Bartenev's "instant freezing" assumption, the approach of Indenbom takes into account the compatibility of strains on both sides of the transition zone. The time dependent strain, which is assumed to be uniform through the thickness of the plate, is a combination of three components: γ_e is the elastic strain, experienced by the material at temperatures below its glass transition temperature; γ_p is the plastic (viscous) strain trapped into the material upon solidification; and finally a thermal component of strain with reference to the initial temperature T_o. The total strain can thus be stated as

$$\gamma(t) = \gamma_e(x_1,t) + \gamma_p(x_1,t) + \beta(T(x_1,t) - T_o) \qquad \text{(II.10)}$$

With these considerations Bartenev's theory, as modified by Indenbom gives for the stress at any point X_1

$$\sigma(x_1) = \frac{E}{1-\nu}[\bar{\gamma}_p(x_1) - \gamma_p(x_1)] \qquad \text{(II.11)}$$

where $\bar{\gamma}(X_1)$ is the average viscous strain through the thickness at the corresponding freezing time for point X_1.

A more rigorous analysis, still based on Bartenev's simplified instant freezing assumption, was presented by Aggarwala and Saibel (2). They made use of the so-called Maxwell model for viscoelastic stress-strain behavior. Above a critical temperature T_c , the material is assumed to behave as an inviscid compressible fluid (the viscosity of the dashpot is zero), whereas as the material goes through T_c the viscosity instantly attains an infinite value, thus allowing for perfectly elastic material response. This assumption implies an abrupt change from zero to infinite relaxation time for the Maxwell viscoelastic model.

With this and other simplifying assumptions regarding the components of the stress tensor for this particular geometry, they arrived at the following expression for stress as a function of both position and time

$$\sigma(x_1,t) = \int_{\bar{t}(x_1)}^{t} 6\beta\left[\left(\frac{1}{b - x_1(t)}\right)\int_{\bar{x}_1(t)}^{b} \frac{\partial\varepsilon(x_1',t')}{\partial t'}\, dx_1' - \frac{d\varepsilon(x_1,t')}{dt'}\right]dt' \qquad \text{(II.12)}$$

where X_1 is the position of the freeze line at a given time, t is the freezing time for a given position, and

$$\beta = \frac{E}{6(1 - \nu)} \qquad \text{(II.13a)}$$

$$\varepsilon = \int_{T_o}^{T} \alpha \, dT \qquad \text{(II.13b)}$$

with α being the volumetric coefficient of thermal expansion. Aggarwala and Saibel showed that the parabolic law of stress distribution, as previously obtained, is true only for very slow cooling rates.

The theories reviewed thus far all yield residual stresses in good agreement with experimental determinations on quenched glass plates. However, as pointed out by Narayanaswamy and Gardon (59) , the instant freezing assumption fails to predict the transient stresses observable in the material as it cools down to ambient temperature. He showed also the inapplicability of such theories for cases in which the initial temperature of the material is close to its glass transition temperature.

Another group of theories treat the temperature dependent relaxation of the material in a more realistic way. The theories developed by Muki and Sternberg (57) and later Lee, Rogers and Woo (46,47), take into account the viscoelastic nature of the material, the latter using experimentally measured stress relaxation data.

Based on non-isothermal linear viscoelasticity and treating glass as a thermorheologically simple material, Lee, Rogers and Woo (47) obtained for the final stress distribution

$$\sigma(x_1,t) = 3\int_0^t R[\xi(x_1,t) - \xi(x_1,t')] \quad \frac{\partial}{\partial t'}\Big[\varepsilon_2(t') - \alpha\, T(x_1,t')\Big]\, dt' \qquad \text{(II.14)}$$

with the additional condition of internal stress equilibrium

$$\int_0^b \sigma(x_1,t)\, dx_1 = 0 \qquad \text{(II.15)}$$

where $\varepsilon(t')$ is the isotropic plane strain, ξ is the reduced time defined by

$$\xi(x_1,t) = \int_0^t \Phi[T(x_1,t')]\, dt' \qquad \text{(II.16)}$$

Φ is a physical property that determines the adjusted time scale, its logarithm being known as the shift function, and R is an auxiliary modulus function satisfying

$$\frac{4}{3K}\int_0^\xi G(\xi-\xi')\frac{\partial R(\xi')}{\partial \xi'}\, d\xi' + R(\xi) = 2G(\xi) \qquad \text{(II.17)}$$

where k and G are the bulk and shear modulus, respectively.

In this treatment, which may be regarded as a generalization of the theory of Aggarwala and Saibel (2), Lee, Rogers and Woo (47) showed

how the continuous effect of temperature change on the variation of the relaxation time spectrum markedly influences the final stress distribution. The comparative stress profiles, as calculated from both treatments, show a sharper peak of compressive stress at the surface and a much steeper subsurface gradient in the solution derived from the theory of Aggarwala and Saibel.

Narayanaswamy and Gardon (59) evaluated the theory presented by Lee et al. by comparison with experimental data. Their studies proved the validity of the thermoviscoelastic model in determining not only the residual stress distribution but also transient (thermal) stresses during quenching, for initial temperatures well above the strain point. However, a modification of the scheme of integration was needed to fit theoretical predictions to experimental values. The thermoviscoelastic theory failed, however, when quenching from low initial temperatures. Here the residual stress levels predicted by the theory were considerably lower than the ones obtained experimentally. Gardon and Narayanaswamy (26) and later Narayanaswamy (58) extended the theoretical analysis of stress generation to quenching from low initial temperatures by taking into account structural effects. They estimated that such structural effects are responsible for approximately one fourth of the total residual stresses in the quenched part.

The foregoing discussion has thus far dealt with theories developed for evaluation of residual stresses in inorganic glasses. Only recently has the importance of such residual effects in polymeric materials been given consideration. The following paragraphs briefly

describe the most relevant parts of the experimental work and the attempts to predict residual stresses in polymers using the theories described above.

Measurement of Residual Stresses and Residual Birefringences in Polymers

Typically, experimental determination of transient and residual stresses in quenched inorganic glass plates has been done indirectly by on-line birefringence measurements (59). The measured birefringence profiles being related to the stress by the simple stress optical law, with the simplifying assumption of a constant stress optical coefficient, valid through the totality of the transformation range. As shown in the previous section, this assumption is not valid when dealing with polymeric materials such as polystyrene, which exhibits a strongly temperature dependent and presumably rate dependent stress optical coefficient (88,98,99).

Despite this complication birefringence determinations have been used by several researchers (13,15,35,36,41,72,93) to obtain an idea as to the shape and magnitude of the stresses present in the quenched part. The most important qualitative conclusions are derived from the work of Isayev et al. (35,36,93). They noted that the areas of positive and negative birefringence are unequal, the more so the higher the initial temperature. When comparing the birefringence and stress distributions, (the latter obtained independently as will be described), they noted that the positions of zero birefringence and zero stress are not coincident. Furthermore, the stress profile always

integrates to zero, whereas the birefringence profile, specially when quenching from high initial temperatures, does not. Based on these observations, Isayev et al. (36) pointed out the impossibility of simply relating the measured birefringence to the residual stress profile by means of a constant stress optical coefficient. They conclude that a considerably more difficult treatment is probably required.

Due to the difficulties involved in relating measured residual birefringences to the actual residual stresses of the fabricated part, an alternative method directly conveying the stress distribution has almost always been used. This direct method is, of course, prescribed when dealing with opaque materials, for which the birefringence approach is unapplicable.

The layer removal method due to Treuting and Read (87) was developed to directly measure through-the-thickness residual stresses in metal plate-like parts. Figure II-6 illustrates the fundamentals in which this method is based. The upper drawing represents the as-quenched sample which exhibits equal residual stress profiles in the 2 and 3 directions. When fine uniform layers of material are removed from one of the surfaces (the lower surface in the drawing), the residual stress equilibrium through the thickness is upset. A redistribution of stress to achieve a new equilibrium state results in the warping of the sample to the shape of a circular arc, as shown in the lower drawing. The curvature may be calculated from the measured length of the chord and the sagitta of the arc. This curvature can

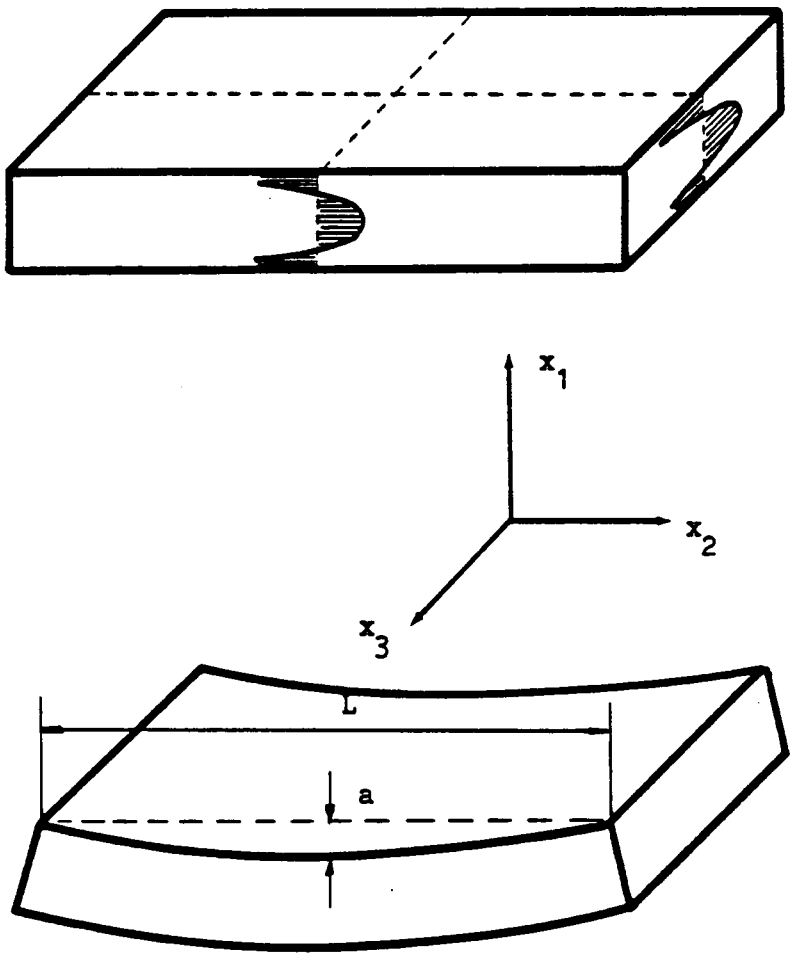

Figure II-6. Illustration of the layer removal method for measuring residual stresses in flat parts.

then be related to the stress profile present in the sample prior to layer removal. For a more complete review of this important method and the actual equations involved the reader is referred to Wust (98). Other methods have been developed to measure residual stresses, as summarized, for instance by Polakowski and Ripling (66).

Several researchers have applied the layer removal method just described to polymeric materials (19,36,73,74,75,78,93). Of these, the extensive work carried out by Isayev et al. (19,36,93) deserves special mention for the implications that it has concerning the reliability of the method when applied to polymer samples. Despite carefully designed experimental procedures in an effort not to introduce additional stresses, they found inconsistencies in the measurements that could not be overcome, thus placing doubt on the accuracy of the determinations and the reliability of the method itself.

Application of Residual Stress Theories to Polymers

Several investigators (19,36,73,83,93) have applied the theories described above to polymer systems. In most cases the theoretical predictions have been judged by contrasting them to measurements based on the layer removal method.

The most complete analysis found in the polymer literature is due to Isayev et al. (19,36,93), in work done with PS and PMMA. They compare the measured residual stress profile to the theories of Bartenev (6,7), Indenbom (33,34), Lee, Rogers and Woo (47), and Struik (83). They conclude that all the theories satisfactorily predict the stress profile in the case of PMMA, with a somewhat overpredicted

surface stress. This is not the case, however, for the PS, for which the theory clearly overpredicts the experimental determinations.

The apparent unreliability of the layer removal technique and the relatively ease by which residual birefringence profiles may be determined, motivated Wust and Bogue (99) to use the birefringence approach. Despite the difficult analyses involved, they applied this approach to polystyrene slab-like samples (1/4"x1"x2"), quenched into various cooling media from an initial temperature of 120°C. Samples so quenched were sliced perpendicularly to the plane of the slab, and the residual through-the-thickness birefringence determined. Wust and Bogue (91) used the theory of Aggarwala and Saibel (2), to describe the generation of residual birefringence, replacing 6β by $C_\varepsilon/(1-\nu)$, where C_ε is the strain optical coefficient. When taking C_ε as a constant (-0.012), or else considering it dependent on an effective temperature, satisfactory fits to the birefringence data were achieved for the ice water and air quenches. For the stress prediction Young's modulus was chosen as a constant (E=3.3 GPa). This resulted in a constant value (4.9 GPa) for 6β, when assuming the constancy of Poisson's ratio (ν=0.33). The stresses so obtained were found to be of the same order of magnitude as the stress data of Isayev et al. (19,93), for the ice water quenches.

CHAPTER III

EXPERIMENTAL

The tensile behavior of variously cooled small, homogeneous fiber-like samples has been investigated at various temperatures. Work on non-homogeneous samples involved rapid quenching from 120°C and 160°C, to 0°C, followed by measurement of the frozen-in birefringence through the cross-section. Finally the possible influence of frozen-in non-homogeneities on the tensile behavior of quenched dumbbell samples was briefly explored. A detailed discussion of the experimental procedures will now be presented.

A. MATERIALS

Two commercial atactic polystyrenes have been used throughout the present work. The samples used for tensile experiments were fabricated of polystyrene Dow Styron 685-D, manufactured by Dow Chemical. This polymer has a rather narrow molecular weight distribution with a number average molecular weight, M_n, of 2.06×10^5 and a weight average molecular weight, M_w, of 1.59×10^5, giving $M_w/M_n = 1.91$.

The material used for residual birefringence determinations was polystyrene Shell TC3-30 furnished by the Shell Chemical Company. This polymer has been quite extensively utilized here at the University of Tennessee, in a variety of rheological studies, including prior work on residual birefringences (Wust (98)). The polydispersity index,

M_w/M_n = 4.62 of this polymer indicates that it has a broad molecular weight distribution; its M_n and M_w values being 6.12×10^4 and 2.83×10^5, respectively. This same material was originally chosen for fabrication of tensile samples. The circumstances that forced the change to the polystyrene that was finally used will be described in the next section.

B. MECHANICAL PROPERTIES OF HOMOGENEOUS SAMPLES AND EXPLORATORY WORK ON NON-HOMOGENEOUS DUMBBELL SAMPLES

Tensile Behavior of Small Fiber-like Samples

Sample fabrication. Prior to sample fabrication the material was dried up for several hours at 97°C. Small, cylindrical samples were obtained by extruding the material from an Instron capillary rheometer through a 0.03 in. die. Very low crosshead speeds (0.01 in./min.) were required to avoid surface defects (melt unstabilities) when extruding at about 220°C. As a consequence of these very low crosshead speeds the fabrication process was extremely slow. Adittionally high temperatures coupled with very slow extrusion rates caused appreciable sample elongation (due to gravity effects), resulting in significant diameter differences along the sample.

To avoid these non-uniformities in diameter, the experimental set-up shown in Figure III-1 was used. In contrast to "free" extrusion processes, the sample is wound on a rotating take-up spool at a carefully controlled angular speed. This velocity of rotation was adjusted to obtain a peripheral linear speed on the take-up spool

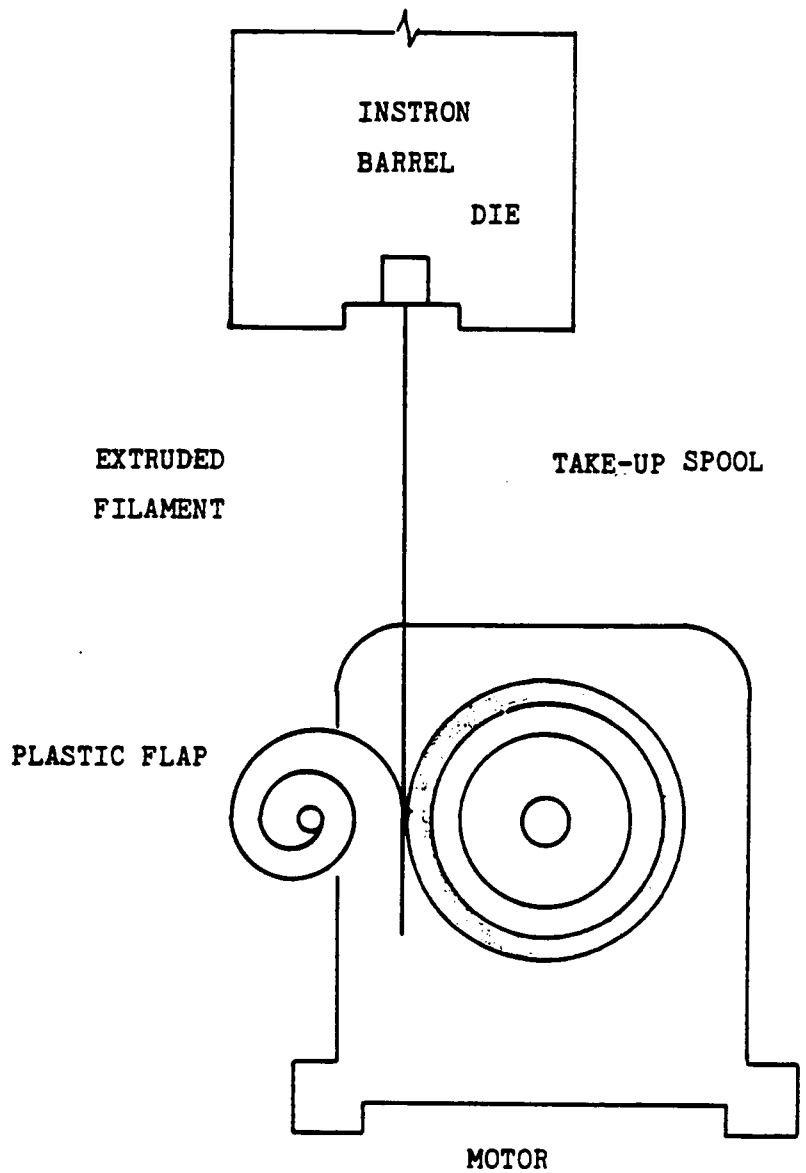

Figure III-1. Experimental set-up for the fabrication of small fiber-like samples.

slightly higher than the extrusion velocity, thus minimizing the "pulling" (orientation) of the filament. Due to the relatively large sample diameter, a flexible plastic flap was needed to constantly apply pressure on the already wound rigid filament, preventing it from pulling the still soft material leaving the die.

Early attempts to use the above experimental set-up gave crazed, unusable filaments. Apparently, the material was being wound while still relatively hot and thus the subsequent thermal contraction resulted in tensile stresses reaching the critical crazing stress of the material. Increasing the distance between the die and the take-up spool was sufficient to obtain craze-free samples. A more complete cooling was alternatively achieved by means of a room temperature air stream (hair dryer) impinging perpendicular to the filament axis.

The resulting filament had a uniform diameter of about 0.45 mm, as opposed to 0.50 mm maximum diameter for the free extruded samples.

Despite the apparent sample uniformity obtained with the above procedure, comparative tensile tests were made as a check; these were done using both the free extruded samples and the wound filaments. The annealing treatment was judged to be necessary, to eliminate any trace of molecular orientation, especially in the wound samples. Within experimental scatter all samples yielded identical results.

Typically the sample fabrication process took place over a 4 to 5 hour period without reloading. It was thought necessary to make sure that such an extended time lapse would not result in detectable polymer degradation. To that end, tensile tests were performed on samples

extruded during the first 2 hours and on samples fabricated after about 4 hours. Determinations of the modulus, yield strength and elongation to break, when compared, showed no signs of thermal degradation.

Shortly after fabrication, the filaments were cut in approximately 20 cm long pieces and stored. Particular care was observed to avoid touching the samples with the bare hand. Surgical gloves were always used to manipulate the specimens from the moment of fabrication, until final testing.

Thermal treatments. Thermal treatments were performed in a forced convection air chamber designed to fit the grips of the Instron tensile tester. This chamber, which can achieve a variety of cooling (or heating) histories (rates as low as 0.0036^{o}C/sec), has been described in detail in prior U.T. work (16,98).

The samples were annealed for no less than an hour and then either slowly cooled to room temperature or quenched into ice water or liquid nitrogen.

A sample holder was built to provide a good support for the soft fibers during annealing and subsequent thermal treatments. Of major concern were the size of the holder and the material of construction (chosen to have good heat transfer properties), to minimize thermal effects on the samples.

As shown in Figure III-2 it consists of upper and lower aluminum support plates with perforations to accomodate a maximum of 10 specimens. These plates can be fastened to a pair of stainless steel rods, forming a frame of variable dimensions, thus allowing for

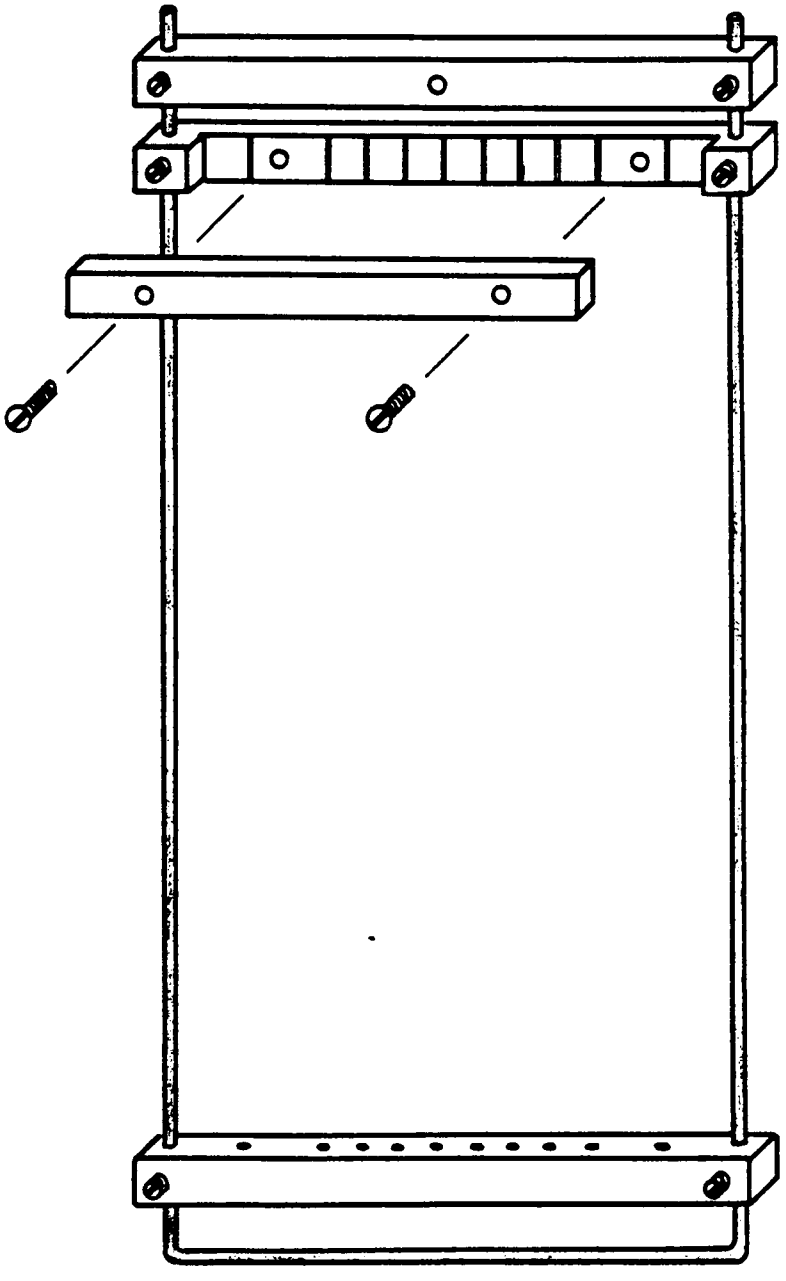

Figure III-2. Sample holder for thermal treatments of fiber-like samples.

different sample lengths. The upper support plate is a two-piece clamp arrangement which constitutes the only true physical constraint for the samples. The lower plate is perforated from top to bottom with oversized (0.7 mm diameter) holes to allow for free contraction (or expansion) of the samples. Finally, the sample holder was equipped with a hanging ring and four guides to allow for fast sample quenching, as will now be described.

The experimental set-up for thermal treatments is illustrated in Figure III-3. Here, the sample holder is shown inside the chamber, hanging from a pulley located at the top. An aluminum cylinder (not shown in the figure) was placed around the sample holder. Its function was to serve as a wind screen preventing the soft samples from becoming curved. The temperature could be continuously monitored and recorded on paper by means of a thermocouple placed through a hole in the screen close to the samples.

The ice water quenching bath arrangement, as was finally used, is shown beneath the chamber. It consists of a cylindrical metal container centered inside a well insulated glass beaker. A mixture of water and finely crushed ice fills the annular space, completely surrounding the metal container filled with distilled water. A cast plastic (epoxy) bottom allows for constant magnetic stirring of the actual quenching medium, thus maintaining a uniform temperature of about $2^{o}C$ throughout the bath.

In the original design, the sample holder was plunged directly into the mixture of crushed ice and water. Considerable scatter of the

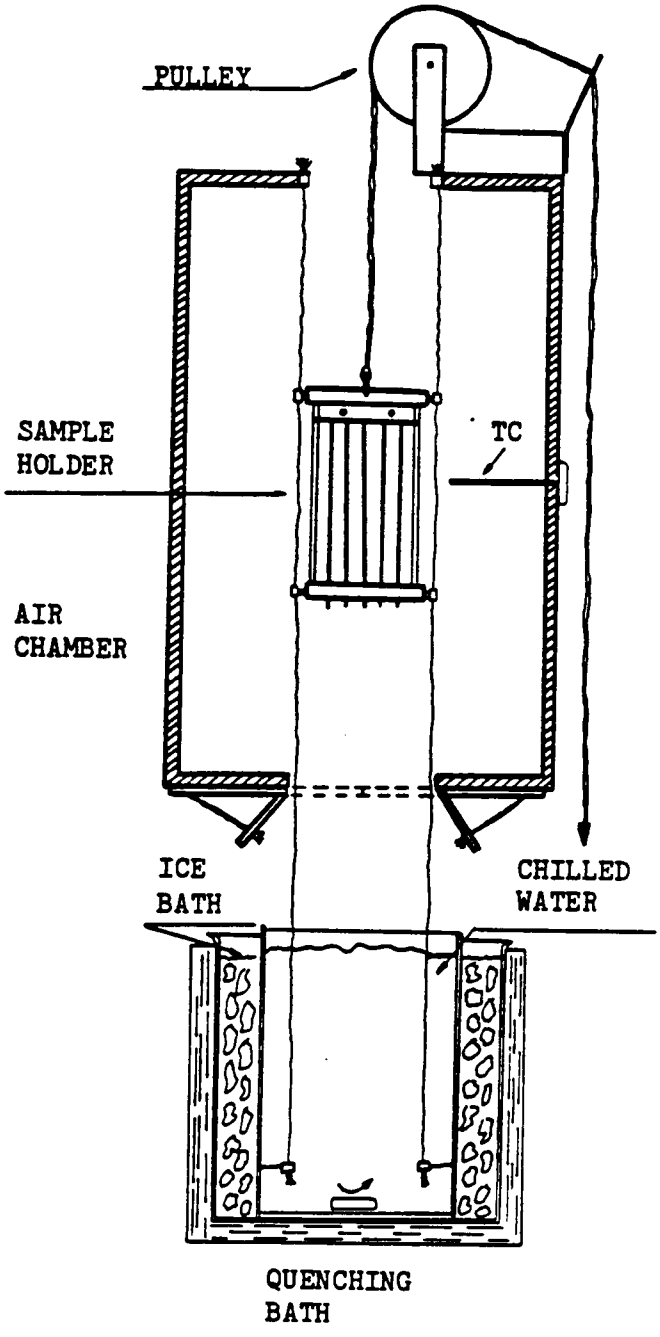

Figure III-3. Experimental set-up for thermally treating fiber-like samples.

tensile test determinations and almost no observable effect of quenching on these properties caused concern about the soundness of the method. Possible damage to the samples could result from their impact with chunks of ice. The existence of two phases (ice and water) was also thought to be detrimental to a uniform cooling of the samples along their length.

Since the hot air intakes for the chamber are located at its bottom, a circular gate was needed to close the bottom aperture, preventing excessive heat loss. A few seconds prior to quenching, the air blowers were shut off and the gate was quickly opened with the aid of rubber bands (shown in Figure III-3). Almost simultaneously the pinched string fixing the sample holder in place was released, allowing it to slide down on its guides and through the opened gate into the quenching bath. For the slow cooling treatments the sample holder was kept in place until room temperature was achieved.

The final samples, typically about 10 cm long, were carefully removed from the holder and stored in a safe place until testing (usually on the same day).

Sample testing. The tensile experiments were performed inside the air chamber mentioned above, attached to a Table Model 1122 Instron Universal Testing Instrument. Testing was done at 30°C (room temperature), 55°C and 70°C. For the sake of consistency the chamber was always used even when testing at room temperature. A set of 10 lb capacity high temperature action pneumatic grips were used for pulling the samples. The gauge pressure on the grips was fixed at the

maximum allowable limit of 75 psi to prevent slippage.

Fiber-like samples, originally made of polystyrene Shell TC3-30, were given thermal treatments as described above. At least ten samples were tested at each temperature and the load elongation curve recorded on chart paper. Initially, a 6 cm gage length was used, pulling at a rate of 2 mm/min (strain rate: 3.33 %/min).

A few preliminary tests showed a clear tendency for the samples to break at the edge of the grip. To minimize this effect the clamping surfaces were lined with self adherent emery paper. This seemed to work very satisfactorily at room temperature but when testing at 70°C the adhesive on the lining material softened and visible slippage occurred. It was necessary to take the grips apart and literally wrap them up with emery paper. This finally solved the problem of systematic breaking near the grips, while also avoiding slippage.

Despite these precautions a great deal of scatter was obtained in the determination of the ultimate elongation. The modulus and yield strength, however, showed much more consistent results. Additionally, as was mentioned earlier, quenching seemed to have very little effect on the tensile properties of these filaments.

At this point the crushed ice and water mix used for quenching was replaced by the chilled water bath described above. Several sets of new samples were prepared by quenching into this bath and subsequently tested. However, no improvement was observed.

A few samples were inspected for flaws under an optical microscope . It was observed that a considerable amount of relatively

large dirt specks were present throughout the samples. Most certainly these randomnly distributed "imperfections" were impairing the expected ductile behavior of the quenched samples.

New samples were prepared, this time using polystyrene Dow Styron 685-D, following the procedures described above. Optical miscropic inspection showed no trace of dirt; this material was therefore used in the subsequent work.

In an effort to reduce the possibility of existing flaws, the sample gage length was reduced from an original value of 6 cm to 1 cm. Despite this reduction in gage length, 8 cm long filaments were quenched and mounted in the pneumatic grips. The actual testing region (1 cm long) was always made to coincide with the central part of the quenched filament. This was thought to minimize the effect of the frame on the "quality" of the quench, also resulting in better sample uniformity. Additionally, the extra filament length (7 cm) made it much easier to mount and center the specimen in the grips.

This new set of experiments were performed at a constant pulling rate of 0.5 mm/min (strain rate: 5 %/min). The new material and the changes in the experimental procedures brought about a marked improvement in the tests results. The quenched specimens now exhibited a sometimes dramatic ductile behavior at the higher testing temperature ($70^{o}C$). Unfortunately the detrimental scattering of the elongations-to-break could not be eliminated. A possible factor influencing this scatter is the swinging of the grips due to the air blowing inside the chamber. Also, a detectable misalignment of the

upper and lower grips was seen to strain the mounted sample, especially near the clamping region, possibly impairing its performance.

Exploratory Work on the Tensile Properties of Non-homogeneous Dumbbell Samples

Material and sample preparation. Polystyrene Dow Styron 685-D was also chosen for the fabrication of the 1/8" thick dumbbell samples used in these experiments.

A Wabash Hydraulic Press was used to compression mold the samples. A two cavity plate (shown in figure III-4) and two Apollo Chrome Ferrotype plates constituted the mold. The preparation of flawless samples involved some trial and error. The following procedure was finally used.

1. The press heating elements were connected and the temperature allowed to equilibrate at about 205°C (400°F).

2. The lower Ferrotype plate and the cavity plate were allowed to heat for about 5 minutes in the press with the platens just touching them.

3. Measured quantities of dry polymer were evenly spread in the two cavities of the mold. Next, the press was closed until the heaped polymer almost touched the upper platen.

4. About 7 minutes later, the press was opened and the upper Ferrotype plate located in place. The press platens were again brought together just barely touching the molding arrangement.

5. After 5 minutes the mold was squeezed down gently and then

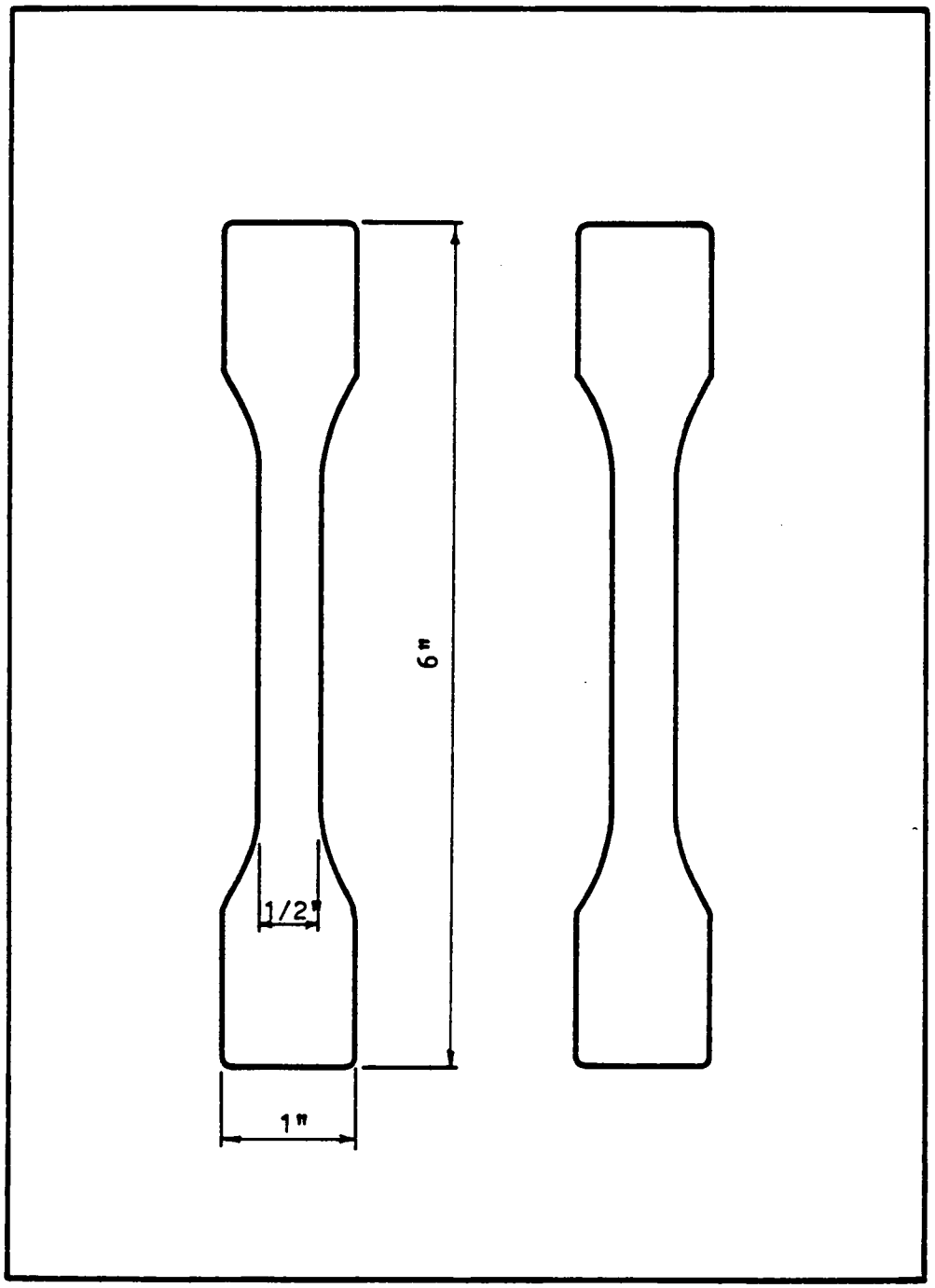

Figure III-4. Illustration of the cavity plate for molding dumbbell samples.

released, to eliminate the existing air; this was repeated 2 or 3 times.

6. Finally, the mold was firmly pressed at approximately 12 tons. This situation was held for about 5 minutes, after which the press was opened and the mold turned over on its other side, repeating the compression process for about 2 or 3 more minutes.

7. The mold was then grabbed with an insulated glove and placed in a quenching bath of room temperature water.

Thermal treatments. Prior to annealing, the flash was carefully removed from the samples. Slight pressure from the edge of one's thumb nail was sufficient to tear off the fine film. The side surfaces where then smoothed by means of 3/0 grit emery paper.

A standard Fisher Isotemp laboratory oven was used for the annealing and slow cooling treatments. The dumbbell samples were suspended from a transverse wire placed inside the oven by means of hook-ended microalligator clips. Annealing was done at 120^{o}C and lasted approximately 24 hours. The resulting sample proved to be stress free (homogeneous) when the birefringence transverse was measured. Slow cooling histories (0.01^{o}C/sec) were achieved by disconnecting the oven and allowing it to naturally cool down to room temperature. Alternatively the samples were quenched in ice water or liquid nitrogen baths placed next to the oven. A well-insulated beaker containing a stirred mixture of crushed ice and water (or liquid nitrogen) was used for the quenches. The actual quenching operation typically lasted about 3 seconds; this was just the time needed to

open the oven door, grab the sample by its hanger and plunge it into the bath. These samples were allowed to equilibrate in the bath for approximately 10 minutes.

Sample testing. Testing was made in the table model Instron testing machine equipped with standard wedge-type grips. The thermally treated samples were tested at room temperature (30°C) and 70°C inside the air chamber mentioned above. Prior to testing a gage length of 2 1/4" was inscribed on the sample surface with a permanent ink marking pen.

Before pulling, the samples were allowed to achieve thermal equilibrium inside the chamber for about 15 minutes. Testing was then performed at a pulling rate of 1 mm/min (strain rate: 1.7%/min), and the load-elongation curve recorded on a chart.

C. RESIDUAL STRESSES AN RESIDUAL BIREFRINGENCES IN NON-HOMOGENEOUS SAMPLES

Sample Fabrication

Slab-like samples (1/4" (or 1/8") x 1" x 2") were molded in the Wabash Hydraulic press following the procedure described by Wust (98) in his doctoral dissertation.

Equipment Used and Quenching Procedure

A Fisher Isotemp laboratory oven was used to preheat the samples at the two initial temperatures investigated (120°C and 160°C). In prior work, Wust(98) quenched such samples from a fixed initial

temperature of 120°C. These samples were placed inside the oven, resting on their short edge, until thermal equilibrium was achieved. Then they were grabbed with a pair of pliers and plunged into the quenching bath.

In the present research, when significantly higher temperatures (such as 160°C) were used, the above procedure was found to be unusable, as one might expect. At approximately 60°C above its glass transition temperature, the material softens to such an extent that it behaves as a viscoelastic fluid. Obviously some kind of physical support for the soft polymer was needed.

Originally an aluminum foil "frame" was built around the sample. A few extra millimeters of foil were folded on to the top, forming a tongue, which enabled one to suspend the framed sample by means of a hooked microalligator clip. An alternate design involved the fabrication of an epoxy frame around the sample. A thick layer of 3M brand quick-setting epoxy resin preparation was applied to the slab edges. A small aluminum foil tongue was also glued on the top for hanging purposes. Figure III-5 shows these supporting arrangements, as finally used.

The framed slabs were then suspended from a transverse wire inside the oven for temperature equilibration. After about 30 minutes, the samples were taken out of the oven and rapidly placed on a wire laid across a beaker completely filled with a mixture of crushed ice and water. The samples remained in the bath for about 15 minutes.

The experimental pros and cons of using the two framing methods

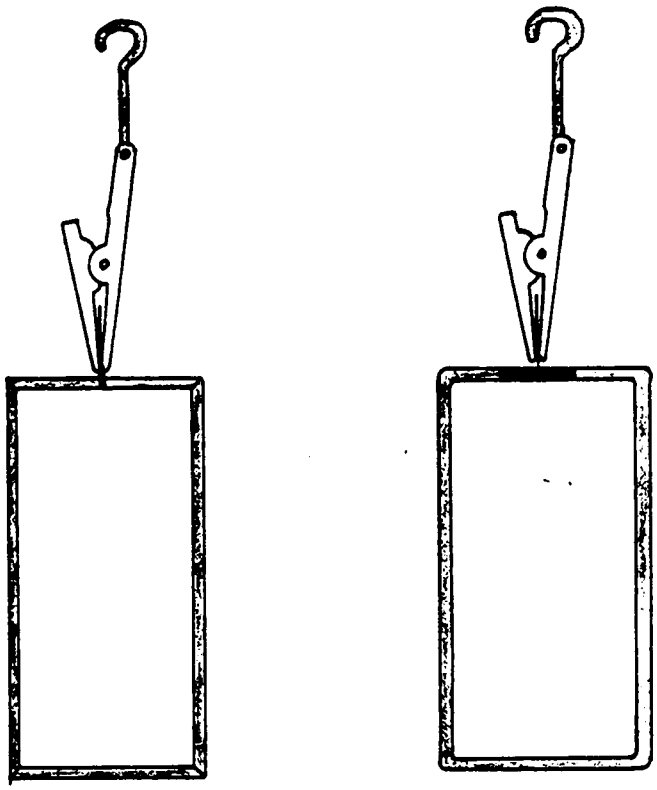

ALUMINUM FRAMED SAMPLE

EPOXY FRAMED SAMPLE

Figure III-5. Supporting arrangements for quenching slab-like samples from high initial temperatures.

will now be discussed. When using the aluminum frame at 170°C, the sample was not able to maintain a uniform shape. The soft material from the top tended to creep out of the frame under the influence of gravity. There was also a significant accumulation of material near the bottom, making the specimen considerably thicker in this region. When reducing the temperature down to 160°C, however, the above detrimental effects almost disappeared. A clear advantage of the aluminum frame was the fact that it could be reused almost indefinitely.

Of major concern, though, was the great difference in heat transfer and thermal expansion parameters of these two materials (polystyrene and aluminum). The use of a plastic thermosetting material (such as epoxy resin) would certainly minimize the difference in these properties.

The ability of the epoxy frame to maintain a reasonable specimen shape was clearly demonstrated, even at 170°C. The resulting quenched sample appeared only slightly longer than the original slab. The distortion of shape was also minimal and, most important, the thickness was very close to being uniform throughout the sample.

The above quenching procedures were preferred to the ones reported by Isayev et al (93) for quenching from high initial temperatures. They immersed the specimens, face up, in a hot silicon oil bath. The high viscosity of this substance was sufficient to support the shape of the soft material. After thermal equilibration, the samples were taken out, lying flat on a spatule, and plunged into

the quenching bath. The main difficulties of this quenching procedure are related to the heat transfer problem. Firstly, the temperature uniformity in the slab prior to quenching is questionable, one side (that closest to the bath surface) being significantly cooler than the other. Secondly, the subsequent cooling is surely impaired by the silicon oil wetting the sample.

Sample Slicing and Polishing

The quenched samples were taken out of the frames and sliced perpendicular to the plane of the slab. Figure III-6 illustrates the reference coordinate axes and the slicing of the slab.

A Gillins-Hamco thin-sectioning machine was used to cut approximately 2.5 mm (1/10") thick slices as close to the slab center as possible. A continuous water stream cooled the cutting area to prevent excessive heat built-up which might modify the frozen-in inhomogeneities. The resulting slices were then carefully polished to remove possible additional stresses from the cutting process.

Polishing was done in two stages. A first stage involved dry-polishing on standard metallurgical tables using decreasingly smaller grit abrasive materials (1, 0, 2/0, 3/0 and 4/0 grit emery paper). A mirror-like finish was obtained on a Buehler polishing turntable using a water suspension of 9.5 m aluminum oxide powder. The actual polishing procedures have been described in great detail by Wust (98).

The final slices, approximately 2 mm thick (20% thickness reduction by polishing), were mounted on standard slide frames for

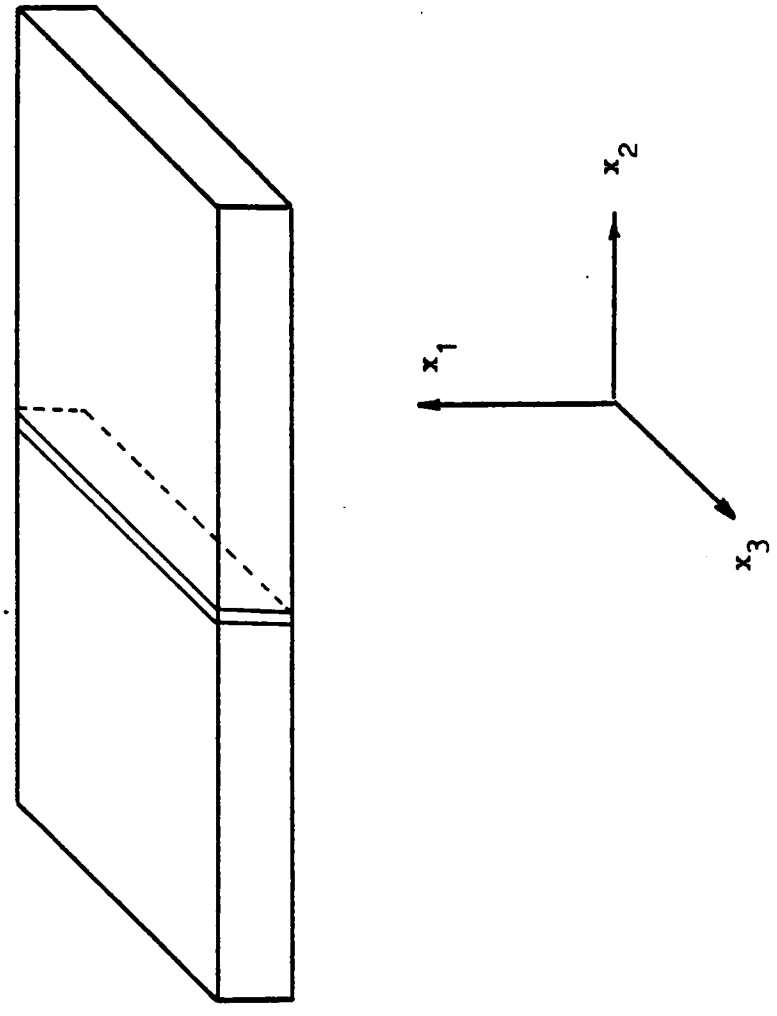

Figure III-6. Slicing of slab-like samples for birefringence determinations.

birefringence measurements. Prior to mounting, it was necessary to estimate the specimen thickness in the actual measurement region. The following procedure was used:

1. A red dot was inscribed centered on the long edge of the specimen. Its function was to allow for easy identification of the measurement region in the birefringence determinations.

2. The thickness on the four corners of the specimen was carefully measured (with 1/1000" precision) by means of a caliper.

3. Assuming linear thickness variation, the thickness on the red dot region was computed from the values obtained for the corners on that side. The thickness on the center of the other side was analogously determined, using the other two thickness values from the corners of the specimen.

4. Finally, the "thickness profile" through the measurement region (approximately the center of the slab) was computed, from the values obtained in 3., also assuming linear thickness variation.

In an effort to minimize edge effects, considerable care was taken to always measure the through-the-thickness birefringence profile in a region as close to the slab center as possible.

Birefringence Measurements

The optical bench used for birefringence measurements is shown in Figure III-7. The specimen is mounted on a rotating stage located between a light source and a microscope with an attached compensator. The light source is an ordinary filament bulb with a polarizing filter in its front. The microscope, which has a polarized 10 X eyepiece, is

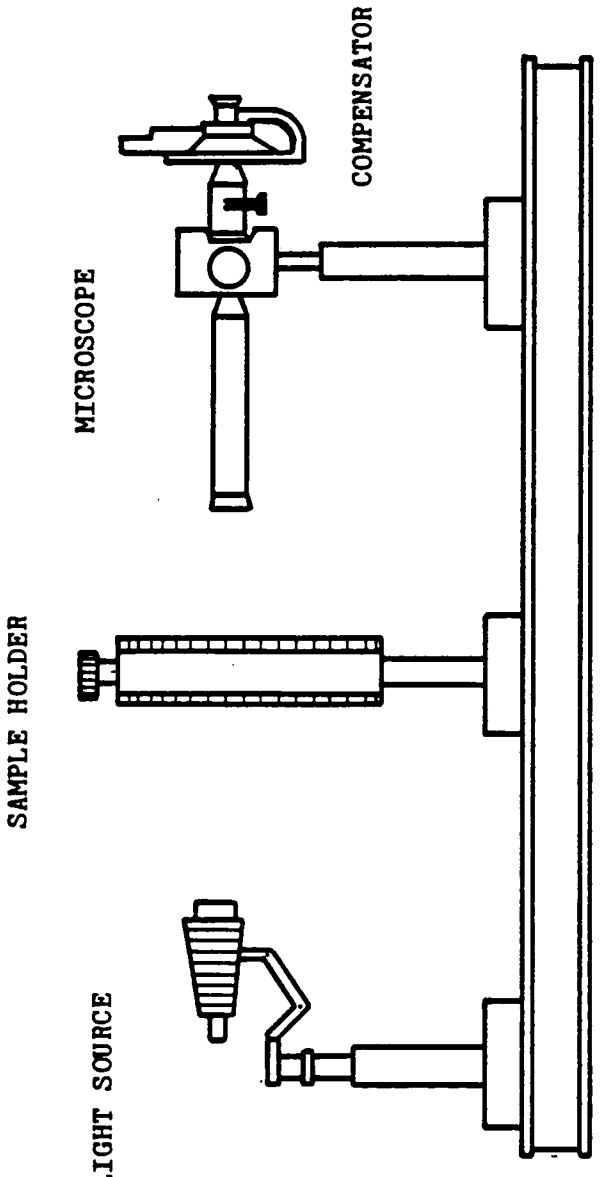

Figure III-7. Optical bench for measuring birefringence.

mounted on a micrometer slide allowing it to travel sideways parallel to its optical axis. A Babinet compensator fits in the microscope between the objective and eyepiece and is used to measure birefringence.

This set-up is the same that was used in earlier work by Wust (98) to determine the residual birefringence profile in quenched polystyrene slabs. The birefringence needs to be determined in a step by step manner, starting from one edge (slab surface), moving to the center and continuing to the other edge. The horizontal distance travelled by the microscope in each step is accurately measured with the attached micrometer. The difference between the micrometer readings at any point and at the edge, gives the actual distance (in mm) of that point to the slab surface. Thus, birefringence as a function of distance to the surface may be determined.

A major experimental difficulty, already noted by Wust (98), was the lack of a vertical reference line in the compensator. Without such a feature the identification of the actual points of measurement was a difficult, eye-straining task. In his work Wust had to use a "speck of dirt" from the compensator as a reference.

Retardation measurements are made at two mutually perpendicular positions of the compensator (0° and 90°). Therefore, the point chosen as reference needs to be on the rotation axis (center) of the compensator, if it is to remain always in the same position. Most important, the reference point needs to remain stationary throughout the experiment. These conditions are, to say the least, very difficult

to meet when such an arbitrary reference as a speck of dirt is used.

For the present work a detachable reference insert (shown in Figure III-8) was built and used as an alternative method. A copper disk fitting snuggly in the compensator front cavity was used to make a support for the monofilar reference. Two holes were drilled on the disk to match a pair of pins in the compensator, thus allowing only one mounting position. A square opening, matching that of the compensator, was then cut in the disk completing the supporting frame. An ultra thin polymer filament was then fixed to the disk by means of an epoxy adhesive preparation. The completed reference insert was coated with flat black paint to avoid internal reflections during measurement. By just slight pressure (no screws needed) this reference insert can be attached to the compensator. It thus provides a very reliable and convenient way to pin-point the birefringence profile across the sample thickness.

The following measuring procedure was used:

1. The microscope and light source were roughly aligned by slightly rotating the former around its supporting column until "even illumination" could be observed on both sides of the microscope barrel.

2. With the analyzer and polarizer in the position of minimum light transmission (crossed polarizers), a check was made to assure that the fringe lines, observable when looking through the microscope, vanished at approximately the 45° angle position of the compensator.

3. With the specimen mounted on the stage, the microscope was then adjusted (raised or lowered) to the height of the red dot

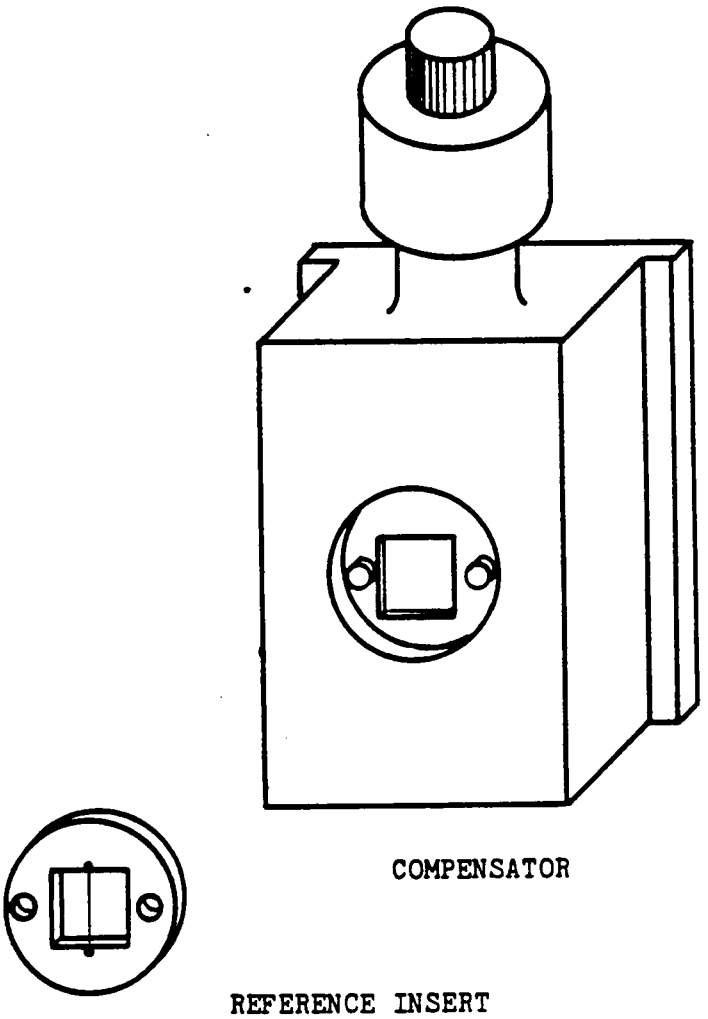

Figure III-8. Vertical reference insert for the optical compensator.

inscribed on the specimen. By means of the attached micrometer slide, the microscope was horizontally displaced, superimposing the vertical reference line of the compensator and the specimen's edge. The micrometer reading at this point corresponds to the slab surface.

4. Finally, the 0° and 90° angle compensator readings were obtained twice at each point, typically 0.2 to 0.3 mm apart, throughout the slab thickness.

The experimental procedures used throughout this research have been extensively discussed in this chapter. The next two chapters of the thesis will be devoted to the presentation and discussion of results and calculations involved in their determination.

CHAPTER IV

MECHANICAL PROPERTIES STUDIES: RESULTS AND DISCUSSION

This research on mechanical properties deals with the effect of thermal history on the tensile behavior of glassy, amorphous polymers. The main effort was given to the case of small, presumably homogeneous, fiber-like samples. The possible influence of residual non-homogeneities on the tensile behavior of quenched dumbbell samples was also investigated.

The experimental results will be presented first, followed by a detailed discussion.

A. CALCULATIONS AND PRESENTATION OF RESULTS

Calculation of Modulus, Yield Strength and Ultimate Elongation

As indicated in the experimental chapter of this thesis (Chapter III), the tensile testing results were recorded on chart paper in the form of load-elongation curves.

Figure IV-1 illustrates a typical load-elongation curve obtained when testing polystyrene fiber-like samples. The modulus, yield strength and ultimate elongation (elongation-to-break) can be calculated from the chart as will now be described.

Young's modulus is taken as the initial slope of the stress-strain curve, i.e.,

$$E = \frac{\sigma}{\varepsilon} \qquad \text{(IV.1)}$$

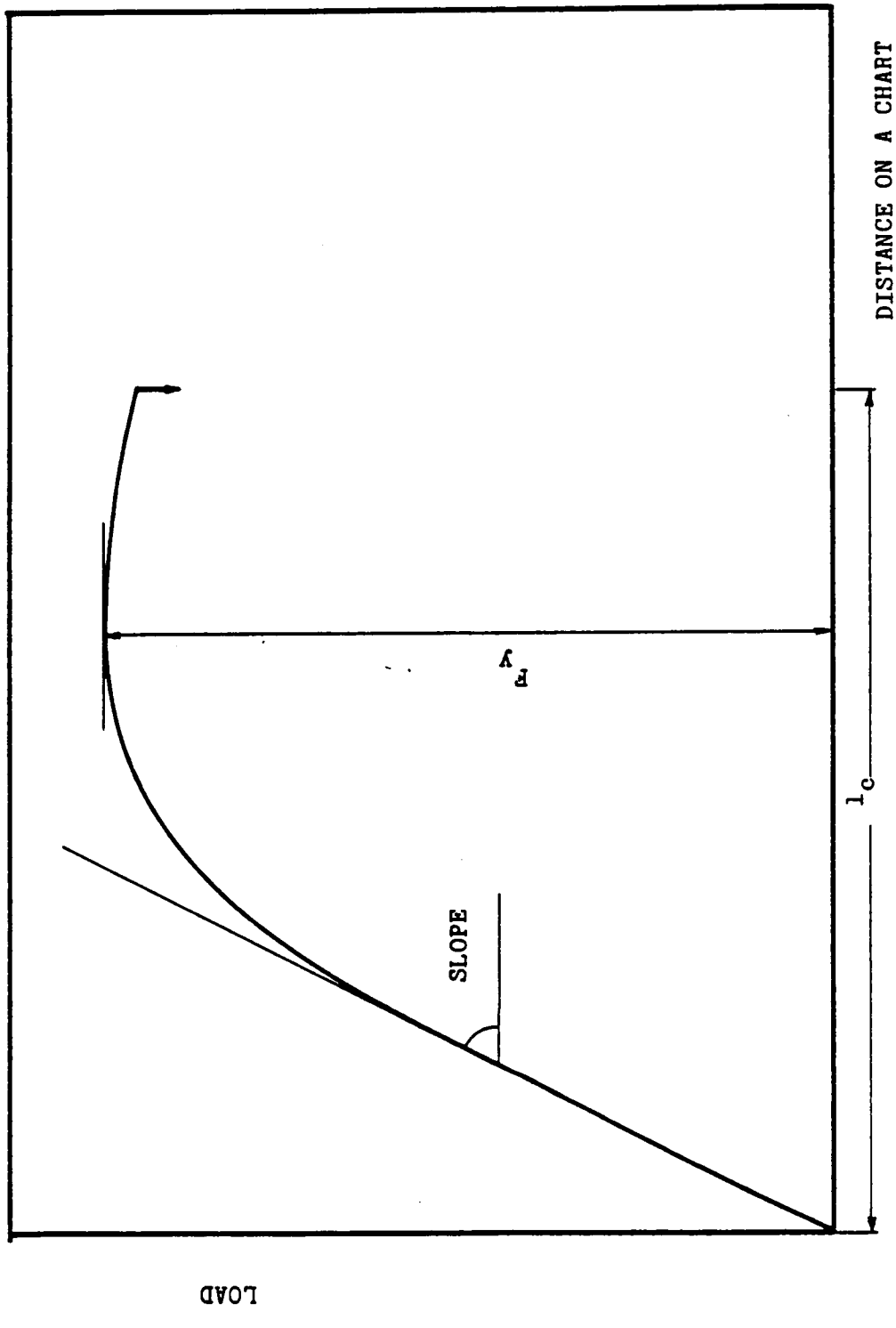

Figure IV-1. Typical load-elongation curve for polystyrene showing the parameters involved in the calculations.

where σ and ε are the engineering stress and strain respectively.

The equivalent of this when dealing with load-elongation data can be obtained from the expressions for stress and strain

$$\sigma = \frac{F}{A_o} \tag{IV.2}$$

and

$$\varepsilon = \frac{l}{l_o} = \frac{l - l_o}{l_o} \tag{IV.3}$$

where F is the load, A_o is the initial cross-section area of the sample, and l_o and l are the initial and final sample lengths respectively.

Instead of measuring the final sample length l, it is more convenient to measure the distance traveled by the chart l_c, during the pulling of the sample. These two quantities are easily connected.

Assuming that there is no slippage at the grips, the "elapsed time" during the experiment can be expressed by

$$t = \frac{l - l_o}{V_x} \tag{IV.4}$$

where V_x is the pulling rate (crosshead speed).

During the time span of the experiment, the chart has traveled a

distance l_c at a preset speed V_c. Thus,

$$t = \frac{l_c}{V_c} \tag{IV.5}$$

Combining IV.4 and IV.5 we obtain

$$\dot{l} = l - l_o = l_c \frac{V_x}{V_c} \tag{IV.6}$$

Substituting this result into IV.3 we finally obtain for the strain

$$\varepsilon = \frac{l_c}{l_o} = \frac{V_x}{V_c} \tag{IV.7}$$

Combining IV.1, IV.2 and IV.7, the final expression for Young's modulus is given by

$$E = \frac{F}{A_o} \frac{l_o}{l_c} \frac{V_c}{V_x} \tag{IV.8}$$

The expression for the yield strength is

$$\sigma_y = \frac{F_y}{A_o} \tag{IV.9}$$

where F_y is the load at the top of the "yield peak" (see Figure IV-1).

Finally, the elongation-to-break can be calculated from IV.7, taking l_c as the final chart length and multiplying the result by 100 to obtain percent elongation.

Tensile Testing Results on Fiber-like Samples

Fiber-like polystyrene samples were annealed for one hour at 120°C and subsequently cooled down to room temperature in various ways. Cooling rates ranging from approximately 160°C/sec (ice water quench) to about 0.008°C/sec (oven cooled) were achieved. Testing of the resulting samples was done at 30°C (room temperature), 55°C and 70°C. Some samples were also quenched in a liquid nitrogen bath.

As has been mentioned in Chapter III, two major difficulties were encountered during tensile testing of these samples. Firstly, the presence of dirt in the original polymer (PS Shell TC3-30) hampered the expected effects of cooling histories on the mechanical performance of the samples. The second difficulty, that could not be solved, was a dramatic scatter of the ultimate elongation results, particularly at the higher temperature. It is for this reason that at least eight typical calculated values for modulus, yield strength and ultimate elongations are presented in each case.

Table IV-1 contains the calculated tensile results for the iced water quenched samples, tested at 30°C, 55°C and 70°C.

At 30°C the modulus and yield stress exhibit average values of 1.5×10^{10} dyne/cm^2 and 4.5×10^{8} dyne/cm^2, respectively. Both properties exhibit quite good reproducibility at this temperature. The elongations-to-break are also relatively uniform at this low temperature with an average value of 4.7%.

When raising the testing temperature to 55°C the resulting modulus is smaller, as expected. Its average value is now 1.2×10^{10}

Table IV-1

Tensile results for ice water quenched fiber-like samples (cooling rate 160°C/sec)

Property	Temperature	Determination										Average	Standard Deviation
	(°C)	1	2	3	4	5	6	7	8	9	10		
Modulus	30	1.4	1.3	1.5	1.4	1.4	1.5	1.5	1.6	1.6	1.6	1.5	.10
	55	1.1	1.1	1.1	1.2	1.2	1.2	1.2	1.1	-	-	1.2	.052
(x 10^{10} dyne/cm^2)	70	.92	.90	.94	.91	.91	.94	.99	.98	.98	.98	.95	.35
Yield Strength	30	4.5	4.5	4.5	4.5	4.5	4.5	4.4	4.4	4.5	4.5	4.5	.042
	55	3.7	3.7	3.7	3.7	3.7	3.6	3.7	3.5	-	-	3.7	.074
(x 10^{8} dyne/cm^2)	70	2.7	2.8	2.8	2.8	2.8	2.8	2.8	2.9	2.8	2.8	2.8	.047
Ultimate	30	4.5	5.1	4.1	4.1	5.3	4.7	4.5	4.8	5.6	4.0	4.7	.54
Elongation	55	6.0	4.3	6.4	5.8	9.4	7.0	5.7	4.5	-	-	6.1	1.6
(%)	70	21	9.6	47	18	69	19	130	53	50	140	56	46

dyne/cm^2, with also very little scatter. Similarly, at 55°C the quenched samples exhibit lower, rather uniform yield stress levels averaging 3.7 x 10^8 dyne/cm^2. In contrast, the elongation-to-break is now greater (average value 6.1%), and so is the dispersion of results (scatter).

With further increase of the temperature to 70°C all properties exhibit the expected tendencies, with decreasing modulus and yield strength and increasing elongations-to-break. Even better reproducibility is now observed in the modulus determinations resulting in an average value of 9.5 x 10^9 dyne/cm^2 with rather small scatter. The yield stress, averaging 2.8 x 10^8 dyne/cm^2 again shows good reproducibility.

The most significant effect when testing at 70°C, however, is the sometimes very dramatic increase in sample ductility. Elongations-to-break as high as 140% were observed. Unfortunately, with supposedly identical specimens (same thermal history), and under identical testing conditions, elongations-to-break of ony 18% were also obtained.

Phenomenologically, a neck was clearly seen to form in the strained samples. This neck, when initiated at a point near the midpoint of the sample, would propagate with further pulling, giving as a result the dramatic ductility mentioned above. However, if the point of initiation was located near the clamps, the neck could not propagate successfully, resulting in much lower ultimate elongations. These widely varying results are reflected in a standard deviation value of

46% elongation obtained for this set of experiments.

In contrast to this, Table IV-2 shows the tensile results for the slowly cooled samples (cooling rate: 0.008°C/sec) at the same testing temperatures (30°C, 55°C and 70°C). These slowly cooled specimens gave a room temperature (30°C) average modulus value of 1.7 x 10^{10} dyne/cm^2. The yield strength is quite uniform at this temperature with an average value of 4.5 x 10^8 dyne/cm^2. Considerable scatter, however, was again obtained for the ultimate elongations, which averaged to 6.0%.

Raising the temperature to 55°C did not seem to affect the modulus results (average value 1.7 x 10^{10} dyne/cm^2). The yield stress did show the expected diminishing trend, averaging 3.7 x 10^8 dyne/cm^2, with rather good reproducibility. A marked scatter was again obtained for the elongations-to-break, reaching an average level of 4.2%.

At 70°C the modulus now exhibits a somewhat lower average value of 1.5 x 10^{10} dyne/cm^2. The yield strength is also lower at an average level of 3.0 x 10^8 dyne/cm^2; rather consistent results were obtained for both properties with good reproducibility at this temperature. The ultimate elongations (average value 8.5%), however, were once more plagued with scatter.

A general observation for the slowly cooled samples in the temperature range investigated, was the presence of crazes in the fractured specimens. These crazes were seen as fine lines appearing perpendicular to the fiber axis, the pulling direction. In contrast,

Table IV-2

Tensile results for oven cooled fiber-like samples (cooling rate 0.008°C/sec)

Property	Temperature (°C)	Determination 1	2	3	4	5	6	7	8	9	10	Average	Standard Deviation
Modulus	30	1.7	1.6	1.7	1.8	1.7	1.7	1.7	1.5	1.7	-	1.7	.083
	55	1.7	1.8	1.7	1.7	1,6	1.7	1.7	1.7	-	-	1.7	.053
(x 10^{10} dyne/cm^2)	70	1.5	1.4	1.3	1.5	1.6	1.5	1.5	1.6	1.6	1.4	1.5	.099
Yield Strength	30	4.4	4.4	4.6	4.5	4.6	4.6	4.6	4.6	4.4	-	4.5	.097
	55	3.7	3.7	3.6	3.6	3.7	3.6	3.7	3.7	-	-	3.7	.052
(x 10^{8} dyne/cm^2)	70	3.0	3.0	2.9	2.9	2.9	3.0	3.0	2.9	3.0	2.9	3.0	.053
Ultimate	30	5.6	4.9	6.5	7.2	4.6	4.0	7.6	7.2	6.4	-	6.0	1.3
Elongation	55	4.4	6.4	3.6	3.8	3.2	4.4	3.2	4.7	-	-	4.2	1.0
(%)	70	5.5	6.1	7.3	12	7.1	12	11	8.4	3.3	12	8.5	3.1

no crazes could be observed in the rapidly cooled samples, but at the lowest testing temperature (30°C), at which some whitening of the sample could be visually detected.

Liquid nitrogen quenched samples were only tested at 70 °C and the results are presented in Table IV-3. The modulus determinations (average 1.0×10^{10} dyne/cm^2) are somewhat higher than the ones obtained for the ice water quenched samples at the same testing temperature. This is also the case for the yield strength, averaging 3.0×10^{8} dyne/cm^2. Regarding ductility, only one case exhibited elongations in a range over 100%, with most determinations lying in the region of 20-30%.

Figure IV-2 is included here as a contrast of the very different ductilities exhibited at 70°C depending on the sample thermal history.

Tensile Testing Results on Dumbbell Samples

As described in Chapter III, some exploratory work was done involving 1/8" thick standard dumbbell samples. These samples were first annealed at 120°C for about 24 hours to relieve residual inhomogeneities from the fabrication process. Cooling down to room temperature was achieved in a variety of ways, analogously to the case of fiber-like samples.

Table IV-4 shows the averages of the calculated moduli, breaking stresses, and ultimate elongations for the different cooling histories, at both 30°C and 70°C. When testing at room temperature (30°C) no difference in modulus is observed between a liquid nitrogen and an

Table IV-3

Tensile results for liquid nitrogen quenched fiber-like samples

Property	Temperature (^{o}C)	Determination 1	2	3	4	5	6	7	8	9	10	Average	Standard Deviation
Modulus ($\times 10^{10}$ dyne/cm^2)	70	.97	1.0	1.0	1.0	1.0	.87	1.0	.98	-	-	1.0	.045
Yield Strength ($\times 10^{8}$ dyne/cm^2)	70	3.0	3.0	3.0	3.0	3.0	2.9	2.9	2.8	-	-	3.0	.076
Ultimate Elongation (%)	70	33	20	28	23	20	28	43	130	-	-	41	37

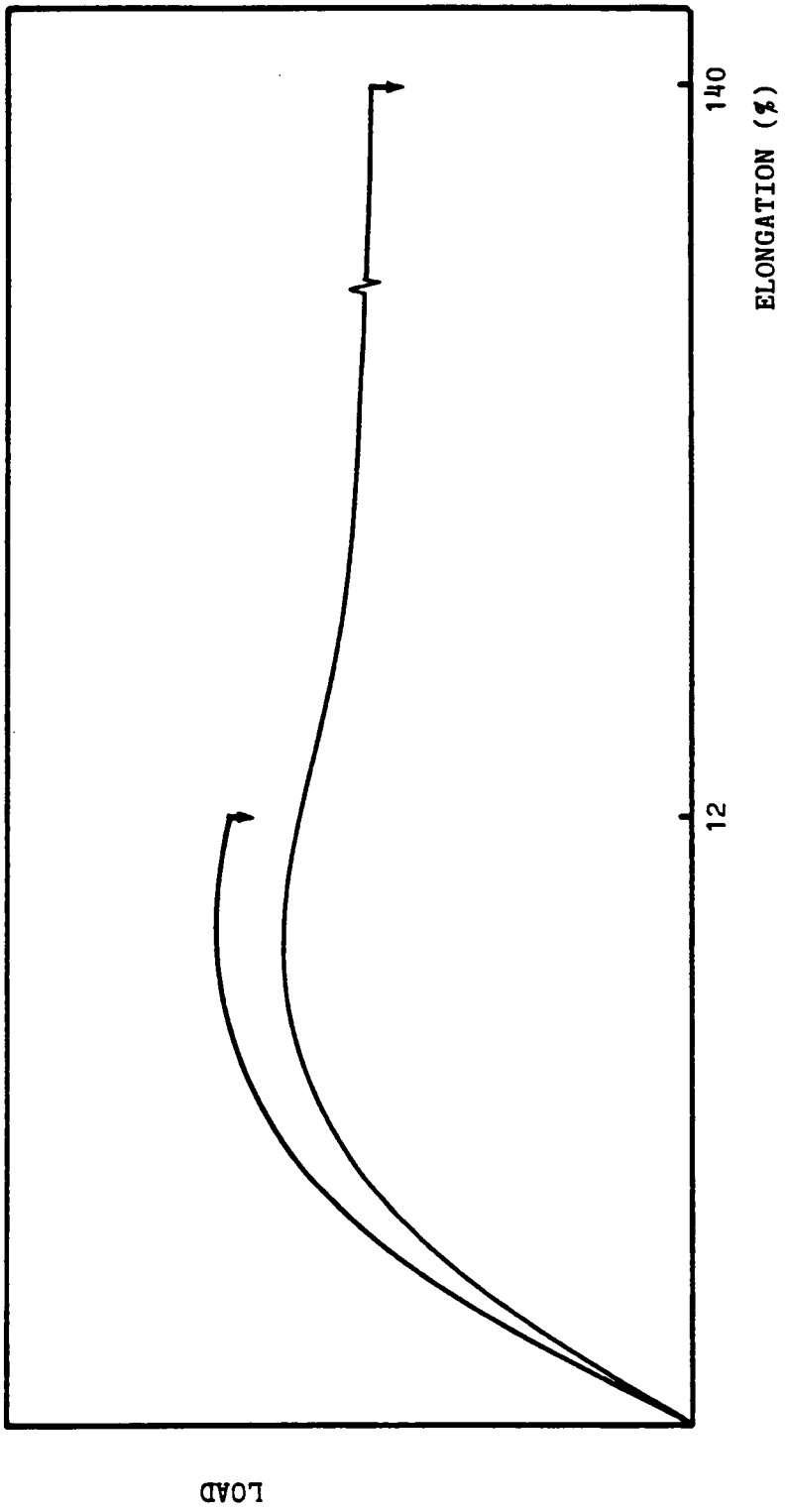

Figure IV-2. Effect of the thermal history on the ductility of small fiber-like samples at 70°C.

Table IV-4

Tensile results for variously cooled dumbbell samples at $30^{o}C$ and $70^{o}C$

Cooling Rate (^{o}C/sec)	Temperature (^{o}C)	Modulus (x 10^{10} dyne/cm^2)	Breaking Stress (x 10^{8} dyne/cm^2)	Ultimate Elongation (%)
-	30	1.8 (.058)(*)	3.7 (.70)	2.5 (.59)
(liquid N_2)	70	1.1 (.058)	2.2 (.20)	2.9 (.45)
160	30	1.8 (0.0)	4.5 (.27)	3.2 (.25)
(ice w.q.)	70	1.1 (0.0)	2.5 (.058)	3.8 (.38)
.01	30	1.9 (.071)	4.9 (.27)	3.3 (.42)
(Oven cool.)	70	1.3 (0.0)	2.6 (.27)	2.3 (.31)

(*): The numbers in parenthesis are the standard deviations of 3 results.

ice water quench. Furthermore, the modulus of the slowly cooled samples (cooling rate: 0.01°C/sec) is only slightly higher than that of the quenched specimens. The breaking stress shows perhaps more consistent results, with some tendency to increase as the cooling rate is lowered.

Similar effects of the cooling history on the modulus and breaking stress are observed at 70°C. In contrast to the case of the fiber-like samples, no change in ductility was detected. A device for on-line measurement of the sample elongation was not available. Thus, a 2" gauge length was inscribed on the sample to allow for the determination of the elongation after fracture. Due to the very small elongations achieved in all cases, it was not possible to make reasonably accurate determinations of the final lengths by this method. To obtain an idea of the breaking elongations with which to establish comparisons, however, estimations were made based on the separation of the Instron jaws during pulling; these are also presented in Table IV-4.

B. DISCUSSION

Tensile Testing of Fiber-like Samples

As mentioned in the background chapter of this thesis (Chapter II), the stress-strain behavior of polymers is strongly temperature dependent. Figure II-1 shows this effect for annealed polystyrene specimens at atmospheric pressure, as presented by Matsushige et al (52). The following discussion will primarily deal with how cooling

histories modify the tensile stress-strain behavior of this polymer. In studying the effect of temperature on this behavior, special consideration will be given to the influence of cooling histories on the brittle-to-ductile transition temperature.

A comparative discussion of the data gathered in Table IV-1 (ice water quenched specimens) and Table IV-2 (slowly cooled samples) will now be made.

Regarding the modulus, small consistent differences are observed at the lower temperature (30°C). As the temperature is increased, however, these differences become larger, the lower the cooling rate the higher the modulus. These changes in rigidity (modulus) with the rate of cooling from above T_g, can perhaps be explained in terms of frozen-in free volume. The ice water quenched samples have more free volume than the slow cooled specimens. The less efficient packing of the polymer chains in the rapidly cooled samples possibly allows for a higher degree of deformation with equal applied stress; this results in lower modulus. This effect is probably enhanced at the higher testing temperatures at which the already existing volume is increased by newly created volume due to thermal expansion.

The observed effect of rapid cooling on the yield strength is not in accordance with what it was expected. One would suppose that a rapidly quenched sample would behave similarly to an annealed specimen tested at a somewhat higher temperature. In the present work both rapidly cooled and annealed samples exhibited the expected decreasing yield strength with temperature. However, the yield strength

determinations at the two lower temperatures (30°C and 55°C) appear to be identical, irrespective of the cooling history of the specimen. Thus, the analogy that a higher quench rate is equivalent to a higher testing temperature does not work. When testing at 70°C, however, the slowly cooled samples exhibited yield strengths about 7% higher (on the average) than those of the quenched specimens. This appears to be a small but rather consistent effect as suggested by the respective standard deviation values.

For the elongations-to-break, Matsushige et al (52) (see Figure II-1) showed a clear diminishing trend with increasing temperature, in the case of annealed polystyrene specimens. This is explained in terms of the monotonically decreasing critical crazing stress temperature dependence. As the temperature increases the critical crazing stress level becomes lower; the breaking stress of the specimen will thus be lower, and so also its ultimate elongation.

When considering the slowly cooled samples in the present research, it is noted that the ultimate elongation value at 55°C is smaller than that at 30°C. By 70°C, however, the ultimate elongation is seen to increase noticeably. This is not the situation for the rapidly cooled samples. In this case the ultimate elongations show a clear increasing trend as the temperature is raised.

Comparing both the slowly cooled and the rapidly cooled samples, the ultimate elongations appear to be larger for the latter case, at all the testing temperatures but the lowest (30°C). The rapidly cooled samples when tested at 70°C exhibited elongations-to-break

considerably above 100% in a few cases (see Table IV-1). Although there is a large amount of scatter, the fact that even a few samples showed this extreme ductility is noteworthy. A great deal of the variation had to do with where in the sample the necking began; if the point of initiation was located near the clamps, the sample soon broke. Such variations must surely have to do with random flaws in the sample, involving such factors as diameter variations in the original sample, property differences caused by non-uniform cooling of the various parts of the sample, dirt particles, and so on. But the appearance of high ductility, even occasionally, gives one hope that such behavior might be reproducible on a consistent basis if the imperfections can be identified and controlled.

It is now relevant to bring into discussion the fact that the ultimate elongations (breaking strains) reported by Matsushige et al (52) are considerably lower than the ones obtained in this research. In the temperature range $-10^{o}C$ to $80^{o}C$, they reported breaking strains of the order of 1-2% for the annealed specimens. In the present work, however, slowly cooled samples exhibited average elongations-to-break in the 4-9% region for the $30^{o}C$ to $70^{o}C$ temperature range.

At least two factors surely account for these possibly significant differences, namely the definition of strain used in each case and the dimensions of the tensile specimens. Matsushige et al reported so-called "true strains" which are defined as $\log_e(l/l_o)$, whereas in the present work strain has been taken as the ratio

$(l-l_o)/l_o$. The former definition of strain yields lower results than the latter, especially at high extensions.

A more important factor is, perhaps, the specimen size as it affects the probability of the existence of imperfections. A polymer glass is not a perfectly homogeneous domain. Dust particles, voids, collections of chain ends and other defects are all a consequence of the fabrication process. These irregularities act as stress concentrators which may induce premature failure of the sample. The larger the cross-section area of the tensile specimen, the more likely it is to find these imperfections in sufficient amount to cause premature fracture. Thus, in a certain size range (excluding the very small samples, in which the size of the imperfections may be comparable to their cross-section dimensions), larger specimens exhibit less ductility, all other conditions constant. Matsushige et al used cylindrical samples of about 3 mm (0.12") in diameter (in the gage length region), approximately six times larger than the ones used in this research.

Leaving aside these possibly explainable differences in strain levels, consideration will now be given to the brittle-to-ductile transition temperature.

When testing annealed polystyrene specimens at atmospheric pressure Matsushige et al (52) found the brittle-to-ductile transition to occur at about 90°C. In the present study, slowly versus rapidly cooled samples showed quite distinct results in this respect, i.e., the brittle-to-ductile transition was found to depend significantly on the

prior thermal history. As mentioned above, the slowly cooled specimens exhibited a drop in the ultimate elongation values between 30°C and 55°C. This is, of course, in agreement with the observations of Matsushige et al (52). At 70°C, however, the breaking elongation is found to be noticeable higher, although it remains in the same order-of-magnitude level.

On the other hand, rapidly cooled samples exhibited a moderate increase in ultimate elongations between 30°C and 55°C. In contrast the average value of ultimate elongations at 70°C is about nine times as large as its corresponding 55°C value. Furthermore, comparing the highest individual determinations at these two temperatures, the 70°C ultimate elongation is of the order of fifteen times larger than the 55°C result. Thus, by rapidly cooling a polystyrene sample one can make it behave in a ductile fashion at lower temperatures. In other words, the brittle-to-ductile transition temperature becomes lower with increasing cooling rates from the molten state.

This increased ductility of the rapidly quenched samples would seem plausible on purely phenomenological grounds because the rubbery state (above T_g) is inherently ductile; one might then reasonably associate the ductile mechanism with increased free volume. Then it can simply be argued that higher quench rates produce a more rubbery glassy state, i.e., one with more free volume. Thus, an ice water quenched sample at 70°C behaves qualitatively like an annealed sample at 90°C.

As described in the background chapter, increasing temperature and pressure induces a brittle-to-ductile transition in "inherently" brittle polymers such as polystyrene (9,52). To explain this phenomena, Matsushige et al. (52) base their argument on more mechanistic grounds; that is, they observed two competing microplastic processes, i.e., crazing and shear banding, associating the former with brittle failure and the latter with ductile failure. When the critical crazing stress becomes equal to the stress for shear band initiation, a brittle-to-ductile transition is observed and the specimen fails in a ductile manner.

While in the present work there was no provision to monitor these plastic yielding processes, some phenomenological observations were made regarding the type of failure in each case, as already mentioned in the previous section. Particularly, the dramatic ultimate elongations obtained with rapidly cooled samples at 70^{o}C were accompanied by the formation and propagation of a neck. In contrast, the slowly cooled brittle samples showed well developed crazes at the moment of fracture.

Matsushige et al.(52) noted that temperature and pressure have significantly different effects on the crazing and shear banding processes, i.e., increasing temperatures affect the shear band initiation stress more strongly than that of crazing, whereas pressure changes affect crazing more markedly than shear banding. It thus seems plausible that the amount of free volume frozen in a sample must surely affect the relative importance of these two mechanisms. Based on these

considerations and on the experimental results, it might be argued that the relatively large free volume present in a quenched sample modifies the position of the intersection point of the curves for these two microplastic deformation mechanisms, shifting it down to a lower temperature. As a consequence, the brittle-to-ductile transition observed by Matsushige et al.(52) at 90°C (and atmospheric pressure), is now seen to occur at some temperature between 55°C and 70°C.

Tensile Testing of Dumbbell Samples

This exploratory work on the tensile behavior of standard dumbbell samples showed very little effect of cooling rates for testing temperatures up to 70°C (see Table IV-4).

The average modulus determinations appear to be identical for the two quenches, whereas the slowly cooled samples exhibit a slightly higher value at all temperatures. Regarding breaking stress, the ice water quenched specimens achieved a higher stress level than the ones cooled in liquid nitrogen. Slowly cooled samples failed at even higher stresses.

The most significant feature of the observed behavior is certainly the type of fracture obtained. In contrast to the case of the fiber-like samples, no brittle-to-ductile transition was found between the two temperatures investigated (30°C and 70°C). Surprisingly, the lower temperature yielded practically identical breaking strain values for the ice water quenched and slowly cooled samples, whereas the liquid nitrogen quenched specimen gave a noticeably lower result.

At 70°C the ice water quenched specimens showed the most ductility, followed by the liquid nitrogen and oven cooled samples. All three cases, however, showed the same ductility level, i.e., no dramatic increase in ductility was observed.

A plausible explanation for the difference in behavior between the small fiber-like samples and the larger dumbbell specimens may be related to the existence of frozen-in nonhomogeneities. As has been reviewed in Chapter II, cooling a relatively large sample rapidly causes a permanent state of stress, generally referred to as residual stresses. These stresses are of a tensile nature in the core and compressive in the surface. When such a sample is pulled, the resulting tensile stress adds to the already existing tensile component of the frozen-in stresses. As a result, the critical brittle failure stress may be "prematurely" reached, inhibiting the brittle-to-ductile transition.

Also, the "quality of the quench" in the central regions of the sample is significantly lower than at the surface. Like in the case of the small samples (such as the fiber-like samples discussed above), the surface cools almost instantly; the cooling rate of the center is, however, much smaller resulting in considerable less frozen-in free volume. Thus, despite these large samples were quenched identically to the small fiber-like samples of the previous section, the degree of non-equilibrium of the former is significantly lower, and as it appears there is not sufficient free volume present in the material to induce a brittle-to-ductile transition at 70°C.

CHAPTER V

RESIDUAL STRESSES AND RESIDUAL BIREFRINGENCES IN NON-HOMOGENEOUS SAMPLES: EXPERIMENTAL RESULTS AND ANALYSIS

The present chapter deals with the measurement and prediction of residual stresses in quenched (non-homogeneous) polystyrene samples, in contrast to the prior work on small (homogeneous) samples. The work in this chapter is thus divided into two parts: experimental and theoretical. A detailed discussion of the experimental procedures involved was developed elsewhere in this thesis (Chapter III). The well-known theory of Lee, Rogers, and Woo (47) was applied for the prediction of both residual stresses and residual birefringences in the quenched part, as will be discussed.

The experimentally determined residual birefringence profiles will be presented first, followed by a detailed analysis of the theoretical results.

A. BIREFRINGENCE CALCULATION AND PRESENTATION OF EXPERIMENTAL RESULTS

Birefringence Calculation from the Compensator Measurements

As noted when discussing the experimental procedures, retardation measurements were made at the 0° and 90° angle compensator positions for each point in the slab thickness. These values for the retardation were recorded in arbitrary units, i.e., the number of turns of the compensator micrometer (corresponding to a determined displacement of the movable wedge). To obtain the retardations in

actual wave length units (nm), the expression used is

$$\Gamma(\text{nm}) = (+/-)\ (\text{SAMPLE READING} - \text{ZERO READING})\ \lambda(\text{nm})\ \left(\frac{\text{WAVE/TURN}}{K}\right) \tag{V.1}$$

where +/- is taken as negative when the displacement of the movable wedge is in the direction of the long dimension of the slice, (3 axis in the slab), and positive if the line of movement is perpendicular to that direction (1 axis in the slab). The zero reading is the position of the zero retardation line without a sample, λ is the wavelength of light (in nm), wave/turn is the amount of retardation per turn of the micrometer, and K is a constant of the compensator. and K is a constant of the compensator. The average value of the result resulting 0^{o} and 90^{o} retardation determinations, Γ_{AVE} is then used in the calculation of the birefringence at that point. The birefringence is thus given by

$$\Delta n = \frac{\Gamma_{AVE}}{t} \tag{V.2}$$

where t is the thickness of material at the point of measurement (slice thickness).

A computer program was made to perform these calculations based on the compensator readings and the thickness profile of the material in the measurement region. This program, which can be conveniently used with the CALCOM plotting routines to directly convey the experimental birefringence profiles, is presented in Appendix B.

Experimental Residual Birefringence Results

Slab-like homogeneous polystyrene samples 1/4" thick were ice water quenched from two initial temperatures 120°C and 160°C. A few 1/8" thick specimens were also quenched from the lower temperature (120°C).

Following slicing and polishing, the 0° and 90° retardations were measured and from them the residual birefringence profiles calculated, as described above.

Figure V-1 shows the experimental determination for the 1/4" thick slabs quenched from 120°C. The result reported by Wust and Bogue (99) for the same quenching conditions has been included here as a check.

When quenching from 160°C it was noted (see Chapter III) that some means of maintaining the shape of the specimen was needed. Thus, prior to the heating and quenching process, the samples were framed in various ways (using epoxy resin or aluminum sheet as framing materials). To evaluate the effect of these frames on the observed residual birefringence profile, some framed samples were used for the 120°C quenches. The results for the epoxy framed and aluminum framed slabs are shown in Figure V-2; the residual birefringence profile found in a "plain" sample (one without a frame) is also included for comparative purposes. It appears that both framing methods have essentially the same effect on the observed birefringences. The surface determinations remain unaffected, whereas significant

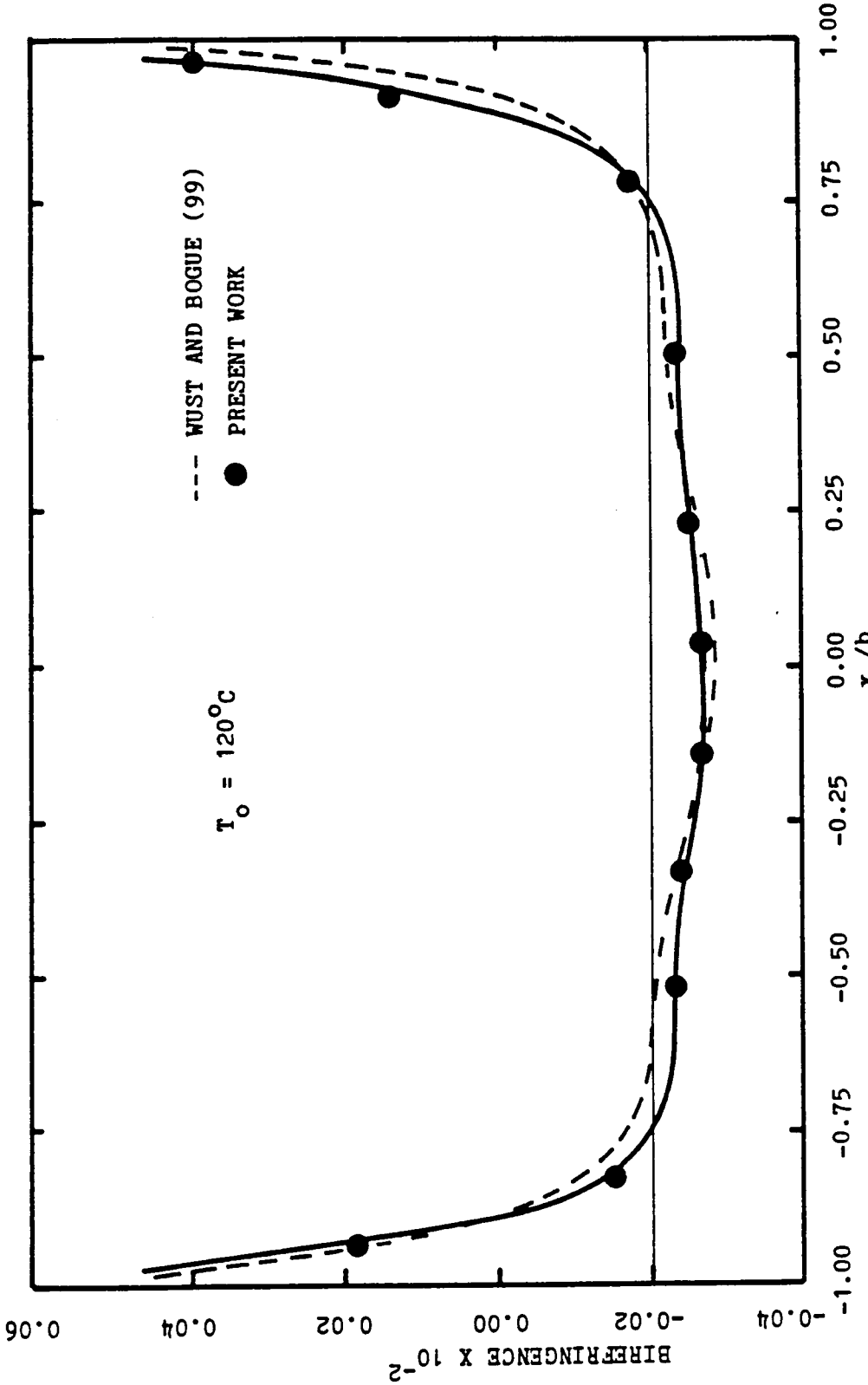

Figure V-1. Experimental residual birefringence profile in unframed slabs for a 120°C initial temperature quench, and comparison with the results of Wust and Bogue (99).

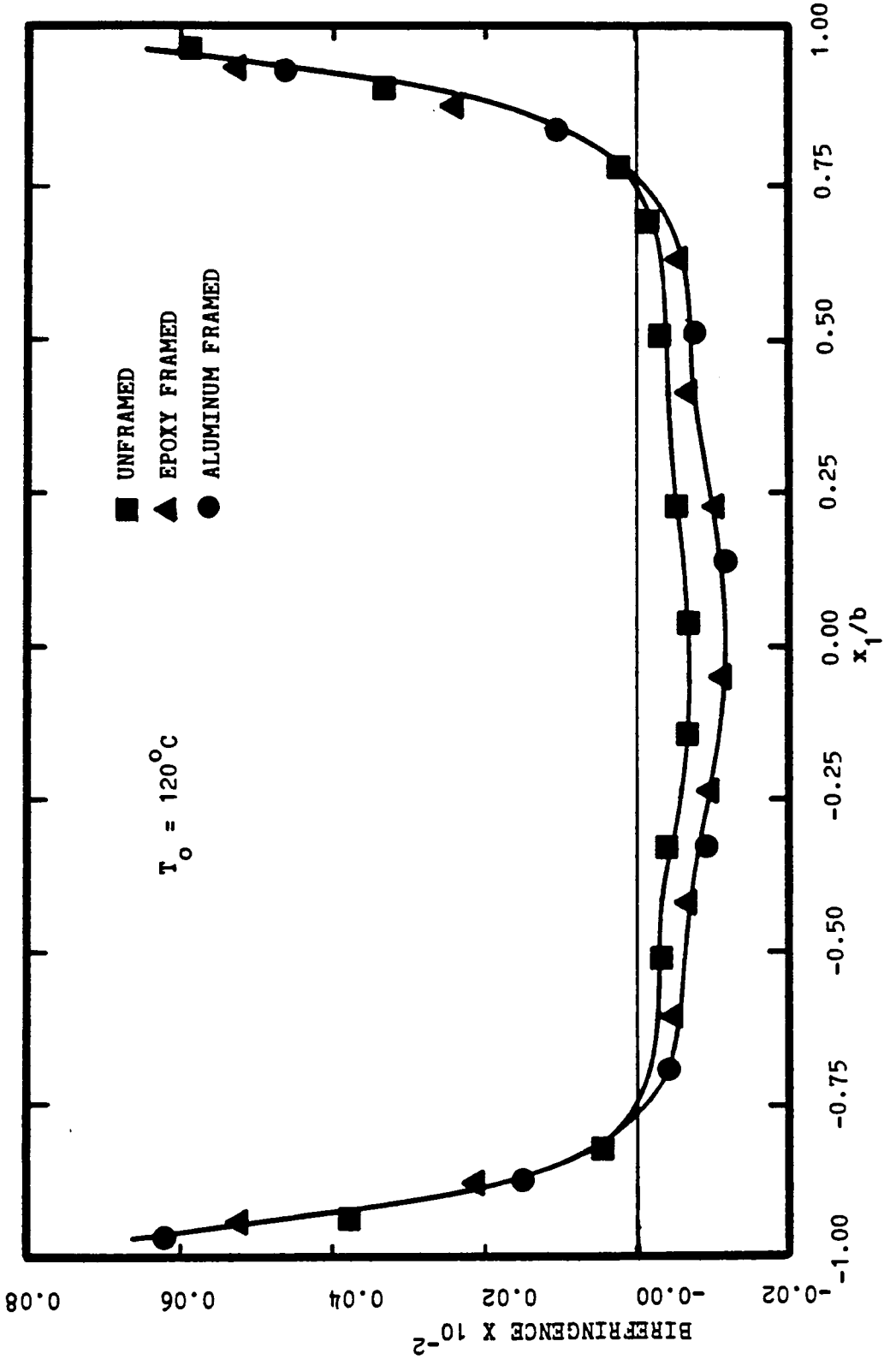

Figure V-2. Effect of the supporting frame on the residual birefringence profile for a 120°C initial temperature quench.

differences can be seen in the central region with higher magnitude negative values.

The practically identical results obtained with these two framing materials, suggest that the observed differences are due to the material being physically constrained during the quenching process, rather than to modifications of the heat transfer problem. The theory of Lee, Rogers, and Woo (47), which will be applied in the next section, requires that the condition of internal stress equilibrium be met at all times. For this to physically happen, however, it is necessary to imagine that the edges of the slab are solid throughout the quenching. The frames used in this work thus seem to provide these rigid edges called for by the theory, resulting in a more balanced profile, as observed in Figure V-2. While this reasoning might be plausible for low initial temperature quenches (120^{o}C), it does not work when quenching from high initial temperatures (160^{o}C) which will be shown that result in highly unbalanced profiles.

An alternative explanation of the effect of the frame on the observed birefringence distributions is based on a more complete constraint of the material as it is being cooled. In both cases the soft polystyrene adheres to the frame (the epoxy frame is actually glued to the sample). During quenching, however, the thermal contraction of the frame and that of the material are different, the latter being greater that the former. The contraction of the slab might thus be partially hindered by the frame, resulting in a tensile stress that gives rise to negative birefringences (since the strain

optical coefficient is negative). This other approach, however, does not explain why the surface birefringences remain essentially unaffected.

For several reasons (see Chapter III) the epoxy frame was preferred to the aluminum one. In order to be consistent, the residual birefringence profile obtained with the epoxy framed slab was used for the evaluation of the theoretical predictions throughout this work.

Figure V-3 shows the respective residual birefringence profiles for epoxy framed samples quenched from 120°C and 160°C. The shapes of these profiles are very similar, with rather steep changes near the surface and gradual levelling-off as the central region is approached. Both cases feature a quite distinct concave "bump" in the center, which is more pronounced in the samples quenched from 160°C.

Quantitatively, however, there are important differences between these two cases. The 120°C profile exhibits large positive birefringences (6×10^{-4}) near the surface and rather low negative values (-9×10^{-5}) in the central region. The cross-over point from positive to negative birefringences is located approximately at one quarter of the half thickness of the slab, taken from the surface inwards. It is noteworthy the fact that this profile is approximately "balanced", i.e., the areas of positive and negative birefringences are nearly equal. This will prove to be of utmost importance when discussing the theoretical attempts to fit the observed birefringence profiles in a later section.

Samples quenched from 160°C show lower surface birefringence

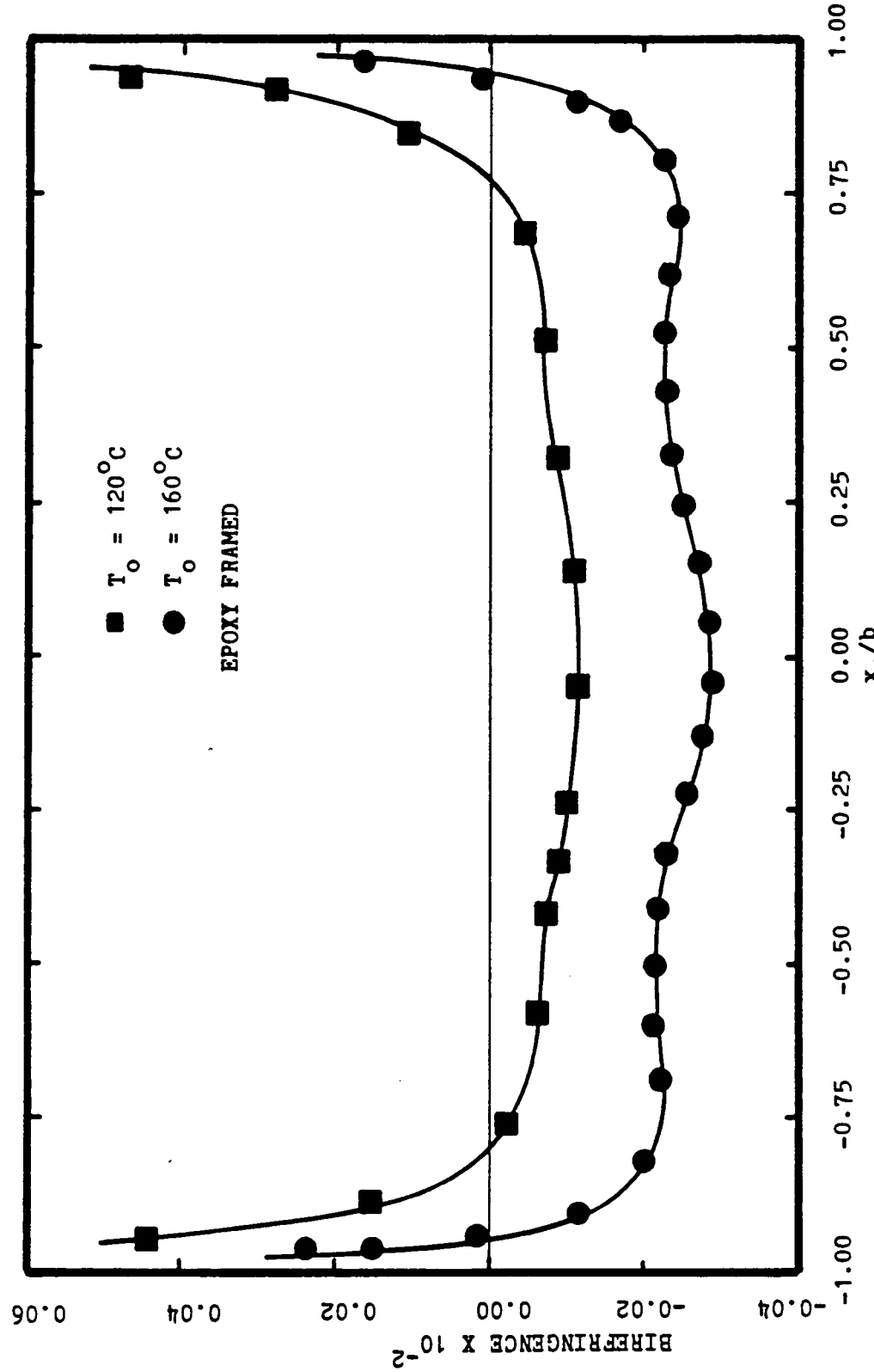

Figure V-3. Residual birefringence profiles for framed slabs quenched from 120°C and 160°C.

values (2×10^{-4}) and much larger negative birefringences internally (-3×10^{-4}). The positive to negative values cross-over point is now much closer to the surface. To state it simply, it appears as if raising the initial temperature has the effect of "shifting down" the residual birefringence profile. Thus, in contrast to the lower initial temperature case, the residual birefringences are not balanced. Here the area of negative birefringence is overwhelmingly larger than the sum of the areas of positive birefringence.

The effect of thickness on the residual birefringence profile is illustrated in Figure V-4. This figure shows the results for 1/4" and 1/8" thick unframed specimens quenched from 120°C in an ice water bath. The birefringence profile for the 1/8" thick sample is both qualitatively and quantitatively different from that of the thicker specimen (1/4"). The levelling-off of the negative birefringence portion observed in the 1/4" thick sample is not present here. The absence of the central bump is also noteworthy. Moving from the surface inwards the birefringence level decreases monotonically, achieving a minimum value at the center of the slab. Symmetry with respect to the slab midplane thus results in a residual birefringence profile of nearly parabolic shape. The cross-over point is now located approximately halfway between the surface and the midplane.

Quantitatively speaking, the near surface birefringences (5×10^{-4}) are considerably larger than their corresponding values for the 1/4" thick specimen (2×10^{-4}). In contrast, similar negative

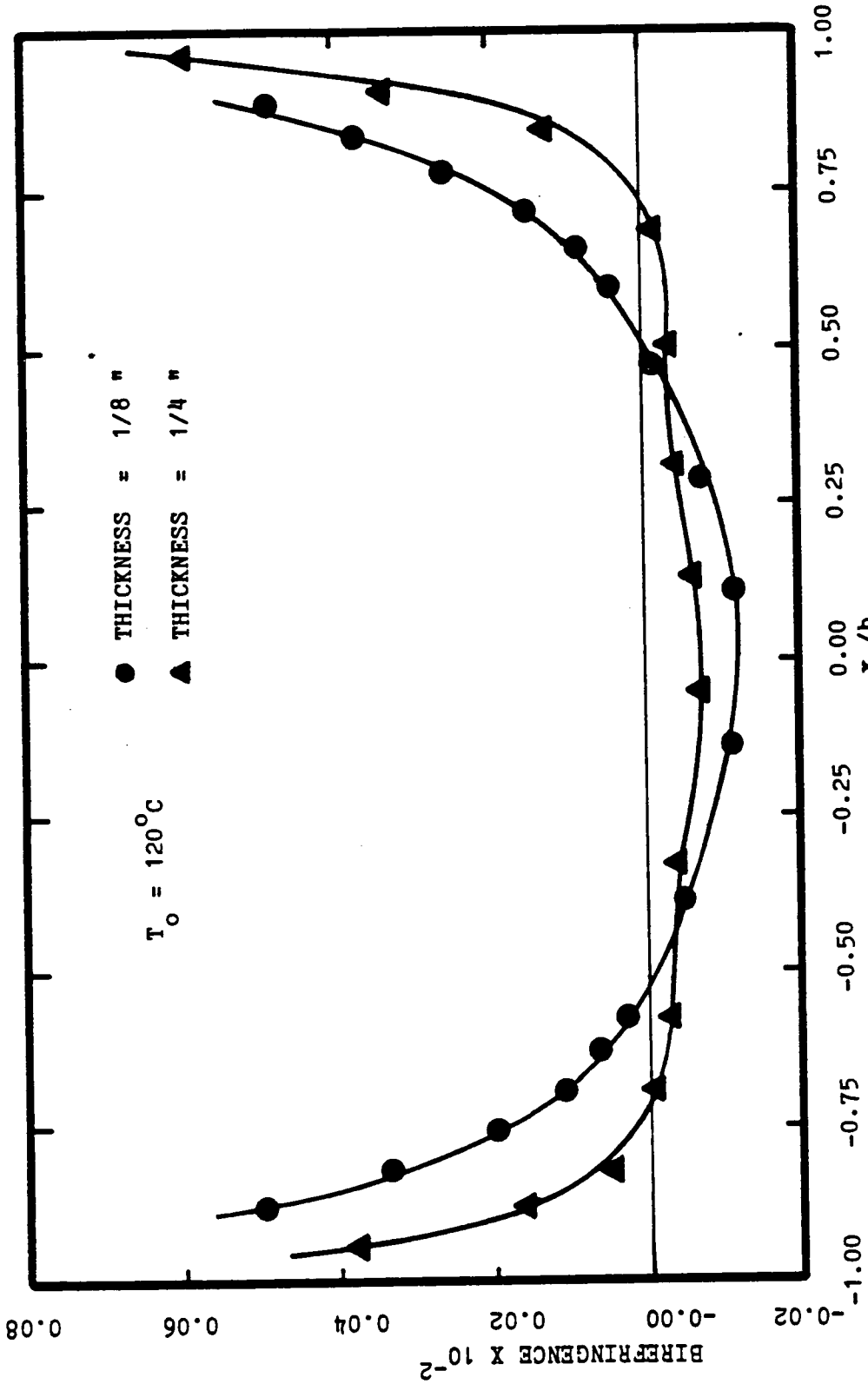

Figure V-4. Effect of sample thickness on the residual birefringence profile in slabs quenched from 120°C.

birefringence levels are observed in both cases, although somewhat larger in the thinner (1/8") sample (1×10^{-4}).

B. ANALYSIS AND DISCUSSION

It is important to keep in mind that a main purpose of this study was to obtain a reasonable theoretical prediction for the residual stress profiles in quenched slabs. Because these stresses are not easy to measure, however, the experimental effort centered on the measurement of birefringence profiles, as an indirect measure of the stresses. Thus, the theoretical analysis must deal with both the mechanical (stress) response and the optical (birefringence) response of the material.

All the present residual stress theories mentioned in Chapter II treat the problem in two steps. A first step involves the calculation of the strains which arise from the decaying temperature gradient during the quench. Subsequently these strains are converted into stresses by multiplying them by a modulus. These generating stresses are then allowed to relax to a greater or lesser extent, depending on the temperature and on the particular theory.

The birefringence approach makes use of the theoretical framework laid down in these treatments. The point of difference comes about after the calculation of the strains has been performed. At this point the calculated strains are converted into birefringences by multiplying them by a strain optical coefficient C_ε. Similar to the stress problem, the developing birefringences undergo various degrees

of relaxation, depending on the temperature and on the particular theoretical framework used. This is accomplished by means of a temperature dependent relaxation function.

The theoretical framework of the residual stress treatments can thus be used to predict residual birefringences in the quenched part as well. Once a reasonable fit to the experimental observations is achieved, the same theory allows for the determination of the stress state frozen into the body.

In the present work the theory of Lee, Rogers, and Woo (47) was used, as defined by expressions II.14 to II.16. Wust (98) has recently shown that this general treatment can be reduced to the simpler theory of Aggarwala and Saibel (2) (see equation II.12), by imagining an abrupt change in the rheological behavior, i.e., the auxiliary modulus function R is zero above T_g and takes on a large constant value R_o below it. This is, of course, the instant freezing assumption which constitutes the basis for an important group of theories, as already described. It will be shown later that the result reported by Wust and Bogue (99) (based on the theory of Aggarwala and Saibel (2)) can also be obtained on the computer by operating in the framework of the more general theory of Lee, Rogers, and Woo (47).

The numerical scheme used in the present work for solving equations II.14 to II.16 is presented in detail in Appendix A. This numerical scheme is essentially the one outlined by Lee et al. (47) with the modifications suggested by Narayanaswamy and Gardon (59). These two groups of investigators pointed out the need for very small

time integration steps in order to obtain sufficient accuracy. Small time integration steps are important during the first stages of the cooling process, particularly near the surface where cooling progresses extremely rapidly. Another factor calling for small time increments is the fact that the auxiliary modulus function $R(\xi)$ shows a nearly exponential dependence on the reduced time ξ, as suggested by the shape of R for inorganic glasses presented in a paper by Narayanaswamy and Gardon (59). Thus, R changes markedly with time at high temperatures and gradually levels off to a constant value R_o as the material cools down.

Small time integration steps are, of course, synonymous with long execution times, which in turn represent high computer costs. In an effort to keep these costs down to a reasonable level without sacrificing accuracy, a variable time scale was developed. This allows for time steps of variable size, starting very small and gradually increasing as time progresses. Despite this provision for an expanding time scale, the execution time in the early runs was found to be excessive (several hours).

Lee, Rogers, and Woo (47), when discussing the numerical solution to their theory, strongly emphasized that the maximum number of time integration steps is bounded by the memory space of the computer. This clearly suggests that in order to keep the execution times low, inter mediate calculations can and must be stored for latter use throughout the computer program. By so doing the execution times were drastically reduced (down to a few minutes). A detailed

discussion of these and other aspects of the computer program, as finally used, are presented in Appendix B, along with the fully documented program.

As mentioned earlier, the residual stress distribution predicted by Wust and Bogue (99), using the theory of Aggarwala and Saibel (2), can also be obtained by means of the more general treatment of Lee, Rogers, and Woo (47). This is accomplished by substituting the experimentally based auxiliary modulus function R by a step function, which is zero above T_g and takes on a constant value R_o below it; i.e., the instant freezing assumption is introduced as "input" to the theory (Lee et al.), rather than being analytically "built-into" the theory (Aggarwala and Saibel).

Figure V-5 shows the predicted residual stress distributions in 1/4" thick polystyrene slabs ice water quenched from 120°C. These predictions are based on a constant value for $6\beta = E/(1-\nu) = 3R_o =$ 4.9 GPa, where E and ν are the instantaneous Young's modulus and Poisson's ratio, respectively. The near total coincidence of the stress profile predicted by Wust and Bogue (99), and the one obtained in the present work, served also as a check for the new computer program.

Shown in Figure V-6 are the respective residual birefringence predictions using a constant strain optical coefficient ($C_\varepsilon = -0.012$) which are also coincident, as expected. Although clearly an oversimplification, this theoretical prediction based on a constant C_ε

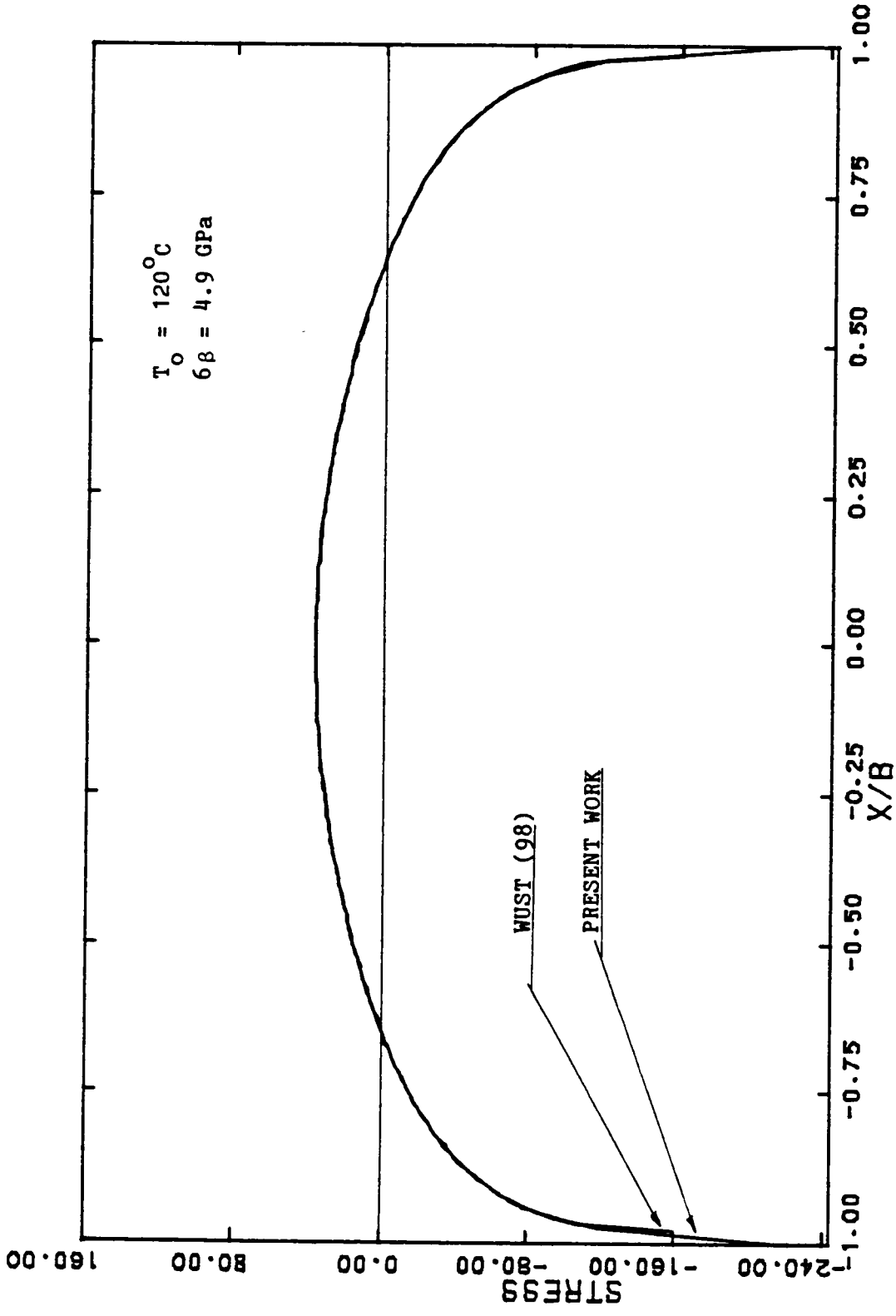

Figure V-5. Comparison of the calculated residual stress profile to the one reported by Wust(98) for a 120°C initial temperature quench, using a constant modulus.

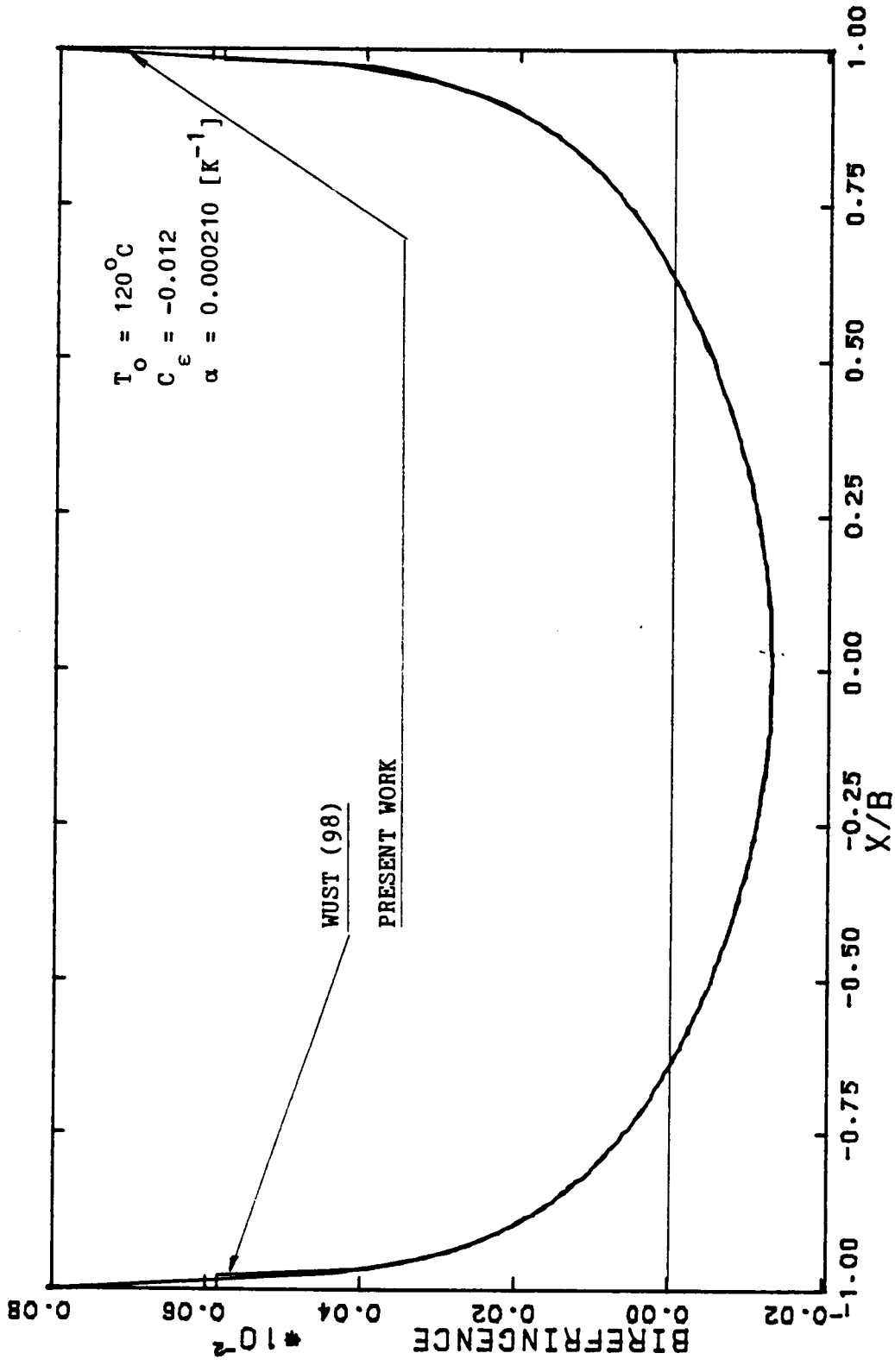

Figure V-6. Comparison of the calculated residual birefringence profile to the one reported by Wust (98) for a 120°C initial temperature quench, using a constant strain optical coefficient.

matches quite closely the experimental observations in slabs quenched from 120°C (98,99).

Despite the marked effect of the initial temperature on the observed residual birefringence profiles (Figure V-3), the theoretical 160°C prediction appears to be, for all practical purposes, identical to the 120°C determination (Figure V-7). This is not at all surprising, since due to the instant freezing assumption the material does not "start to remember" until T_g is reached. Thus, the final profile is only the result of the birefringence generated during cooling from 100°C down to the final temperature. A higher initial temperature, although it affects the overall heat transfer problem, does not appear to have a significant effect on the predicted birefringence profile. This result, however, is not in agreement with the experimental results (Figure V-3) and thus various modifications were introduced.

The next logical step was to use a more realistic auxiliary modulus function R, i.e., one allowing only for partial relaxation at high temperatures (above T_g). Ideally, the theory of Lee, Rogers, and Woo (47) calls for a function $R(\xi)$ which is related to the experimentally determined shear modulus spectrum $G(\xi)$ through equation II.17.

Since a complete set of shear modulus data was not available for this polymer, an exponential function was used instead. As already mentioned, this was thought to be appropriate, judging from the shape of R for inorganic glasses, as presented by Narayanaswamy and Gardon (59). Thus, a plausible form for $R[\xi(x,t)-\xi(x,t')]$, as it appears in the final expression for the stress distribution (equation II.14), may

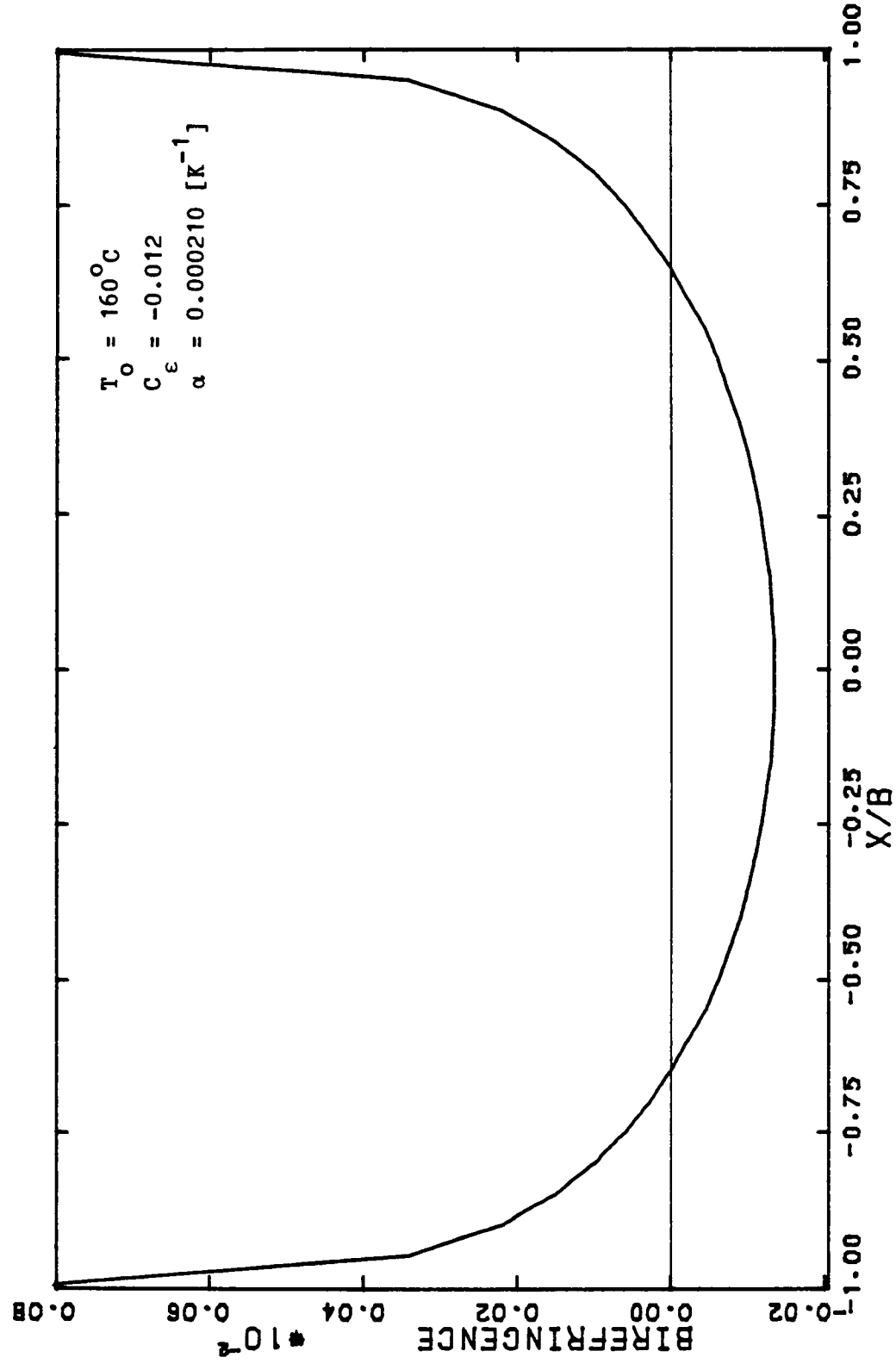

Figure V-7. Birefringence profile calculated from a constant strain optical coefficient for a 160°C initial temperature quench.

be

$$R[\xi(x_1,t) - \xi(x_1,t')] = R_o \exp\left[\frac{-1}{\tau_o}\int_{t'}^{t} e^{K[T(x_1,t'') - T_R]}\, dt''\right] \quad (V.3)$$

where τ_o is a characteristic relaxation time of the material at a reference temperature T_R (usually taken as T_g), K is the slope of the linear fit to the shift function (WLF equation), that determines the adjusted time scale, t is the "present" time, and, finally, t' and t'' are two levels of "past" times. The derivation of equation V.3 from the assumption stated above and the definition of reduced time , has been presented in Appendix A.

For the calculation of K, T_R was taken as T_g (100^oC). The constants for the WLF equation, C_1 and C_2 (12.4 and 41^oC, respectively), were the ones used by Wust (98) in his volume aging experiments; this resulted in a K value of 0.3126. The characteristic relaxation time τ_o was taken as an adjustable parameter.

For the birefringence work, a new memory function was needed. The way this function should behave was estimated using Wust's work (98) on the time dependency (relaxation) of the stress and stress optical coefficient (at constant strain), shown in Figure II-2 of the background chapter.

At temperatures close to T_g the stress (and therefore the modulus) is shown to decay with time, as expected. The stress optical

coefficient , however, builds-up negatively at a rate that depends on the temperature, the higher the temperature the faster it grows. This delayed build-up of the optical coefficient may suggest a memory function of the form

$$C = C_o \left[1 - \exp \left[\frac{-1}{\tau_o} \int_{t'}^{t} e^{K[T(x_1,t'') - T_r]} \, dt'' \right] \right] \quad (V.4)$$

allowing for complete memory at high temperatures and decreasing memory as the temperature is lowered. Such a memory function, however, was found to produce totally erroneous, all positive profiles, with zero birefringence at the surface.

But it is the strain optical coefficient, not the stress optical coefficient, that is used in the birefringence calculations. As shown elsewhere in this thesis, the strain optical coefficient may be obtained by multiplying the strain optical coefficient and the modulus. For stress relaxation experiments at constant strain a decreasing stress is synonymous with a decreasing modulus. Thus, the build-up with time exhibited by the stress optical coefficient does not necessarily apply to the strain optical coefficient because of this decreasing modulus by which the former is multiplyed to give the latter. Also, further inspection of Wust's data shows that in the low temperature range (about 40-60^{o}C), both the stress and the stress optical coefficient decay very similarly with time. Thus, at this

temperature range the strain optical coefficient clearly decreases with time.

Based on the above considerations, an exponential birefringence memory function C was thought to be appropriate. The form of C is identical to the R function used for the stress calculation (equation V.3). For the birefringence work, K was also taken as 0.3126, leaving τ_o as an adjustable parameter.

Figure V-8 shows the effect of τ_o on the predicted birefringence profile (120°C case), as obtained with the new computer program. It is readily appreciated that allowing for partial relaxation at high temperatures does not improve the theoretical predictions. Changing the "fluidity" of the material at T_R (100°C) by adjusting τ_o, produces very different quantitative results, with lower birefringence levels the greater the τ_o; more will be said about this later. Qualitatively, however, it appears as if the theoretical predictions were somehow biased towards a particular result, i.e., a balanced profile. As will now be discussed, this was exactly the case.

It was noted earlier in this section that solving for the stress distribution is done in a two-step process. This involves the calculation of the strains and subsequent multiplication by a modulus or by a strain optical coefficient, resulting in stresses or birefringences, respectively. However, this is not so simple, judging from the effect of the initial temperature on the final birefringence profile, as observed experimentally (Figure V-3). Quenching from high initial temperatures (160°C) produces a highly unbalanced birefringence

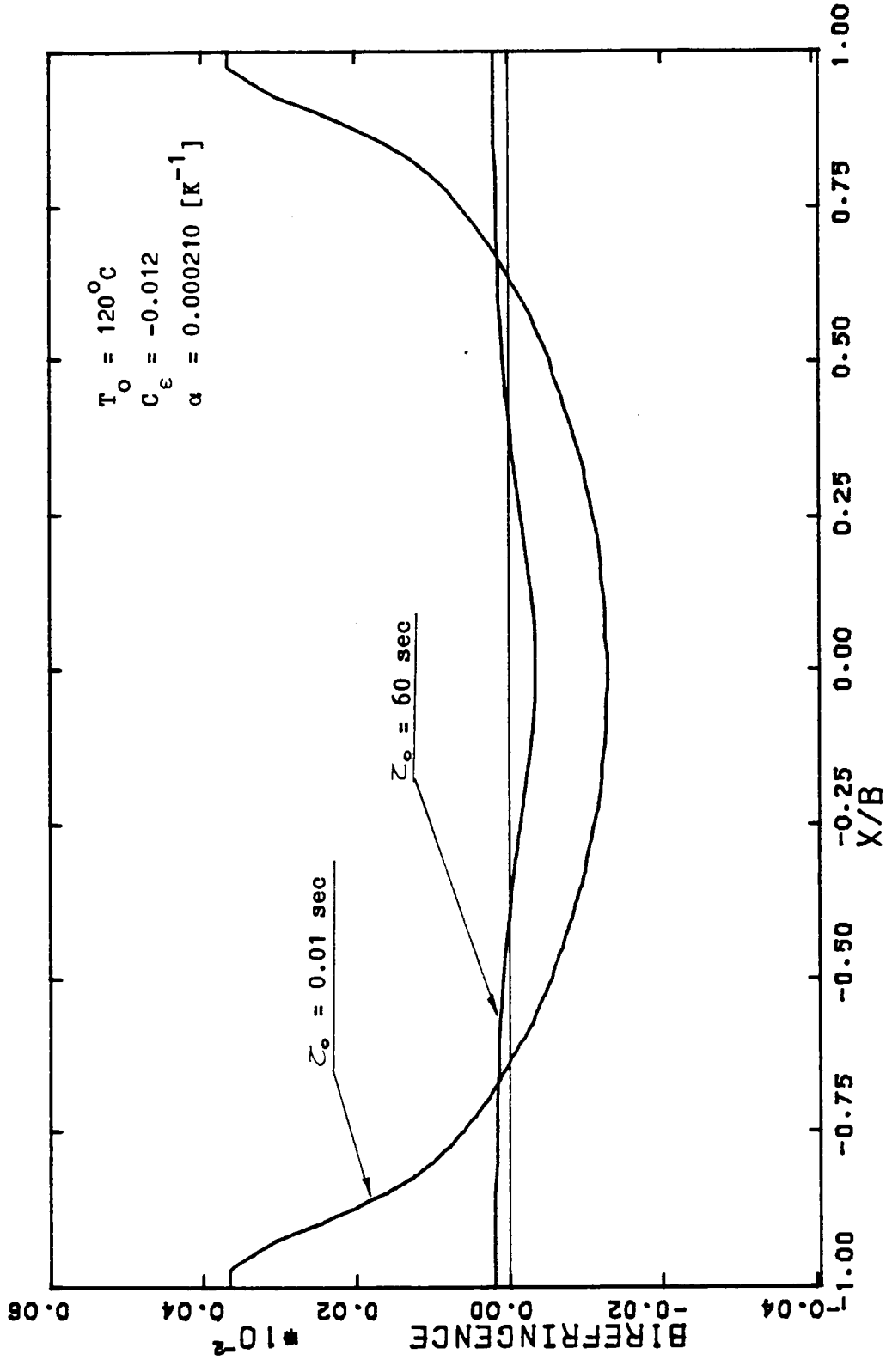

Figure V-8. Effect of the fluidity of the material on the residual birefringence profile calculated from a constant strain optical coefficient and using the balancing condition (120°C initial temperature quench).

profile. This is in contrast to the 120°C case, where the area of negative birefringence is nearly equal to the sum of the areas of positive birefringence.

The residual stress distribution, however, must always be balanced in order to be consistent with the condition of internal stress equilibrium in the quenched part. This condition, given as a complimentary equation (eqn. II.15) in the theory of Lee, Rogers, and Woo (47), is, however, "built-into" the final expression for the stress in the treatment of Aggarwala and Saibel (2). Thus, it is apparent that the prediction of residual birefringences using the latter theory (Aggarwala and Saibel), will generally not be possible. An exception to this assertion is, of course, the fit obtained by Wust and Bogue (99) for slabs quenched from 120°C (balanced profile), already indicated, but their fit is probably fortuitous because, in general, the negative and positive portions of the experimental birefringence distributions do not balance.

Returning for a moment to the result shown in Figure V-8, it is apparent that for the condition of internal stress (or birefringence) balancing decreasing the fluidity of the material (large τ_o) produces low levels of birefringence profiles, whereas increasing the fluidity (small τ_o) has the opposite effect, both cases, however being balanced in the sense described above. The physical interpretation of these results is that with increasing τ_o, the material approaches the condition of complete elastic response, and the thermal stresses (or in this case birefringences) that arise during the first stages of the

quenching are cancelled out to some extent by stresses (or birefringences) of opposite sign that originate during subsequent cooling. It will be shown later that removing the balancing condition from the calculations, the effect of τ_o on the predicted birefringence distributions is both qualitatively and quantitatively very different than that for balanced profiles.

A clear advantage of the treatment of Lee, Rogers, and Woo is thus the fact that the condition for balanced profiles may be disregarded when solving for birefringences. In this case, the strains are first calculated using the condition of internal stress equilibrium, as for the stress case; the evaluation of the birefringences then follows without forcing a balanced profile. A detailed discussion of how this is actually done is presented in Appendix B. The final expression used for calculating the birefringence as a function of both position and time is shown there to be

$$\Delta n(x_1,t_n) = \sum_{i=1}^{n-1} \frac{C_\varepsilon(T_g)}{1-\nu}\,\varepsilon_2(t_{i+1}) - \varepsilon_2(t_i) - \alpha\,[T(x_1,t_{i+1}) - T(x_1,t_i)] \qquad (A.23)$$

where the $\varepsilon_2(\ )$ are the strains at immediate consecutive times (t_i and t_{i+1} and C^*_i is defined by

$$C_i^* = \frac{1}{t_{i+1}-t_i}\int_{t_i}^{t_{i+1}} \bar{C}[\xi(x_1,t_n) - \xi(x_1,t')]\,dt' \qquad (A.22)$$

where C is the dimensionless birefringence memory function (C/C_o).

For the remaining birefringence work, the strains were calculated using the simplifying instant freezing condition for stress calculation as described elsewhere in this thesis. The birefringence generation, however, was controlled by means of the exponential memory function discussed above.

The elimination of the balancing condition from the birefringence calculation induced great changes in the theoretical predictions for samples quenched from 120°C. As shown in Figure V-9, changes in τ_o now have dramatic effects on the final result, both qualitatively and quantitatively. Considering the material as relatively solid at 100°C (τ_o = 60 sec) results in all positive birefringences with a concave profile. Lower relaxation times (τ_o = 10 sec) produce a birefringence distribution of nearly parabolic shape, with both positive and negative regions and some levelling-off at the surface. With further increasing of the fluidity of the material (lowering τ_o), the resultant profile becomes more and more balanced. Finally, at τ_o = 0.01 sec the predicted birefringence distribution practically coincides with the result of Wust and Bogue (99).

A physical interpretation of these results is that the early near-the- center compressive history is "remembered" in the case of high relaxation times, giving a large positive value to the birefringence (recall that the strain optical coefficient is negative).

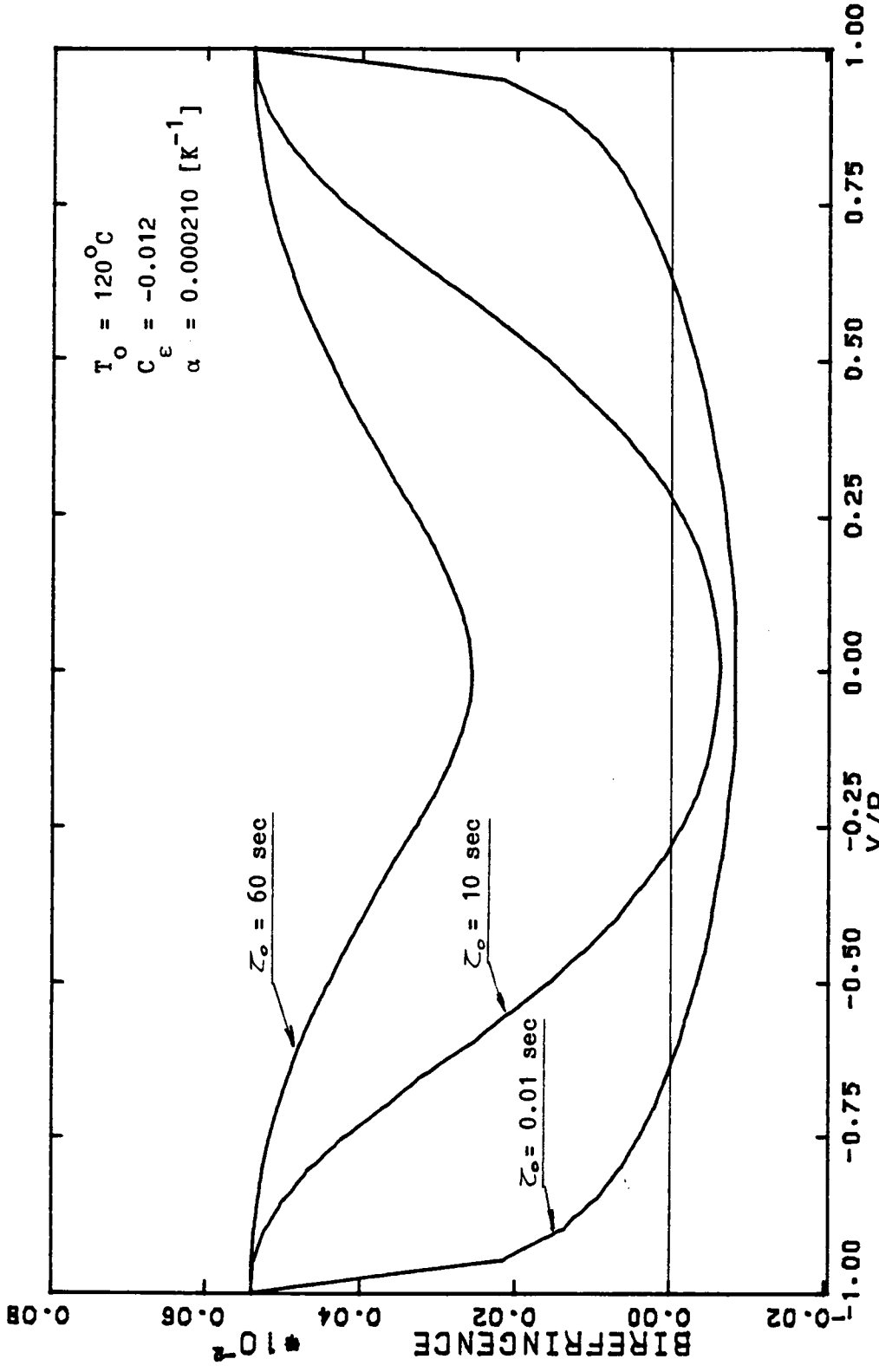

Figure V-9. Effect of the fluidity of the material on the residual birefringence profiles calculated from a constant strain optical coefficient without the balancing condition (120°C initial temperature quench).

Obviously this part of the history must be "forgotten" by using a small τ_o, in order to obtain the correct results.

It now being possible to eliminate the balancing condition from the birefringence calculation, as shown above, a theoretical fit of the 160°C data could be attempted. In contrast to the 120°C case discussed above, changing τ_o was found to have very little effect on the birefringence prediction for this high initial temperature quench (160°C), as shown in Figure V-10. More surprisingly, the changing trend is now in the opposite direction, i.e., increasing τ_o results in a slightly more negatively unbalanced profile. The position of the positive to negative values cross-over point and the overall profile shape, however, differ greatly from the experimental observation.

The physical interpretation of this apparently very different qualitative behavior of the high initial temperature (160°C) case might be explained in terms of the nature of the memory function used in the calculations. In quenches performed from relatively low initial temperatures (close to the reference temperature T_R), relatively small changes in τ_o (0.01 to 60 sec) are sufficient to change drastically the temperature range at which the material "remembers"; thus, dramatic changes are observed in the final birefringence profiles. If the initial temperature is considerably higher than T_R, however, even apparently great τ_o values (10,000 sec) do not suffice for significant birefringence "remembering" in the first stage of quenching (high temperatures). To state it simply, no matter how large a value one might choose for τ_o (within any reasonable range), the

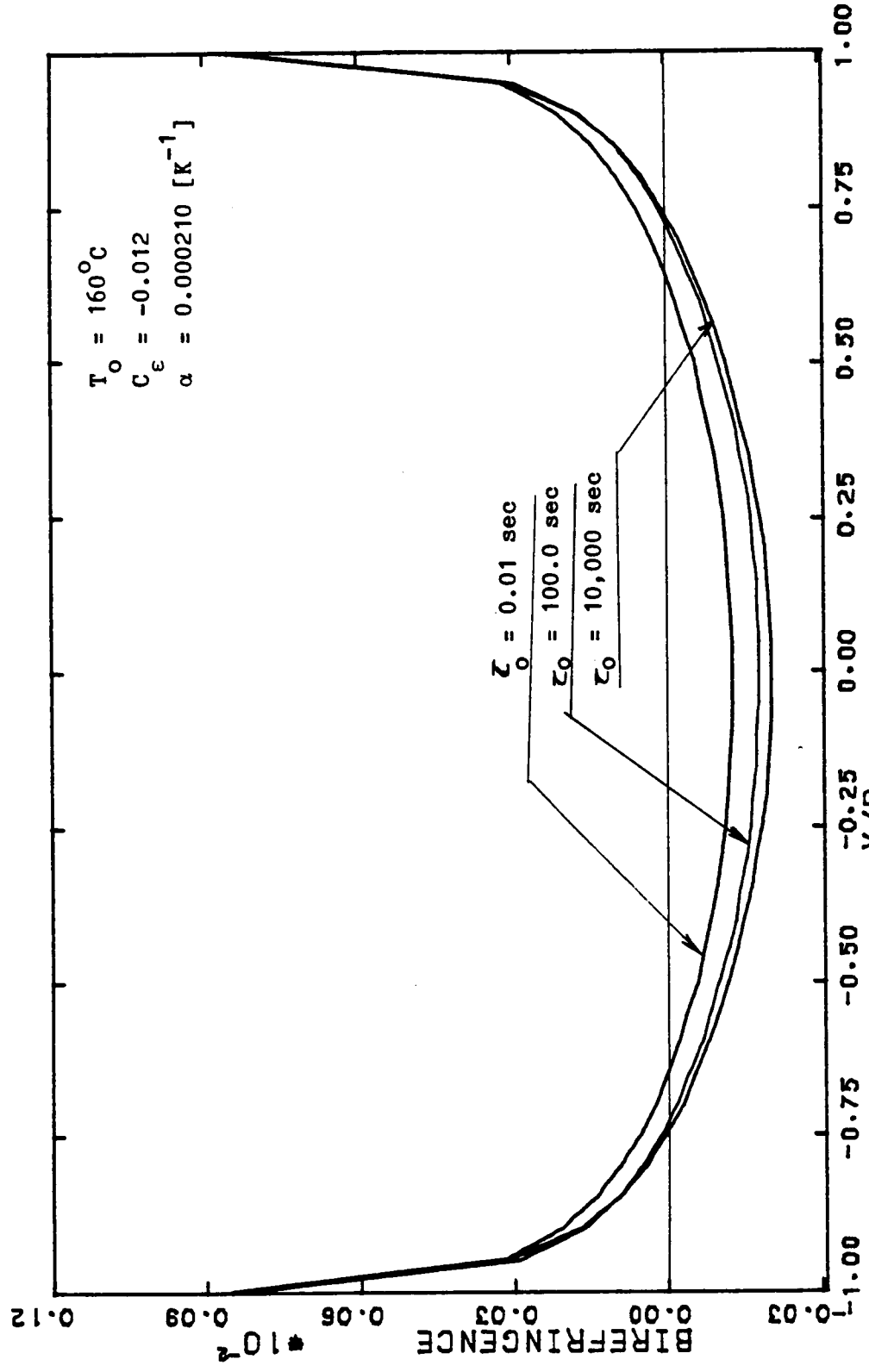

Figure V-10. Effect of the fluidity of the material on the residual birefringence profiles calculated from a constant strain optical coefficient without the balancing condition (160°C initial temperature quench).

material, at say 160°C would still be very fluid-like and almost total relaxation would occur. Thus, in this case, the early near-the-center compressive history is not remembered and the central region of the final birefringence profile reflects more of the subsequent sweeping through of what might be called the "tensile stress wave".

But the extent of relaxation of this near-the-center tensile stress history naturally depends on the value of τ_o. Therefore, the higher the relaxation time the more of the near-the-center tensile history will be remembered, resulting in higher negative birefringences in the central region.

The above analysis was made using a constant strain optical coefficient (C_ε = -0.012) throughout the whole temperature range. A more realistic approach would certainly involve a temperature dependent strain optical coefficient.

As indicated in the background chapter, Wust(98) studied the temperature dependence of the strain optical coefficient , in both tension and compression, over a range of temperature (from room temperature to about 120°C). As Wust did, the tension rather than the compression data were arbitrarily chosen for the present birefringence theoretical work. As shown in Figure II-3, which also includes the 0°C determination of Rudd and Gurnee (68), the strain optical coefficient of polystyrene exhibits a rather distinct temperature dependence. It features two clearly distinguishable regions on both sides of T_g (100°C). In the low temperature region

the strain optical coefficient initially shows a relatively mild monotonically decreasing trend, starting with a 0°C value of about 0.035, and reaching the transition from positive to negative values at about 87°C. Further temperature increase causes the strain optical coefficient to grow in a negative sense very rapidly, almost precipitously droping to very high values (-0.20) in the vicinity of T_g (100°C). On the other side of T_g, however, the above situation is essentially reversed. This high temperature region now exhibits a rapidly diminishing negative strain optical coefficient which eventually levels off at approximately 120°C, with a value of about -0.0037. As already mentioned, the strain optical coefficient data below T_g were fit empirically by Wust(98); the analytical expression is included in Figure II-3. For the present work a fit of the high temperature data was also needed. This was simply performed by drawing straight lines through the data points; for temperatures higher than 120°C the strain optical coefficient was assumed to be constant with a value of -0.0037. The actual expressions used are included in Appendix B.

As reported by Wust and Bogue (99), attempting to predict the residual birefringence distribution, based on this temperature dependent C_ε, results in totally inverted profiles, i.e., the birefringences are negative at the surface and positive in the central regions. The above result is certainly due to the importance of the temperature history corresponding to the cooling from about 87°C down to the final temperature, when C_ε takes on a positive value. However,

giving excessive importance to the final cooling stages is, actually, inherent to the instant freezing assumption, since it calls for total property relaxation above T_g. Thus, the birefringences generated at temperatures above T_g, when C_ε is negative and relatively large, are completely eliminated, resulting in a birefringence distribution, which excessively reflects the effect of the final cooling history.

Motivated by these considerations, a fit was attempted using the theory of Lee et al. (47), with the temperature dependent strain optical coefficient described above. The resulting inverted profile for the 160°C case, shown in Figure V-11, seem to confirm Wust's observation that the birefringence is not simply additive.

A more promising approach, as suggested by Gardon and Narayanaswamy (26,58), and shown by Wust and Bogue (99), appears to be the introduction of structural effects via the fictive temperature concept. This approach is centered around the idea that the properties of the nonequilibrium glass are determined by a fictive (or effective) temperature, rather than by the actual temperature of the material.

Following these ideas a fit was attempted using an effective temperature T_e and an apparent glass transition temperature T_g(app.) of 106.7°C and 109.2°C, respectively, as calculated by Wust (98) for the ice water quenched samples, by means of a rate equation due to Rusch(70). As shown by Wust (98), T_e remains almost constant after the material goes through T_g(app.). Thus, the strain optical coefficient will remain negative at a constant level (determined by T_e) during subsequent cooling from T_e to the final

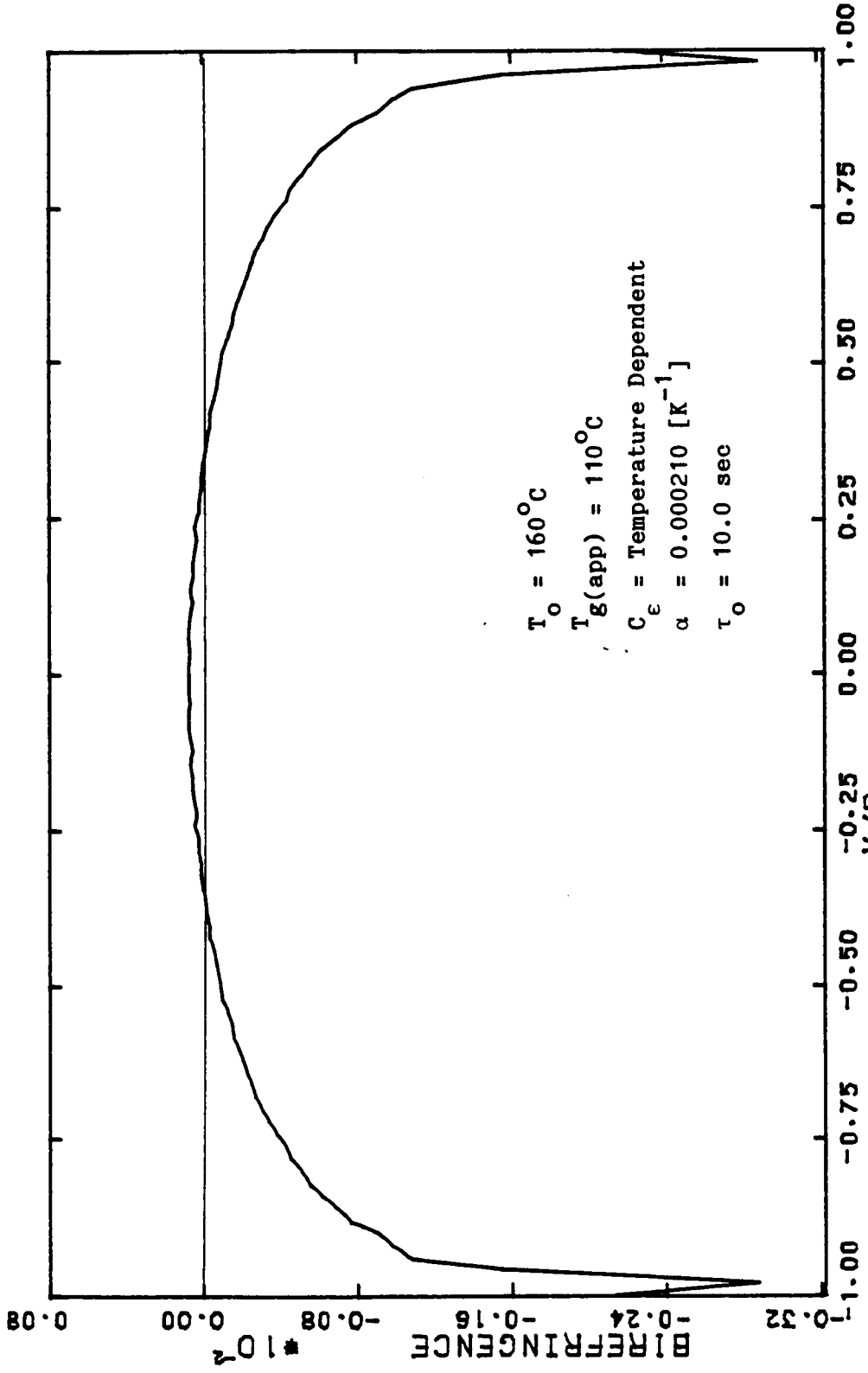

Figure V-11. Birefringence profile calculated from the temperature dependent strain optical coefficient for a slab quenched from 160°C.

temperature. For the calculations, the experimental strain optical coefficient curve of Figure II-3 was horizontally shifted, so as to obtain the point of discontinuity (ocurring in the data at 100°C), at the new T_g(app.). For the following work a τ_o value of 1 sec was used throughout, unless otherwise specified.

The predicted birefringences profile for samples quenched from 160°C is shown in Figure V-12, along with the experimental profile. This theoretical birefringence distribution appears to be both qualitatively and quantitatively in error. While the cross-over point from positive to negative values is experimentally observed to be very near the surface, the theory predicts its position to be about three quarters of the half thickness of the slab, taken from the center outwards. Also, the predicted birefringence levels both in the central regions and at the surface are much higher than the experimental determinations.

As shown in Figure V-13, however, great changes are observed in the predicted birefringence distribution if one arbitrarily varies the value of the effective temperature T_e, keeping T_g constant. Thus, lowering T_e results in lower birefringence levels both at the the surface and in the center, while the cross-over point is shifted towards the surface. The same trends are observed for the low initial temperature quenches (120°C) shown in Figure V-14. Wust (98) recently showed this effect of T_e on the levels of surface and center birefringences; his result, however, does not show any variation of the position of the cross-over point, observed in the present work.

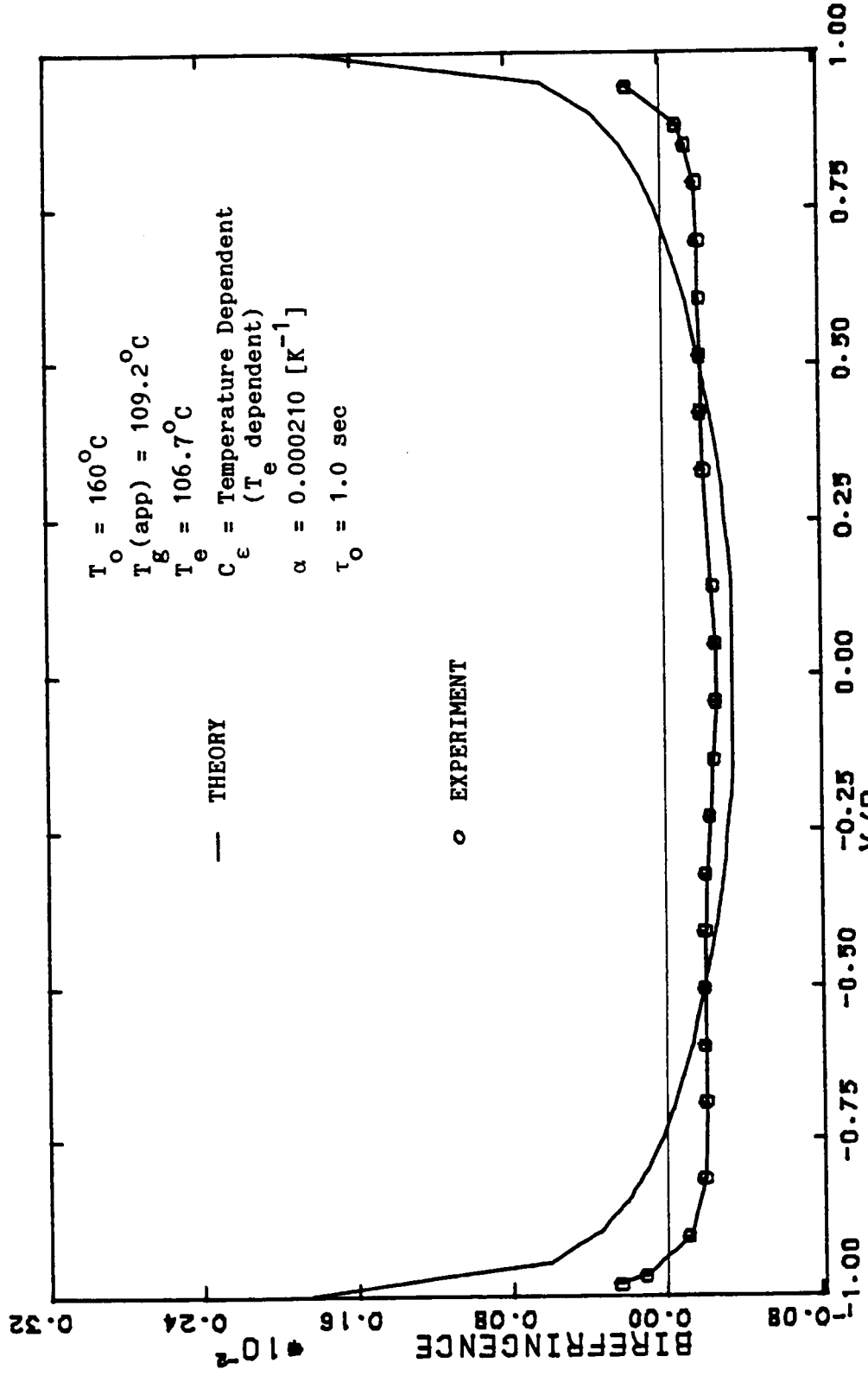

Figure V-12. Birefringence profile calculated using the effective temperature and a temperature dependent strain optical coefficient for a 160°C initial temperature quench.

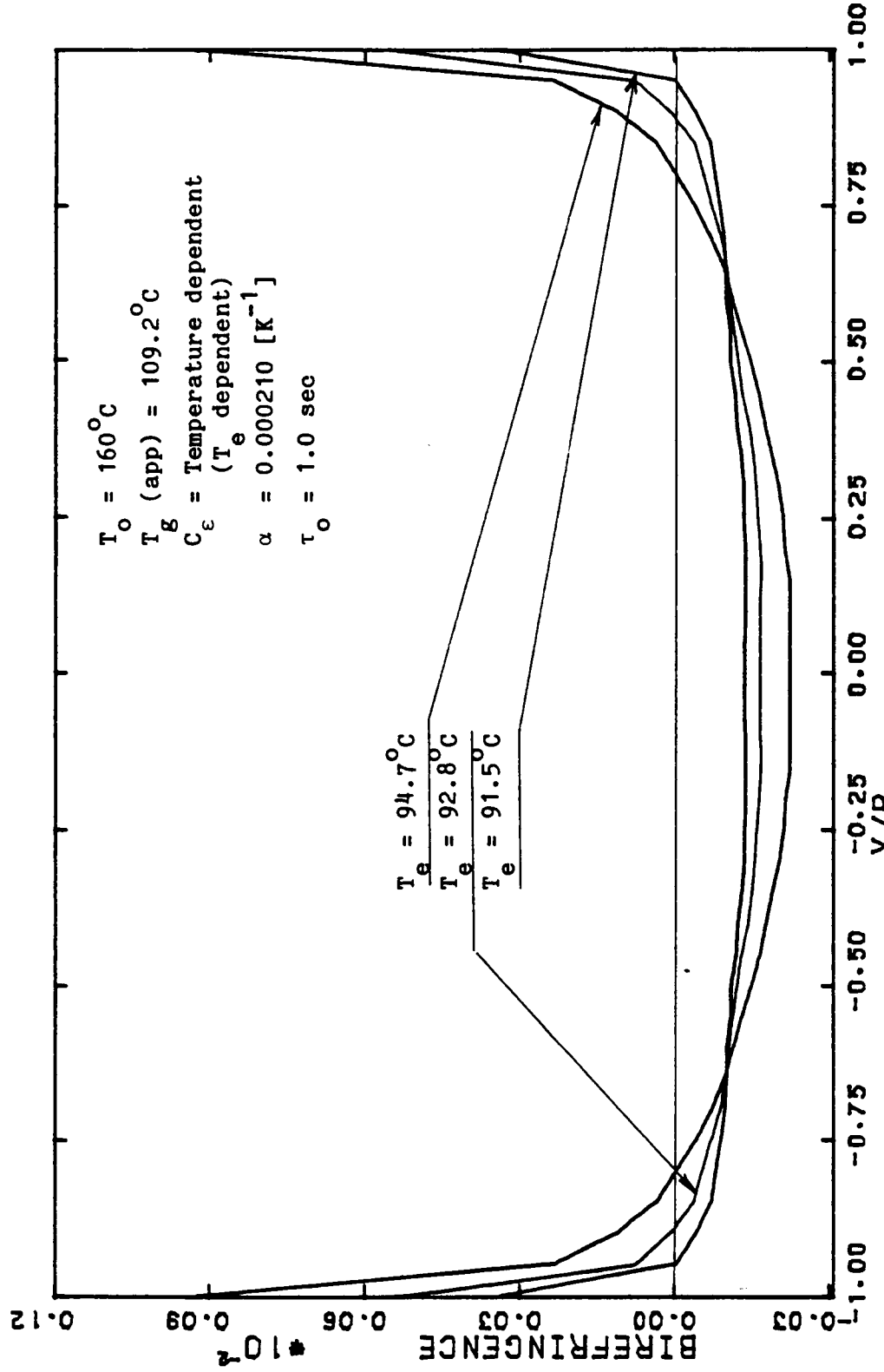

Figure V-13. Dependence of the residual birefringence profile on the effective temperature for a 160°C initial temperature quench and constant glass transition temperature.

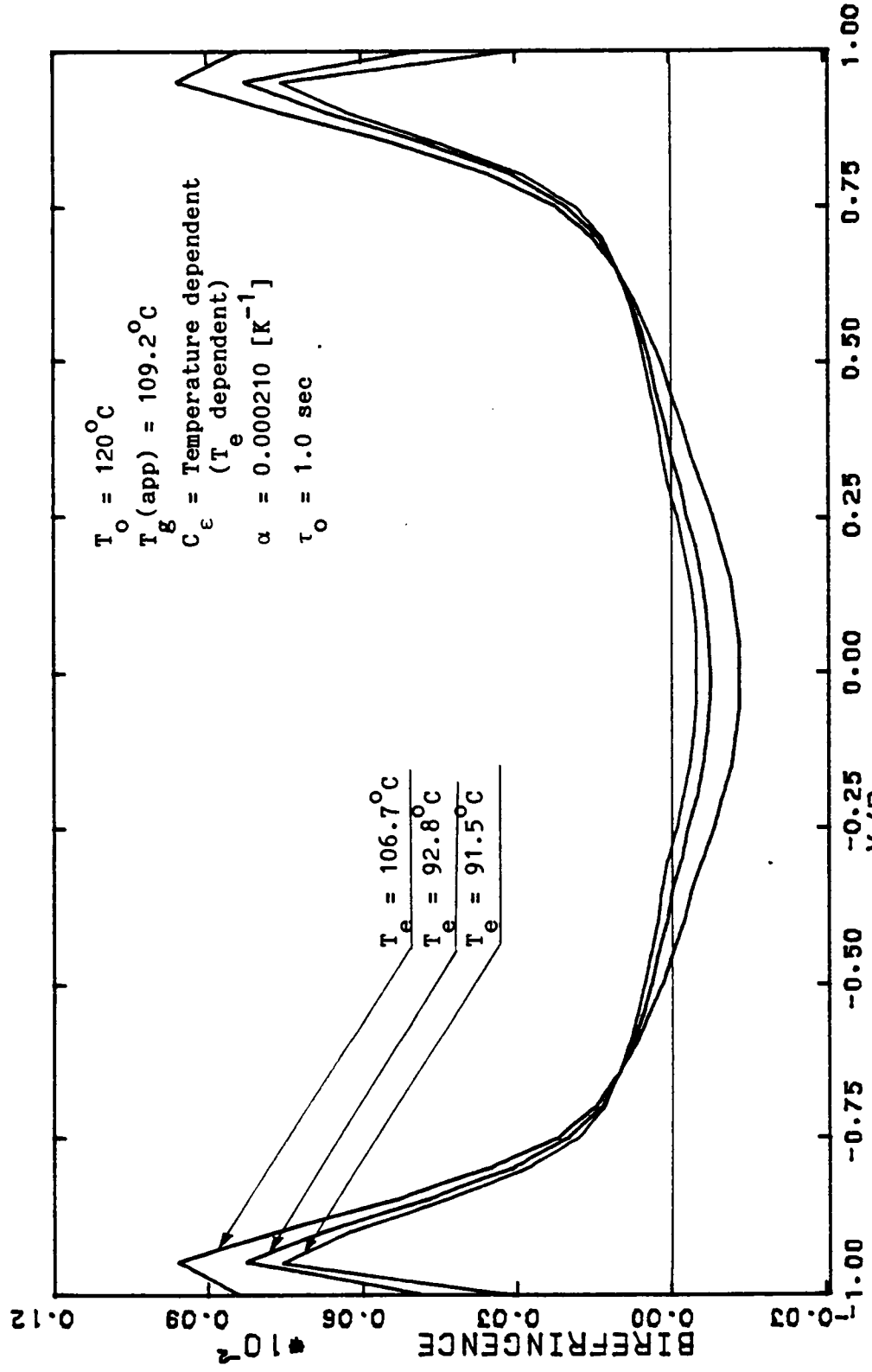

Figure V-14. Dependence of the residual birefringence profile on the effective temperature for a 120°C initial temperature quench and constant glass transition temperature.

The predicted profiles for the 120°C quenches exhibit a sharp discontinuity point near the surface, a difficulty not present in the higher initial temperature quenches (160°C). A discontinuous birefringence profile does not have, of course, any physical meaning. It must certainly be due to the superposition of the various very steep functions involved in the calculations, namely the step memory function for stain (stress) calculation, the exponential memory function for birefringence calculation, and the temperature dependent strain optical coefficient. All these coupled with the extremely rapid cooling experience of the near the surface region probably cause this mathematical difficulty.

The sharp surface discontinuity was found to disappear by increasing the fluidity of the material (τ_o=0.01 sec) or by lowering the glass transition temperature (T_g=100°C). Increasing the fluidity of the material allows for less complete memory, i.e., the material forgets more of its high temperature history.

The effect of T_g(app.) on the final birefringence profile, holding T_e and τ_o constant, is illustrated in Figures V-15 and V-16 for the 120°C and 160°C initial temperature quenches, respectively. It is readily appreciated that raising T_g(app.) produces lower negative birefringences in the central regions and almost no changes at the surface. The physical interpretation of this behavior is based on the extent to which the birefringences that originate in the material at temperatures close to T_g(app.), when C_ε takes on very large values, are remembered. Raising T_g(app.) brings the point of

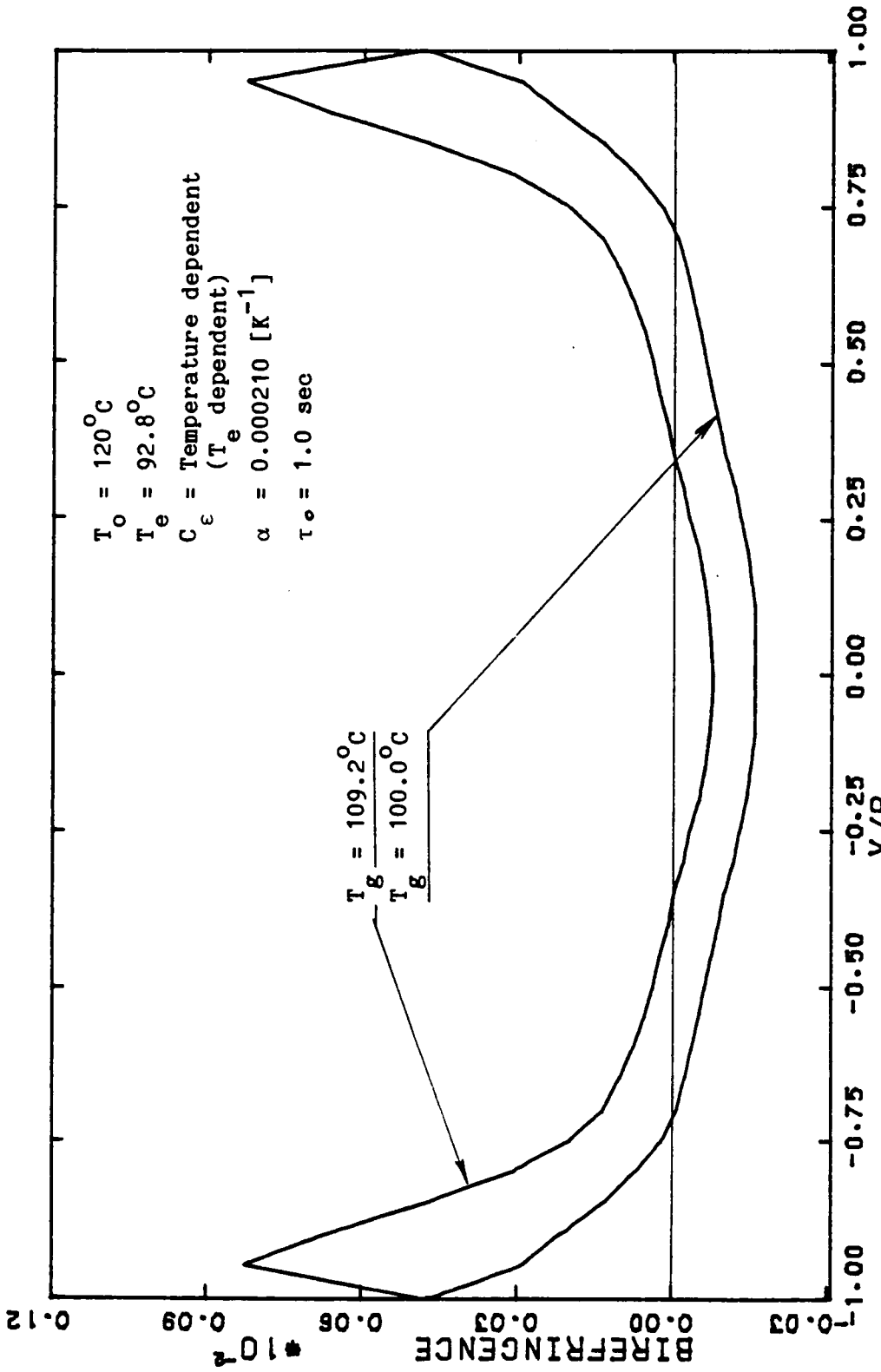

Figure V-15. Dependence of the residual birefringence profile on the glass transition temperature for a slab quench from 120°C and with constant effective temperature.

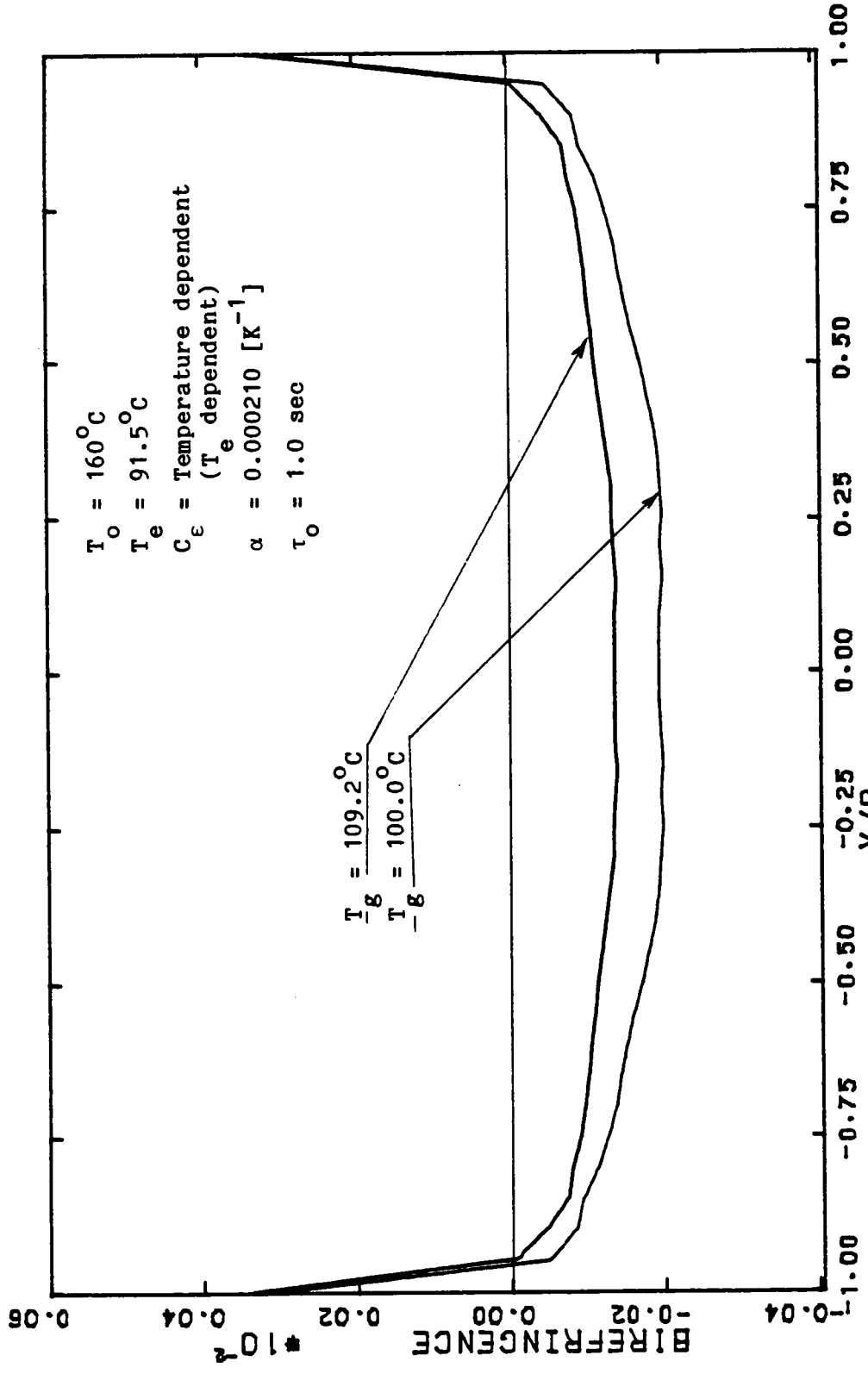

Figure V-16. Dependence of the residual birefringence profile on the glass transition temperature for a slab quenched from 160°C and with constant effective temperature.

discontinuity of the C_ε function (large negative values) to a higher temperature at which property relaxation is more complete. Thus, the higher the T_g(app.) is the less influence will the "dip" in the C_ε function have in the final birefringence profile, resulting in smaller negative center birefringences.

The best theoretical predictions for samples quenched from 120°C and 160°C are shown in Figure V-17, along with the experimental profiles. These "fortuituous" fits were obtained with the combinations of values for the various parameters shown in Figure V-17. It is relevant to point out that both these fits were ob tained with the same values for the material parameters τ_o and T_g(app.) for birefringence and stress relaxation, respectively. The effective temperature value required for these fits, however, is slightly larger in the lower initial temperature quench case (T_e=92.8°C) than in the samples quenched from 160°C (T_e=91.5°C).

The predicted profile for the 120°C case is now seen to be in very good qualitative agreement with the experimental observations. Even though the gradual levelling-off birefringence observed in the data is not present here, the position of the cross-over point and the concave bump reproduce quite closely those of the experimental observation. In a quantitative sense the levels of surface and center birefringence are also rather satisfactorily predicted.

The theoretical prediction for the high temperature quench (160°C) is also in rough qualitative agreement with the experimental observations. With the cross-over point from positive to negative

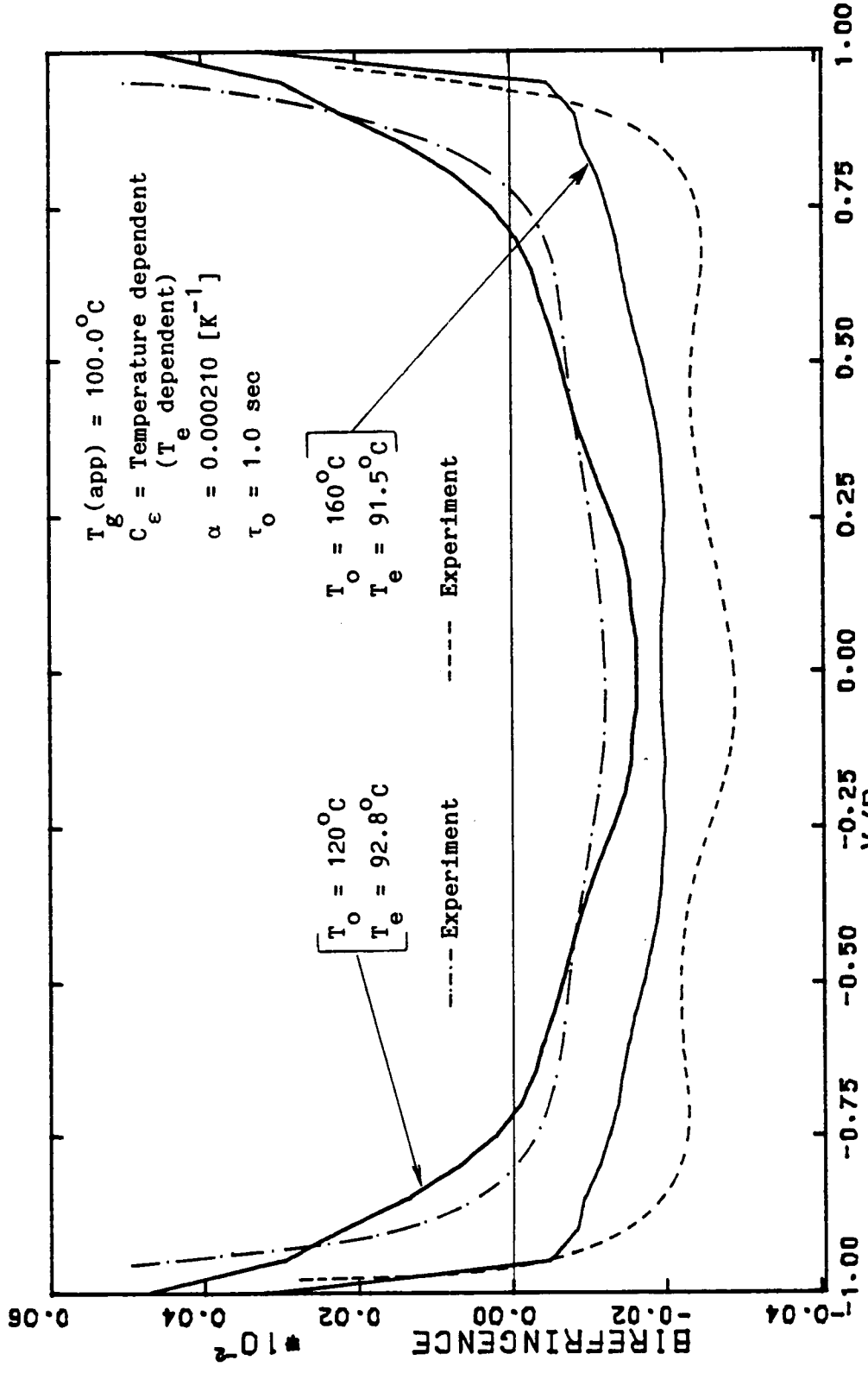

Figure V-17. Best theoretical fits of the experimental residual birefringence profiles calculated using the effective temperature concept for 120°C and 160°C initial temperature quenches.

birefringences very close to the surface, the resultant profile is now highly negatively unbalanced. The theory fails to reflect, however, the details of the experimental profile observed in the central regions, i.e., the slight birefringence increase and the central concave bump. Quantitatively the surface birefringence values are quite accurately predicted, whereas the negative central birefringences are significantly lower than the experimental.

Up to this point the theoretical efforts to fit the observed birefringence profiles involved a constant value for the coefficient of thermal expansion, i.e., $\alpha=0.000210\ K^{-1}$, used throughout the temperature range of the experiment. Certainly a more realistic approach would involve at least two values, a large α (rubbery) for temperatures above T_g(app.), and a smaller α (glassy) for the lower than T_g(app.) temperatures. But the transition from the rubbery to the glassy α generally is not a sharp one, instantly occurring at T_g(app.); it rather takes place over a certain temperature range in the vicinity of T_g(app.). As shown in Appendix B, a Subroutine was developed allowing one to chose the temperature range in which the transition from rubbery to glassy α takes place. The α values were averages of literature determinations taken from a table of physical constants of polystyrene recently presented by Wust(98). The steepness of the transition could be varied on the computer by means of the variables DELTHI and DELTLO; these are the temperature increments on both sides of T_g(app.) that define the temperature transition range from the rubbery to the glassy α values (see Appendix B).

Figure V-18 shows the influence of varying the temperature range for the transition from rubbery to glassy α. It may be seen that making this transition steeper results in significant shifting down of the final birefringence profile. Also, when α drops sharply from the rubbery value to the glassy level at T_g(app.), a considerably less smooth profile is obtained. This "bumpy" profile is once more probably due to the many very steep functions involved in the calculations. To obtain smooth profiles in such a case it would be necessary to further increase the number of time and space integration steps.

Figure V-19 shows the best fit that was obtained for the 120°C initial temperature quench birefringence data. The larger α values involved required a higher value of T_g(app.) (recall that raising T_g(app.) has the effect of shifting up the resultant birefringence profile). A larger value of τ_o (τ_o=300 sec) was also required to obtain this fit. Although the levels of surface and center birefringence are closely predicted, the resulting profile is clearly more negatively unbalanced than the experimental.

Shown in Figure V-20 is the theoretical prediction for the residual birefringence profile of samples quenched from 160°C, using a temperature dependent α. This result is again in rough qualitative agreement with the data, but the level of negative birefringences is in this case highly overpredicted.

Thus, in summary one can say that the thermoviscoelastic treatment of Lee, Rogers, and Woo (47), developed for the calculation of residual stresses in quenched inorganic glass plates, can be

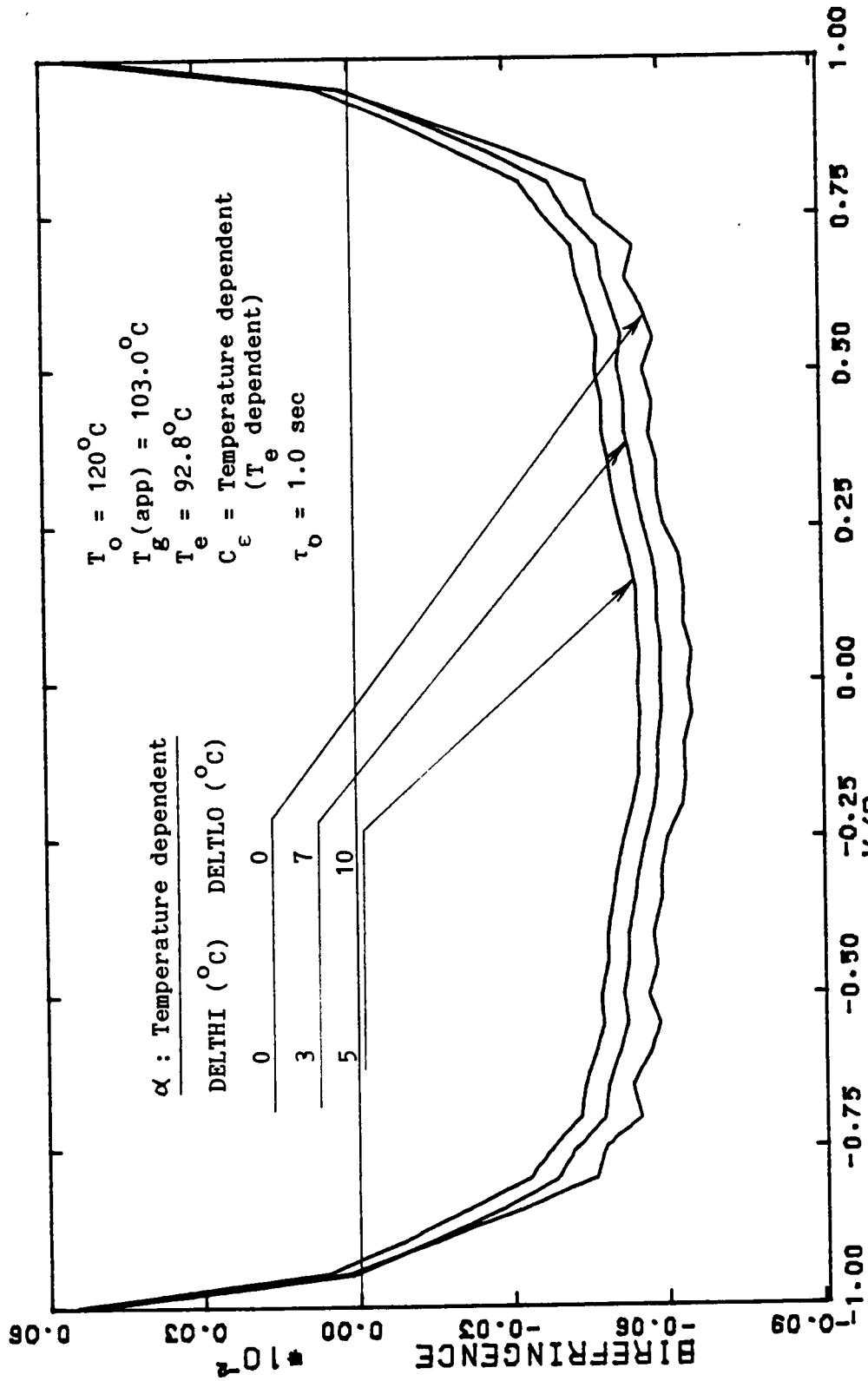

Figure V-18. Dependence of the temperature range for the transition from a rubbery to a glassy coefficient of thermal expansion on the residual birefringence profile for a 120°C initial temperature quench.

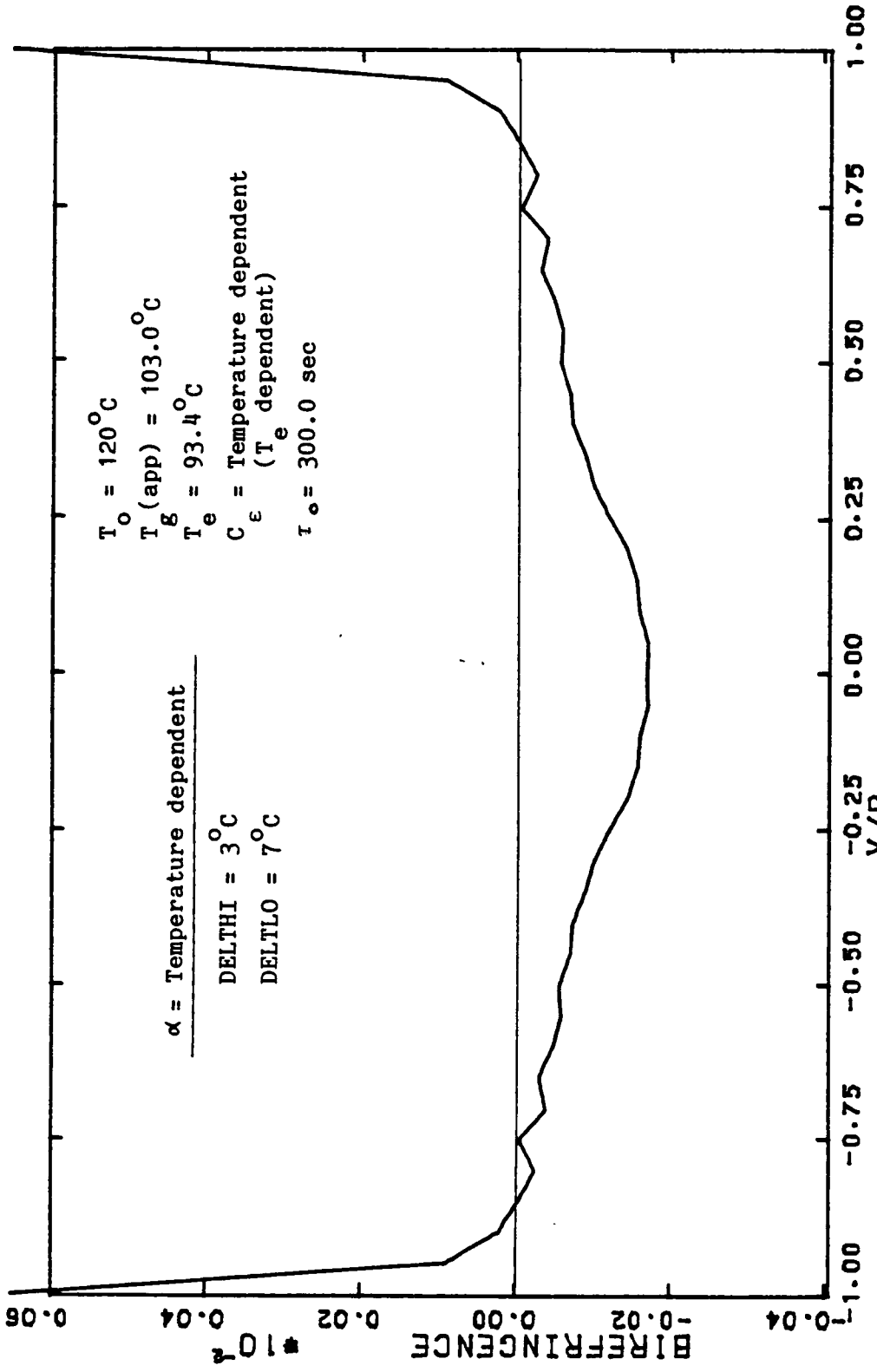

Figure V-19. Theoretical fit of the residual birefringence profile for a 120°C initial temperature quench using a temperature dependent coefficient of thermal expansion.

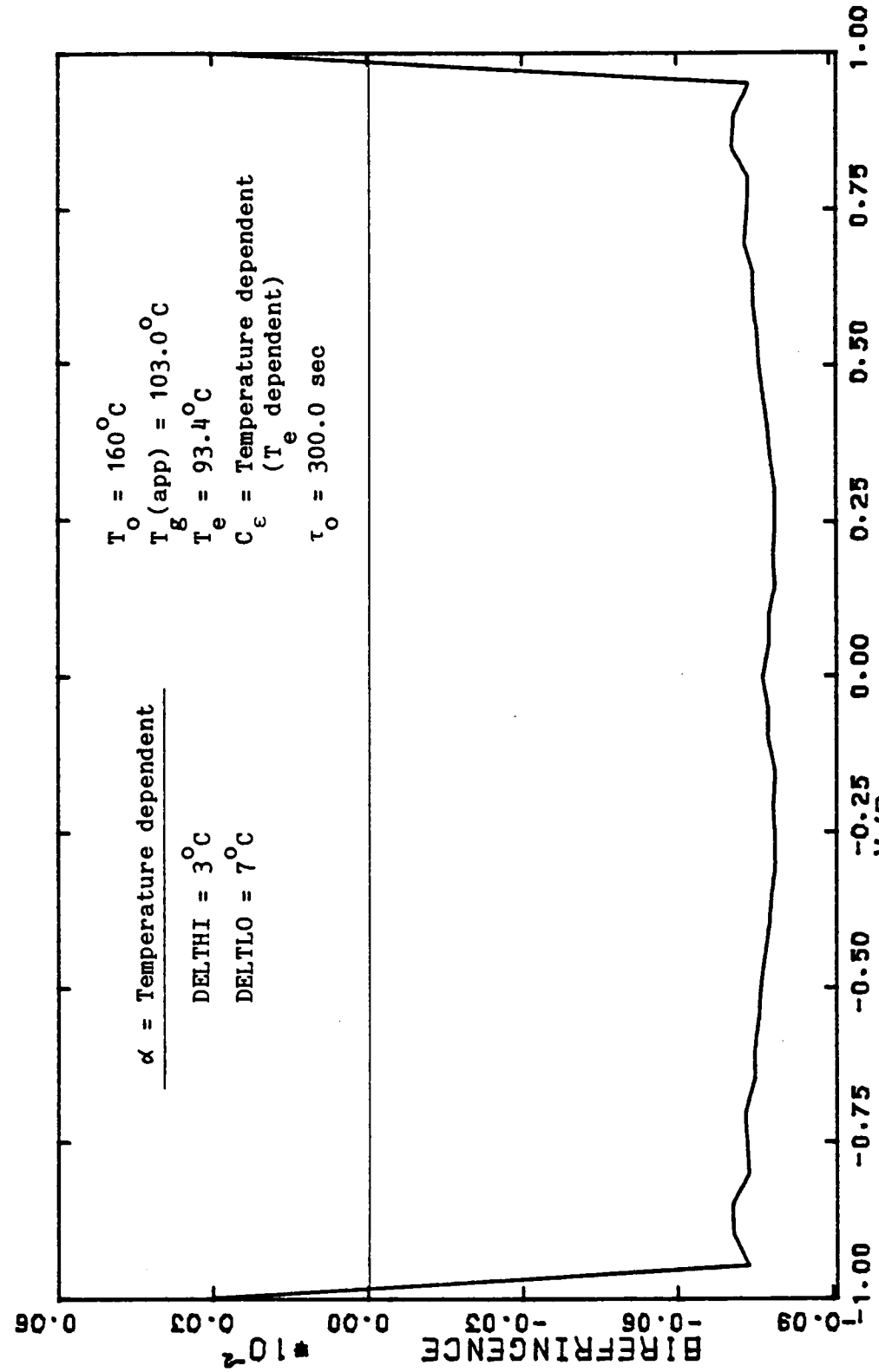

Figure V-20. Birefringence profile calculated using a temperature dependent coefficient of thermal expansion for a 160°C initial temperature quench.

conveniently modified for the calculation of residual birefringences in the quenched part, by eliminating the balancing condition for birefringence, while maintaining the balancing condition for stress. By a somewhat arbitrary selection of parameters, fair fits to the experimental profiles can be obtained; but in view of the large number of parameters and the relative absence of independent data, one cannot say that the fits are unique ones.

CHAPTER VI

CONCLUSIONS

The present work constitutes a basic study of the effect of thermal history on the glassy state properties of amorphous polymers. In this research separate consideration has been given to small, homogeneous samples and large, non-homogeneous samples. The extent to which the degree of non-equilibrium (free volume) affects the mechanical (tensile) properties was investigated for fiber-like homogeneous specimens. The work on non-homogeneous samples involved the measurement and theoretical prediction of the gradient of birefringence frozen into large quenched slab-like specimens. For the birefringence theoretical work the well- known theory of Lee, Rogers, and Woo (47) was conveniently modified. Finally, the effect of these non-homogeneities on the tensile behavior of dumbbell samples was also investigated.

A. MECHANICAL PROPERTIES OF SMALL HOMOGENEOUS FIBER-LIKE SAMPLES AND NON-HOMOGENEOUS DUMBBELL SPECIMENS

Small Homogeneous Fiber-like Samples

The effect of thermal history on the tensile behavior of polystyrene samples at various temperatures was investigated. The major emphasis was placed on small fiber-like samples, i.e., those which do not have a gradient of properties through the cross-section. Specifically, the degree of non-equilibrium frozen into the body (free

volume) was shown to affect the ductility of the material. Prior literature (52) shows that slowly cooled (annealed) polystyrene samples (an inherently brittle polymer at room temperature) suddenly fail in a ductile fashion when tested at temperatures close to T_g (90°C) at atmospheric pressure. The literature also acknowledges a diversity of factors that influence the brittle-to-ductile transition temperature, ranging from the polymer itself (molecular weight, crystallinity, side groups, etc...), to the testing conditions (pressure, strain rate, etc...)(90,91).

In the present work it was shown that increasing the amount of frozen-in free volume in the tensile specimens, by rapidly quenching into an ice water bath, produces dramatic ductilities at temperatures as low as 70°C. In contrast, slowly cooled samples in a temperature controlled environment did not exhibit any significant ductility increase, when tested under identical conditions.

The phenomenological observations made when testing these variously cooled specimens seem to corroborate the idea suggested by Matsushige et al. (52), that two essentially different failure mechanisms are taking place, i.e., crazing and shear banding. The slowly cooled specimens showed welldeveloped crazes at the breaking point, regardless of the testing temperature. Quenched samples, however, did not craze at the higher temperatures, but rather a neck would start and more or less completely propagate prior to fracture.

Despite the high degree of scatter that plagued the ductility determinations, the fact that a few quenched samples exhibited

elongations-to-break above 100%, when tested at 70°C, is in itself of considerable interest. Various factors were found to impair the mechanical performance of these specimens, as described elsewhere in this thesis. Some of these factors have to do with uncontrollable random imperfections such as slight diameter variations in the original sample and dirt particles. Other factors such as the quality of the quench and the actual testing conditions, i.e., controlled environment, clamping device, etc..., however, might be improved so as to be able to obtain more reproducible results. Particularly, the quenching arrangement used throughout this research (which involved a metal sample holder) was found to produce denser samples than the ones recently used by Snow (77) in his aging experiments, obtained by directly plunging the bare sample into the quenching bath.

It thus seems plausible that somehow improving both the quality of the quench and the clamping device used for pulling the samples would produce better reproducibility and perhaps even result in a lower brittle-to-ductile transition temperature.

Non-homogeneous Dumbbell Samples

Relatively large (1/8") thick dumbbell samples were given similar thermal treatments as was previously applied to the fiber-like samples. As expected, this samples were found to be large enough so as to develop significant gradients of properties through the cross-section when rapidly cooled from above T_g. Particularly, as evidenced by birefringence determinations, important levels of residual stresses were present in the quenched specimens.

In contrast to the case of small fiber-like samples mentioned above, rapidly quenching a large sample does not induce ductile behavior at temperatures as low as 70°C. In fact very little changes in behavior were found among the variously cooled specimens at the two temperatures investigated. A plausible explanation for this strikingly different behavior was thought to be related to the non-homogeneous cooling of the specimens, as it creates gradients of properties through their cross-section.

B. RESIDUAL STRESSES AND RESIDUAL BIREFRINGENCES IN NON-HOMOGENEOUS SAMPLES

Following prior work at the University of Tennessee (98,99), the determination of the residual stress state frozen into a quenched sample, as measured by the experimental birefringence distribution, was investigated further.

Birefringence profiles were measured on slab-like samples quenched from 120°C and 160°C. Quenching from the higher temperature (160°C) required a means of supporting the soft material during temperature equilibration and subsequent cooling. This was achieved by framing the samples in various ways. Both the high and the low initial temperature quenches produced birefringences that were positive at the surface and negative in the center. The 120°C profile was compared to the one reported by Wust and Bogue (99) and it was found to be identical within experimental error. Analogously, the high initial temperature quench profile (160°C) was seen to be in

rough qualitative agreement with the ones reported by Isayev et al. (93) for quenches performed from similar initial temperatures.

The main feature that distinguishes a low temperature quench from a high temperature quench is the degree of balancing of the positive and negative birefringences in the final profile. Quenching from relatively low temperatures (120^{o}C) produces approximately balanced profiles, whereas high initial temperatures (160^{o}C) result in highly negative, unbalanced profiles. This non-balance cannot be accomodated by the simplified theory of Aggarwala and Saibel (2), as was used by Wust and Bogue (99), which neglects all time dependent effects.

Because of this limitation the more general theory of Lee, Rogers and Woo (47) was used in the present work. This more general framework, which does include time dependent effects, permits one to introduce a relationship between stress and strain that is different from that between birefringence and strain. Thus one can have a balance of the stresses, which is a necessary physical constraint, without necessarily having a balance of the birefringences. To actually use the general theory, however, one must deal with a number of unknown functions and parameters, notably the relaxation functions for both the mechanical and optical behavior (each with a leading coefficient and a relaxation time) and a function for the thermal coefficient of expansions, all of these qualities being dependent on temperature. In order to move forward with the analysis, certain arbitrary decisions were necessary.

The analysis of the stress was simplified by using a discontinuous memory function as did Wust and Bogue (99); that is, one assumes a perfect fluid above T_g and a perfect solid below it. The analysis of the birefrigence was not treated so simply and a relaxation function for it, involving a strongly temperature-dependent leading coefficient (strain optical coefficient) and a time constant based on the WLF equation was introduced. In this form the theory was qualitatively correct (i.e., it showed the desired non-balance of the birefringence profiles) and could be made nearly quantitative as well by a particular, though quite arbitrary, choice of parameters. The quantitative results depend strongly on the numerical values and the forms of the functions for the strain optical coefficient and the thermal coefficient of expansion. One finally concludes that the "memory" of the mechanical and optical response near and above (but not too far above) the glass transition temperature largely determines the final birefringence profile, but that a complete quantification of all of the relevant parameters would require extensive independent measurements.

REFERENCES

REFERENCES

1. Adams, L. H., and E. D. Williamson, J. Franklin Inst., 190, 835 (1920).

2. Aggarwala, B. D., and E. Saibel, Phys. Chem. Glasses, 2, 137 (1961).

3. Ainbinder, S. B., M. G. Laka, and I. Y. Maiors, Mekhanika and Polimerov, 1, 65 (1965).

4. Amborski, L. E., and T. D. Mecca, J. Appl. Poly. Sci., 4, 332 (1960).

5. Argon, A. S., R. D. Andrews, J. D. Godrick, and W. Whitney, J. Appl. Phys., 39, 1899 (1968).

6. Bartenev, G. M., J. Tech. Phys., 18, 383 (1948).

7. Bartenev, G. M., J. Tech. Phys., 19, 1423 (1949).

8. Bevis, M., and D. Hull, J. Mater. Sci., 5, 357 (1970).

9. Biglione, G., E. Baer, and S. V. Radcliffe, Paper presented at Brighton Conference on Fracture, 1969.

10. Bowden, P. W., and S. Raha, Phil. Mag., 22, 463 (1970).

11. Brady, T. E., and G. S. Yeh, J. Appl. Phys., 42, 4622 (1971).

12. Broutman, L. J., and S. M. Krishnakumar, Poly. Engr. Sci., 14, 4 (1974).

13. Broutman, L. J., and S. M. Krishnakumar, Poly. Engr. Sci., 14, 249 (1974).

14. Broutman, L. J., and S. M. Krishnakumar, Poly. Engr. Sci., 16, 2 (1976).

15. Broutman, L. J., and S. M. Krishnakumar, Poly. Engr. Sci., 16, 74 (1976).

16. Carey, D. A., C. J. Wust, Jr., and D. C. Bogue, J. Appl. Poly. Sci., 25, 575 (1980).

17. Cheatham, R. G., and A. G. H. Dietz, Modern Plastics, 29, 113 (Sept., 1951).

18. Cheatham, R. G., and A. G. H. Dietz, Trans. Am. Soc. Mech. Engr., 74, 31 (1952).

19. Crouthamel, D. L., A. I. Isayev, and K. K. Wang, SPE ANTEC Technical Papers, 28, 295 (1982).

20. Desper, C. R., and R. S. Stein, J. Appl. Phys., 37, 3990 (1966).

21. Dietz, A. G. H., and F. J. Mc Garry, "Symposium on Speed of Testing," Spec. Tech. Publ. No. 185, p. 30, Philadelphia, Pa. Am. Soc. Testing Materials, 1956.

22. Dietz, W., J. L. White, and E. S. Clark, Poly. Engr. Sci., 18, 273 (1978).

23. Ely, R. E., Plastics Tech., 3, 900 (1957).

24. Fellers, J. F., and B. F. Kee, J. Appl. Poly. Sci., 18, 2355 (1974).

25. Gardon, R., in "Glass: Science and Technology," vol. 5, D. R. Uhlmann and N. J. Kreidl, Eds., Academic, New York, 1980.

26. Gardon, R., and O. S. Narayanaswamy, J. Am. Cer. Soc., 53, 380 (1970).

27. Golden, J. H., B. L. Hammat, and E. A. Hazell, J. Appl. Poly. Sci., 11, 1571 (1967).

28. Gurnee, E. F., L. T. Patterson, and R. D. Andrews, J. Appl. Phys., 26, 1106 (1955).

29. Han, C. D., and L. H. Drexler, J. Appl. Poly. Sci., 17, 2329 (1973).

30. Haward, R. N., editor, "The Physics of Glassy Polymers," Wiley, NY 1973.

31. Haward, R.N., B. M. Murphy, and E. F. T. White, Symposium on Fracture, Paper 45, Session IV, Brighton, England, 1970.

32. Huck, N. D., and P. L. Clegg, Soc. Plastics Engr. Trans., 1, 121 (1961).

33. Indenbom, V. L., J. Tech. Phys., 24, 925 (1954).

34. Indenbom, V. L., Fizika Tverdogo Tela, Sbornik Statey, 1, 236 (1959).

35. Isayev, A. I., SPE ANTEC Technical Papers, 28, 288 (1982).

36. Isayev, A. I., C. A. Hieber, and D. L. Crouthamel, SPE ANTEC Technical Papers, 27, 110 (1981).

37. Ito, E., T. Horie, and Y. Kobayashi, J. Appl. Poly. Sci., 22, 3193 (1978).

38. Jackson, G. B., and R. L. Ballman, Soc. Plastics Engr. J., 16, No. 10, 1147 (1960).

39. Jones, T. T., Pure Appl. Chem., 45, 39 (1976).

40. Kahar, N., R. A. Duckett, and I. M. Ward, Polymer, 19, 136 (1978).

41. Kamal, M. R., and V. Tan, Poly. Engr. Sci, 19, 558 (1979).

42. Kambour, R. P., J. Poly. Sci. Macromol. Rev., 7, 1 (1973).

43. Knowles, J. K., and A. G. H. Dietz, Trans. Am. Soc. Mech. Engr., 77, 177 (1955).

44. Kolsky, H., Nature, 166, 235 (1950).

45. Kovacs, A. J., Rheol. Acta, 5, 262 (1966).

46. Lee, E. H., and T. G. Rogers, J. Appl. Mech., 30, 127 (1963).

47. Lee, E. H., T. G. Rogers, and T. C. Woo, J. Am. Cer. Soc., 48, 480 (1965).

48. Litt, M. H., and A. V. Tobolsky, J. Macromol. Sci. Phys., B 1 (3), 433 (1967).

49. Litt, M. H., and P. J. Koch, Polymer Letters, 5, 251 (1967)

50. Litt, M. H., P.J. Koch, and A. V. Tobolsky, J. Macromol. Sci. Phys., B 1 (3), 587 (1967).

51. Martin, J. R., J. F. Johnson, and A. R. Cooper, J. Macromol. Sci. C, 8, 57 (1972).

52. Matsushige, K., S. V. Radcliffe, and E. Baer, J. Appl. Poly. Sci., 20, 1853 (1976).

53. Matsushige, K., S. V. Radcliffe, and E. Baer, Report from Department of Macromolecular Science, Case Western Reserve University, TR No. 270, Feb. 1975, to be published.

54. Matsumoto, T., and D. C. Bogue, J. Poly. Sci.-Phys., 15, 1663 (1977).

55. Matsumoto, K., J. F. Fellers, and J. L. White, J. Appl. Poly. Sci., 26, 85 (1981).

56. Merz, E. H., L. E. Nielsen, and R. Buchdahl, Ind. Engr. Chem., 43, 1396 (1951).

57. Muki, R., and E. Sternberg, J. Appl. Mech., 28, 193 (1961).

58. Narayanaswamy, O. S., J. Am. Cer. Soc., 61, 146 (1978).

59. Narayanaswamy, O. S., and R. Gardon, J. Am. Cer. Soc., 52, 554 (1969).

60. Nielsen, L. E., "Mechanical Properties of Polymers," Reinhold, New York, 1962.

61. Nielsen, L. E., and R. Buchdahl, J. Chem. Phys., 17, 839 (1949).

62. Nielsen, L. E., and R. Buchdahl, J. Colloid Sci., 5, 282 (1950).

63. Nielsen, L. E., and R. Buchdahl, J. Appl. Phys., 21, 488 (1950).

64. Oda, K., J. L. White, and E. S. Clark, Poly. Engr. Sci., 18, 53 (1978).

65. Patel, P. D., and D. C. Bogue, Poly. Engr. Sci., 21, 449 (1981).

66. Polakowski, N. H., and E. J. Ripling, "Strength and Structure of Engineering Materials," Prentice-Hall, New Jersey, 1966.

67. Potnis, P., M.S. Thesis, The University of Tennessee, Knoxville, 1982.

68. Rudd, J. F., and E. F. Gurnee, J. Appl. Phys., 28, 1096 (1957).

69. Rudd, J. F., and E. F. Gurnee, J. Poly. Sci.-Chem., 1, 2857 (1963).

70. Rusch, K. C., J. Macromol. Sci., B2, 179 (1968).

71. Rusch, K. C., and R. H. Beck, Jr, J. Macromol. Sci.-Phys., B3, 365 (1969).

72. Saffell, J. R., and A. H. Windle, J. Appl. Poly. Sci., 25, 1117 (1980).

73. Shen, Y. C., M.S. Thesis, The University of Tennessee, Knoxville, 1981.

74. Siegmann, A., A. Buchman, and S. Kenig, Poly. Engr. Sci., 22, 40 (1982).

75. Siegman, A., M. Narkis, and N. Rosenzweig, Poly. Engr. Sci., 19, 223 (1979).

76. Smith, T. L., J. Poly. Sci., 32, 99 (1958).

77. Snow, B. D., M.S. Thesis, The University of Tennessee, Knoxville, 1982.

78. So, P., and L. J. Broutman, Poly. Engr. Sci., 16, 785 (1976).

79. Sookne, A. M., and M. Harris, J. Research, 34, 467 (1945).

80. Sookne, A. M., and M. Harris, Ind. Engr. Chem., 37, 478 (1945).

81. Stein, R. S., and F. H. Norris, J. Poly. Sci., 21, 381 (1956).

82. Struik, L. C. E., "Physical Aging in Amorphous Polymers and Other Materials," Elsevier, New York, 1978.

83. Struik, L. C. E., Poly. Engr. Sci., 718, 799 (1978).

84. Tanabe, Y., and H. Kanetsuna, Polymer, 20, 1121 (1979).

85. Thomas, L. S., and K. J. Cleereman, SPE J., 28, 61 (April 1972).

86. Timoshenko, S. P., and J. N. Goodier, "Theory of Elasticity," McGraw-Hill, New York, 1970.

87. Treuting, R. G., and W. T. Read, Jr., J. Appl. Phys., 22, 130 (1951).

88. Tsevtkov, V. M., and E. A. Krym, Vestnik Leningrad Univ., Ser. Mat. Fiz. Khim, 3, 5 (1956).

89. Van Krevelen, D. W., "Properties of Polymers - Correlation with Chemical Structures," Elsevier - North Holland, Amsterdam, 1972.

90. Vincent, P. I., Polymer, 1, 425, (1960).

91. Vincent, P. I., Plastics (Lond), 27, 115 (1962).

92. Wales, J. L. S., Rheol. Acta, 8, 38 (1969).

93. Wang, K. K., S. F. Shen, C. Cohen, C. A. Hieber, A. I. Isayev, and T. Akiyama, Progress Report No. 7, Injection Molding Project, Cornell University, 1980.

94. Ward, I. M., "Mechanical Properties of Solid Polymers," Wiley, New York, 1971.

95. White, J. L., and J. E. Spruiell, Poly. Engr. Sci., 21, 859 (1981).

96. Wilkes, G. L., and R. S. Stein, J. Poly. Sci.-Phys. _, 1525 (1969).

97. Williams, M. L., R. F. Landel, and J. D. Ferry, J. Am. Chem. Soc., 77, 3701 (1955).

98. Wust, C. J., Jr., Ph.D. Dissertation, The University of Tennessee, Knoxville, 1982.

99. Wust, C. J., Jr., and D. C. Bogue, J. Appl. Poly. Sci., 28, 1931 (1983).

100. Yanko, J. A., J. Poly. Sci., 3, 576 (1948).

101. Ziegler, E. E., and W. W. Brown, Plast. Technol., 341 (1955).

APPENDICES

APPENDIX A

NUMERICAL SCHEME FOR SOLVING THE EQUATIONS OF LEE, ROGERS, AND WOO (47)

The numerical solution to the thermoviscoelastic treatment of Lee, Rogers, and Woo (47) for the calculation of residual stresses in quenched plates will be presented here in detail. The numerical scheme developed here for the calculation of stress (equations II.14 to II.16) is essentially the one outlined by Lee et al.(47) with some modifications suggested by Narayanaswamy and Gardon (59). The calculation of the birefringence, which makes use of the strains evaluated when solving for the stress distribution requires some modifications, as will be described.

Calculation of Stress

The expression for the stress at any point x_1 in the slab as a function of time is given by

$$\sigma(x_1,t) = 3\int_0^t R[\xi(x_1,t) - \xi(x_1,t')] \frac{\partial}{\partial t'}\left[\varepsilon_2(t') - \alpha T(x_1,t')\right] dt' \qquad \text{(II.14)}$$

The auxiliary modulus function R can be made dimensionless by dividing it by $R_o = E(0)/[3(1-\nu)]$, where E(0) is Young's modulus and ν is Poisson's ratio; thus,

$$\bar{R}[\xi(x_1,t) - \xi(x_1,t')] = \frac{R[\xi(x_1,t) - \xi(x_1,t')]}{\frac{E(0)}{3(1-\nu)}} \tag{A.1}$$

Rewriting II.14 in terms of R

$$\sigma(x_1,t) = \int_0^t \bar{R}[\xi(x_1,t) - \xi(x_1,t')] \frac{E(0)}{1-\nu} \frac{\partial}{\partial t}[\varepsilon_2(t') - \alpha T(x_1,t')]\, dt' \tag{A.2}$$

The integrand of equation A.2 can be considered to be the product of two factors, i.e., the dimensionless stress memory function R and the rate of stress generation, which is given by

$$\frac{\partial \sigma_g}{\partial t'} = \frac{E(0)}{1-\nu} \frac{\partial}{\partial t'}[\varepsilon(t') - \alpha T(x_1,t')]\, dt' \tag{A.3}$$

The time interval of consideration may be divided into (n-1) intervals from $t_1=0$ to $t_n=t$.

Substituting A.3 into A.2 and considering this time partion, the expression for the stress can be written

$$\sigma(x_1,t_n) = \sum_{i=1}^{n-1} \int_{t_i}^{t_{i+1}} \bar{R}[\xi(x_1,t_n) - \xi(x_1,t')] \frac{\partial \sigma_g}{\partial t'} \, dt \qquad (A.4)$$

Making the assumption that the rate of stress generation, i.e., $\frac{\partial \sigma_g}{\partial t'}$ is constant in any given time interval of integration A.4 can be expressed

$$\sigma(x_1,t\ ) = \sum_{i=1}^{n-1} \frac{\partial \sigma_g}{\partial t'} \int_{t_i}^{t_{i+1}} \bar{R}[\xi(x_1,t_n) - \xi(x_1,t')] \, dt' \qquad (A.5)$$

Which can be written as

$$\sigma(x_1,t_n) = \sum_{i=1}^{n-1} \frac{\Delta \sigma_g}{\Delta t} \int_{t_i}^{t_{i+1}} \bar{R}[\xi(x_1,t_n) - \xi(x_1,t')] \, dt' \qquad (A.6)$$

or

$$\sigma(x_1,t_n) = \sum_{i=1}^{n-1} (\Delta \sigma_g)_i \, R_i^* \qquad (A.7)$$

where

$$(\Delta\sigma)_i = \frac{E(0)}{1-\nu}\left[[\varepsilon_2(t_{i+1}) - \alpha\, T(x_1,t_{i+1})]\right.$$

$$\left. - [\varepsilon_2(t_i) - \alpha\, T(x_1,t_i)]\right] \qquad (A.8)$$

and

$$R_i^* = \frac{1}{t_{i+1} - t_i}\int_{t_i}^{t_{i+1}} \bar{R}[\xi(x_1,t_n) - \xi(x_1,t')]\, dt' \qquad (A.9)$$

Therefore, the stress in any point of the slab at time t_n is given by

$$\sigma(x_1,t_n) = \sum_{i=1}^{n-1} \frac{E(0)}{1-\nu} \left[\varepsilon_2(t_{i+1}) - \varepsilon_2(t_i)\right.$$

$$\left. - \alpha\,[T(x_1,t_{i+1}) - T(x_1,t_i)]\right] R_i^* \qquad (A.10)$$

Following Lee et al.(47) it is now convenient to take the ε_2 terms out of the summation in equation A.10

$$\sigma(x_1,t_n) = \frac{E(0)}{1-\nu}\left[\varepsilon_2(t_n) - \varepsilon(t_{n-1}) - \alpha\,[T(x_1,t_n) - T(x_1,t_{n-1})]\right] R_{n-1}^*$$

$$+ \sum_{i=1}^{n-1} \frac{E(0)}{1-\nu} \left[\varepsilon_2(t_{i+1}) - \varepsilon_2(t_i) - \alpha\,[T(x_1,t_{i+1}) - T(x_1,t_i)]\right] R_i^* \quad (A.11)$$

Rearranging A.11

$$\sigma(x_1,t_n) = \frac{E(0)}{1-\nu} R_{n-1}^* \varepsilon_2(t_n)$$

$$- \frac{E(0)}{1-\nu}\left[\varepsilon_2(t_{n-1}) + \alpha\,[T(x_1,t_n) - T(x_1,t_{n-1})\right] R_{n-1}^*$$

$$- \sum_{i=1}^{n-2} \varepsilon_2(t_{i+1}) - \varepsilon_2(t_i) - \alpha\,[T(x_1,t_{i+1}) - T(x_1,t_i)]\Big] R_i^*$$

(A.12)

The expression between square brackets in the second term of A.13 can be named P for convenience; thus, with some rearranging

$$\sigma(x_1,t_n) = \frac{E(0)}{1-\nu}[R_{n-1}^* \varepsilon_2(t_n) - P] \quad (A.13)$$

The term P contains only strains (ε_2) corresponding to prior times, i.e., $t<t_n$.

Combining A.14 with the condition of internal stress equilibrium (balancing condition) expressed by equation II.15, i.e.,

$$\int_0^b \sigma(x_1,t)\, dx_1 = 0 \qquad \text{(II.15)}$$

the resulting expression is

$$\int_0^b \frac{E(0)}{1-\nu} \left[R^*_{n-1}\, \varepsilon_2(t_n) - P\right] dx_1 = 0 \qquad \text{(A.14)}$$

But since, $\varepsilon_2(t_n)$ does not depend on x_1, it can be taken out of the integral. Solving for $\varepsilon_2(t_n)$ thus gives

$$\varepsilon_2(t_n) = \frac{\int_0^b P\, dx_1}{\int_0^b R^*_{n-1}\, dx_1} \qquad \text{(A.15)}$$

Equation A.15 allows for the calculation of the $\varepsilon_2(\ )$ on a step-by-step basis. At the beginning of the quench the strain is zero, i.e., $\varepsilon_2(t_1 = 0)$ since the plate is originally unconstrained. Thus, $U2^{(t_2)}$ may be calculated from A.15 in which P is only function of $\varepsilon_2(t_1)$ and other known quantities. Analogously, $\varepsilon_2(t_3)$, $\varepsilon_2(t_4)$,....., $\varepsilon_2(t_n)$, can be subsequently calculated as function of all the previous ones.

Once the strains have been calculated up to a time t_n, the stress profile through the plate thickness at time t_n can be evaluated by means of A.14.

Calculation of Birefringence

For the birefringence calculation, the analogous of A.3 would be

$$\Delta n(x_1,t) = \int_0^t \bar{C}[\xi(x_1,t) - \xi(x_1,t')] \frac{C_\varepsilon(T_g)}{1-\nu} \frac{\partial}{\partial t'} [\varepsilon_2(t') - \alpha\, T(x_1,t')]\, dt' \qquad (A.16)$$

in which the rate of birefringence generation is being multiplied by a dimensionless birefringence memory function C (see A.3 for comparison with the expression for stress).

Dividing the time interval t into (n-1) subintervals results in

$$\Delta n(x_1,t_n) = \sum_{i=1}^{n-1} \int_{t_i}^{t_{i+1}} \bar{C}[\xi(x_1,t_n) - \xi(x_1,t')] \frac{\partial(\Delta n)_g}{\partial t'} dt' \qquad (A.17)$$

Analogously to the stress problem, it can be assumed that the rate of birefringence generation remains approximately constant within any given time interval of integration. Taking it out of the integral thus results in

$$\Delta n(x_1,t_n) = \sum_{i=1}^{n-1} \left(\frac{\partial(\Delta n)_g}{\partial t'}\right)_i \int_{t_i}^{t_{i+1}} \bar{C}[\xi(x_1,t_n) - \xi(x_1,t')]\, dt' \qquad (A.18)$$

which can be written as

$$\Delta n(x_1,t_n) = \sum_{i=1}^{n-1} \frac{\Delta[(\Delta n)_g]_i}{\Delta t_i} \int_{t_i}^{t_{i+1}} \bar{C}[\xi(x_1,t_n) - \xi(x_1,\, t')]\, dt' \qquad (A.19)$$

or

$$\Delta n(x_1,t_n) = \sum_{i=1}^{n-1} \Delta[(\Delta n)_g]_i\, C_i^* \qquad (A.20)$$

where

$$\Delta[(\Delta n)_g]_i = \frac{C_\varepsilon(T_g)}{1-\nu}\left[[\varepsilon_2(t_{i+1}) - \alpha\, T(x_1,t_{i+1})] - [\varepsilon_2(t_i) - \alpha\, T(x_1,t_i)]\right] \qquad (A.21)$$

and

$$C_i^* = \frac{1}{t_{i+1} - t_i} \int_{t_i}^{t_{i+1}} \bar{C}[\xi(x_1, t_n) - \xi(x_1, t')]\, dt' \qquad (A.22)$$

Thus, the expression for the calculation of the birefringence (totally analogous to A.11 for stress) is

$$\Delta n(x_1, t_n) = \sum_{i=1}^{n-1} \frac{C_\varepsilon(T_g)}{1 - \nu} \varepsilon_2(t_{i+1}) - \varepsilon_2(t_i)$$

$$-\alpha [T(x_1, t_{i+1}) - T(x_1, t_i)] \qquad (A.23)$$

Since the strains ($\varepsilon_2(\ )$) have already been calculated when solving for the stress problem, no further developments are required and the residual birefringence profile may be directly obtained from A.23. It is important to realize that A.23 does not include the condition of balanced profiles (balancing condition), needed for the calculation of the stress, which, as confirmed experimentally, does not apply to the residual birefringence distribution.

Stress Memory Function

The thermoviscoelastic theory of Lee, Rogers, and Woo (47) for the calculation of stresses in a quenched plate (see eqn. II.14) requires the use of a temperature dependent memory function R. A rigorous application of the thermoviscoelastic theory requires the

calculation of R from the experimentally determined shear modulus spectrum, via equation II.17. But a complete set of shear modulus data was not available for this polymer, and thus an exponential function was used instead. The derivation of the R function as used throughout this work will now be presented in detail.

Assuming that the material is thermorheologically simple, the time-temperature supperposition can be applied, resulting in a reduced time ξ given by

$$\xi(x_1,t) = \int_0^t \Phi[T(x_1,t')]\, dt' \qquad \text{(II.16)}$$

where $\Phi[T(x_1,t''')$ is a physical property that determines the adjusted time scale (its logarithm is the shift function). The form of Φ is

$$\Phi = e^{K[T(x_1,t') - T_R]} \qquad \text{(A.24)}$$

The reduced time can thus be given by

$$\xi(x_1,t) = \int_0^t e^{K[T(x_1,t') - T_R]}\, dt' \qquad \text{(A.25)}$$

For window glass Narayanaswamy and Gardon (59) showed that the function $R(\xi)$ is approximately exponential. Assuming that this holds true for a polimeric glass, $R(\xi)$ can be written as

$$R(\xi) = R_o \exp\left[\frac{-1}{\tau_o}\,\xi(x_1,t)\right] \tag{A.26}$$

or

$$R(\xi) = R_o \exp\left[\frac{-1}{\tau_o}\int_0^t e^{K[T(x_1,t') - T_R]}\,dt'\right] \tag{A.27}$$

Thus, a plausible form for $R[\xi(x_1,t) - \xi(x_1,t']$, as it appears in the final expression for the stress distribution, is

$$R[\xi(x_1,t) - \xi(x_1,t')] = R_o \exp\left[\frac{-1}{\tau_o}[\xi(x_1,t) - \xi(x_1,t')]\right] \tag{A.28}$$

which can be written as

$$R[\xi(x_1,t) - \xi(x_1,t')] = R_o \exp\left[\frac{-1}{\tau_o}\int_{t'}^t e^{K[T(x_1,t'') - T_R]}\,dt''\right] \tag{A.29}$$

APPENDIX B

COMPUTER PROGRAMS

The two computer programs developed for use in this thesis are presented in this appendix. A description of each program including the main variables involved, input parameters, and final results is presented before each program.

BIREF.FOR

This program calculates the experimental residual birefringence profile through-the-thickness of a quenched polymer slab by solving equations V.2 and V.2. Input to the program consists of sets of data obtained at each particular point in the sample, including the dimensionless position (DLSX), the 0^{o} and 90^{o} compensator readings (SAMZER and SAM90), and the sample thickness (THICK). The 0^{o} and 90^{o} reference compensator readings (with no sample) (ZERZER and ZER90) are also input. The program outputs in a tabular form the 0^{o} and 90^{o} retardations (GAMZER and GAM90), the average retardation (GAMAVG), and the birefringence (BIREF) at each point throughout the thickness. Additionally, pairs of position and birefringence values are conveniently stored in a plotting data file, that allows for direct representation of the birefringence profile by means of the CALCOM plotting routines.

```
C*********************************************************************
C*    PROGRAM:  BIREF.FOR                                            *
C*                                                                   *
C*    CALCULATION OF FROZEN-IN BIREFRINGENCE IN A QUENCHED SLAB      *
C*********************************************************************
C
      REAL GAMZER,GAM90,GAMAVG,BIREF,SAMZER,SAM90,ZERZER,ZER90,
     1 LAM,WAVTUR,K,THICK,COMP(30,4)
C INPUT POSITION COMPENSATOR READINGS AND THICKNESS DATA
      DATA(COMP(1,I),I=1,4)/0.016,9.97,30.36,0.0745/
      DATA(COMP(2,I),I=1,4)/0.024,11.71,29.00,0.0745/
      DATA(COMP(3,I),I=1,4)/0.055,16.75,23.64,0.0745/
      DATA(COMP(4,I),I=1,4)/0.086,18.97,21.22,0.0745/
      DATA(COMP(5,I),I=1,4)/0.118,20.35,19.88,0.0746/
      DATA(COMP(6,I),I=1,4)/0.149,20.93,19.30,0.0746/
      DATA(COMP(7,I),I=1,4)/0.180,21.16,19.07,0.0746/
      DATA(COMP(8,I),I=1,4)/0.227,21.19,18.90,0.0746/
      DATA(COMP(9,I),I=1,4)/0.274,21.21,18.91,0.0746/
      DATA(COMP(10,I),I=1,4)/0.321,21.09,18.86,0.0747/
      DATA(COMP(11,I),I=1,4)/0.368,21.39,18.72,0.0747/
      DATA(COMP(12,I),I=1,4)/0.415,21.56,18.46,0.0747/
      DATA(COMP(13,I),I=1,4)/0.462,21.81,18.33,0.0747/
      DATA(COMP(14,I),I=1,4)/0.509,21.87,18.30,0.0748/
      DATA(COMP(15,I),I=1,4)/0.556,21.76,18.40,0.0748/
      DATA(COMP(16,I),I=1,4)/0.603,21.63,18.48,0.0748/
      DATA(COMP(17,I),I=1,4)/0.650,21.44,18.74,0.0748/
      DATA(COMP(18,I),I=1,4)/0.697,21.30,18.87,0.0748/
      DATA(COMP(19,I),I=1,4)/0.745,21.23,18.92,0.0749/
      DATA(COMP(20,I),I=1,4)/0.792,21.36,18.81,0.0749/
      DATA(COMP(21,I),I=1,4)/0.839,21.19,18.95,0.0749/
      DATA(COMP(22,I),I=1,4)/0.886,20.33,19.80,0.0749/
      DATA(COMP(23,I),I=1,4)/0.917,18.84,21.24,0.0750/
      DATA(COMP(24,I),I=1,4)/0.948,17.10,23.11,0.0750/
      DATA(COMP(25,I),I=1,4)/0.964,14.77,24.92,0.0750/
      DATA(COMP(26,I),I=1,4)/0.980,11.04,28.29,0.0750/
      DATA(COMP(27,I),I=1,4)/0.995,8.35,31.78,0.0750/
      DATA(COMP(28,I),I=1,4)/0.0,0.0,0.0,0.0/
      DATA(COMP(29,I),I=1,4)/0.0,0.0,0.0,0.0/
      DATA(COMP(30,I),I=1,4)/0.0,0.0,0.0,0.0/
C
C OPEN OUTPUT FILE FOR PLOTTING
      OPEN(UNIT=22,FILE='B15.PLT')
C INPUT THE 0 AND 90 DEGREE REFERENCE COMPENSATOR READINGS.
      ZERZER=20.16
      ZER90=20.01
C INPUT THE NUMBER OF POINTS MEASURED (FROM 1 TO 30).
      J=27
      P=27.
C DEFINE THE APPARATUS CONSTANTS.
      LAM=546.
```

```
      WAVTUR=0.1891
      K=0.998
C PRINT THE HEADINGS FOR THE OUTPUT
      WRITE(5,500)
      WRITE(24,500)
500   FORMAT(///,1X,'POINT  ',4X,'X/L',5X,'SAMZER',5X,'SAM90',
      1       8X,'THICK',7X,'GAMMA 0',6X,'GAMMA 90',6X,
      1'GAMMA AVERAGE',6X,'BIREFRINGENCE')
C
      FLAG=0.
C
C CALCULATE THE BIREFRINGENCE AT ALL POINTS.
      DO 100 M=1,J
      DLSX=COMP(M,1)
      SAMZER=COMP(M,2)
      SAM90=COMP(M,3)
      THICK=COMP(M,4)
      GAMZER=(ZERZER-SAMZER)*LAM*WAVTUR/K
      GAM90=(SAM90-ZER90)*LAM*WAVTUR/K
      GAMAVG=(GAMZER+GAM90)/2
      BIREF=GAMAVG/(THICK*25.4E6)
      WRITE(5,1000) M,DLSX,SAMZER,SAM90,THICK,GAMZER,GAM90,
      1 GAMAVG,BIREF
      WRITE(24,1000) M,DLSX,SAMZER,SAM90,THICK,GAMZER,GAM90,
      1 GAMAVG,BIREF
1000  FORMAT(/,2X,I2,6X,F5.3,6X,F5.2,6X,F5.2,6X,F6.4,6X,F8.2,6X,
      1       F8.2,7X,F8.2,12X,E9.3)
      IF(FLAG.NE.0.) GO TO 600
      WRITE(22,2000) P
2000 FORMAT('HEAD',/,'DATA',T15,G15.6)
      FLAG=1.
600   CONTINUE
      WRITE(22,2500) DLSX,BIREF
2500  FORMAT(2G15.7)
100   CONTINUE
      CLOSE(UNIT=22,FILE='B15.PLT')
      STOP
      END
```

LRW.FOR

This program calculates simultaneously the residual stress and residual birefringence profiles in a quenched slab by solving the equations of Lee, Rogers, and Woo (47) (eqns. II.14 to II.16). The strains as a function of time are also calculated. The numerical scheme used in these calculations is presented in Appendix A. The solution to the heat transfer problem, which is needed throughout the calculaton of stress and birefringence, can be obtained with the program TEMP.FOR, recently developed by Wust (98).

The structure of the program is a modular one, consisting in a main calculating routine and a variety of subroutines (subfunctions) interacting with one another. A detailed description of these various routines is now presented.

MAIN PROGRAM

The main program is essentially divided into three major parts. The first part involves the calculation of the hardening time TIHARD (time at which a point goes through T_g), and hardening time counter value ITHARD for all the x "positions" (NXSTE1) throughout the slab thickness. Analogous calculations are subsequently performed for an arbitrary intermediate low temperature, i.e., 60°C, and for the final temperature (TAMB). The reason for this is explained latter when discussing the expanding time scale.

In a second part the stress and birefringence profiles are calculated for times up to the hardening (freezing) of the centerline.

As shown in Appendix A, the calculation of the stress and birefringence at any point and time requires the knowledge of the strains at all the previous times. The calculations are performed by two "nested" DO loops in space and time, respectively, i.e., the values of the stress and birefringence at all the desired intermediate times are calculated at one point at a time. Since the strains are not position dependent, they are calculated once and for all, during the time loop for the first x position (IX=1).

The number of stress and birefringence profiles to be calculated in this first stage of cooling is defined by NSOUT1. Prior to the strain calculation the three storage matrices ALPTEM(IY1,I), TIEXTE(IY1,I), and DIMFAC(IY1,I) are evaluated. These contain the result of alpha times temperature calculations, memory function calculations, and strain optical coefficient calculations, respectively, and are repeteadly used throughout the program. More will be said latter about these storage matrices when dealing with the routines involved in the calculations.

The third major part of the main program consists in the calculation of the stress and birefringence profiles for the second stage of quenching, i.e., for times after the hardening of the centerline and up to total temperature equilibration. The structure of the calculations is in all analogous to the one just described for the first quenching stage.

FUNCTION TIME(IT)

This routine calculates the time (dimensionless time) corresponding to the various values of the time counter, from IT=1 to IT=N, throughout the program. As explained in Chapter V, an expanding time scale was developed to provide for time steps of variable size, starting very small and gradually increasing as time progresses. This is intended to keep the number of steps as low as possible without this being detrimental to the accuracy of the calculations. This expanded time scale in which the FUNCTION TIME(IT) routine is based is now explained in detail.

Expanding time scale. This time scale provides a means for gradually increasing the size of the time steps, as the quenching progresses, up to the hardening of the centerline. It thus allows for very small time steps at the beginning of the quench, when cooling is very rapid near the surface. The initial size of the time step DELTI1 is arbitrarily chosen. After the hardening of the centerline and up to it reaching 60°C, larger time steps can be used, and so a constant time step size is specified by means of DELTIS. Finally, an even larger constant step size may be used from the time the centerline reaches 60°C up to the end of the quench, as defined by DELTIF.

Figure B-1 illustrates the expanding time scale used for the first stage of quenching. The initial time increment is thus defined by DELTI1. Every M time counter values (IT=M, IT=1M,...), the time step is increased by a quantity L*DELTI1, and remains constant during the next M time counter values (generally M time subintervals). The

variable NGROUP indicates the number of groups of (M-1) (just one, the first) and M subintervals that have been accumulated for a given time.

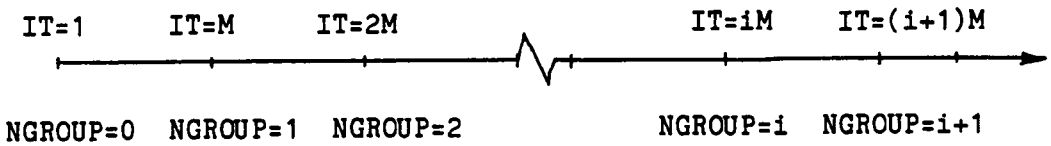

Figure B-1. Expanding time scale for stress and birefringence calculation.

Thus, the computer program starts with NGROUP=0 at time t=0 (IT=1) and steps in time using a constant step size DELTI1 until IT=M. At IT=M, the group counter is incremented in one, i.e., NGROUP=1, and the new step size is DELTI*(1+L). Analogously, this step size remains constant until IT=2M, at which NGROUP=2 and the step size becomes DELTI1*(1+2L). The time step continues its expansion in this fashion until the centerline hardening time is reached. From this time on, the time step size remains constant as described above.

The expression for calculating the time as as a function of the time counter value IT for times up to the centerline hardening time, will now be derived.

The elapsed time (TIME) corresponding to any value of the time counter can be described as the sum of two quantities: T1 and T2.

T1 is the elapsed time that corresponds to an integer number of M subinterval groups, e.g., NGROUP=(i+1) in the case illustrated in Figure B-1.

T2 is the time accumulated in the remaining time subintervals (less than M) up to the time counter value under consideration IT.

The quantity T1 can be written as

$$T1 = (M-1)\ DELTI1 + M\ DELTI1\ [(1+L) + (1+2L) + \ldots$$
$$\ldots + [1 + (NGROUP - 1)\ L\ ]\ ] \qquad (B.1)$$

The quantities between square brackets in the second term of B.1 represent the sum of an arithmetic series. Thus, equation B.1 can be rewritten as

$$T1 = (M-1)\ DELTI1$$
$$+ M\ DELTI1\ [1/2\ (NGROUP-1)\ [2(1+L) + (NGROUP-2)\ L]\ ] \qquad (B.2)$$

or

$$T1 = DELTI1\ [M\ [1 + (NGROUP-1)\ (1 + L\ NGROUP/2)] - 1] \qquad (B.3)$$

The quantity T2 is given by

$$T2 = (IT - NGROUP\ M)\ DELTI \qquad (B.4)$$

where DELTI is the current time increment and is given by

$$DELTI = DELTI1\ (1 + NGROUP\ L) \qquad (B.5)$$

The final expression for the time as a function of IT is thus given by

$$\text{TIME(IT)} = \text{DELTI1 M } [1 + (\text{NGROUP}-1)\ (1 + \text{L NGROUP}/2)] - 1 + (\text{IT} - \text{NGROUP M})\ \text{DELTI} \qquad \text{(B.6)}$$

For times after the hardening of the centerline, the expressions are straightforward, since the size of the time step is kept constant, as described above.

FUNCTION TIME1(IT)

This routine is very similar to FUNCTION TIME(IT) just described. But it allows for the calculation of the dimensionless time (TIME) at any intermediate point in a subinterval. The particular point is specified by means of the variable PART.

TIME1(IT) is used in the evaluation of the memory function R(x,t,t'), which is performed by FUNCTION RBAR(IX,IT,I) using equation A.29.

FUNCTION STRAIN(IT)

This routine calculates the strains at any given time by solving equation A.15. The space integrals involved (INUM and IDEN) are evaluated in a straightforward manner using Simpson's Rule.

FUNCTION P(IX,IT)

This function evaluates the value of the term P, introduced in equation A.13. The calculation of P at a given position (IX) and for a

given time (IT) involves looping in time from IT=1 to IT=IT-1. Thus, it is very convenient to store the calculated values for intermediate times of as many common parameters as possible. The storage matrix ALPTEM(IX,IT), calculated in the main program, constitutes an example of this. It contains the calculated values of α [$T(x_1,t_{i+1})$ - $T(x_1,t_i)$] for any (IX,IT) pair. Thus, each individual α [$T(x_1,t_{i+1})$ - $T(x_1,t_i)$] is only calculated once, saving considerable computer time.

FUNCTION DELTN(IX,IT)

This function calculates the birefringence at any position (IX) and time (IT) by means of equation A.23. To perform the calculations involved, another storage matrix besides ALPTEM(IX,I) is used. This storage matrix, i.e., DIMFAC(IX,I), contains the calculated values of the temperature dependent strain optical coefficient, as defined in FUNCTION SOC(IX,IT).

FUNCTION RBAR(IX,IT,I)

This routine calculates the value of the dimensionless strain memory function with the simplified instant freezing assumption. Thus, RBAR is assigned either a value of 0 or 1 depending on whether or not the temperature of the point under consideration is larger or smaller than T_g, respectively.

FUNCTION RSTAR(IX,IT,I)

This routine simply solves equation A.9 by means of the Trapezoidal Rule, in one single step.

FUNCTION CBAR(IX,IT,I)

This routine solves the exponential equation of the birefringence memory function (analogous to equation A.29 for the stress memory function). The integration is performed by calculating the value of the function at an intermediate point of each time subinterval,i.e, at the midpoint of the subinterval, using FUNCTION TIME1(I), and subsequent multiplication by the subinterval width. The final result is obtained by summing over all the time subintervals from the past time (I) to the time of consideration (IT).

FUNCTION CSTAR(IX,IT,I)

This function calculates the value of C^* in a given subinterval by averaging the values of the function at the interval ends.

FUNCTION SUMSTR(I)

This routine calculates the area under the curve of the calculated stress profiles allowing one to check whether the condition of internal stress equilibrium is met. The calculations are performed in a straightforward manner by means of Simpson's Rule for discrete data.

FUNCTION SUMBIR(I)

This routine, which is identical to FUNCTION SUMSTR(I), calculates the area under the predicted birefringence curves.

FUNCTION RT(X,TIME)

This routine calculates the real temperature (in ^{o}C) as a

function of position and dimensionless time. It actually converts the dimensionless temperature calculated by means of TEMP.FOR into real temperature.

FUNCTION RTI

This function converts the dimensionless time (in the heat transfer sense) into real time by multiplying it by the square of the half thickness of the slab, and subsequently dividing the result by the thermal diffusivity THERDF(TC), which is a routine of TEMP.FOR.

FUNCTION THEDEF(IX,I)

This routine is used to calculate the storage matrix ALPTEM(IX,I) which, as mentioned earlier, contains the results of multiplying the coefficient of thermal expansion (ALPHA) by the temperature increment in each subinterval for all posible combinations of IX and I.

FUNCTION ARGMEM(IX,I)

This routine calculates the storage matrix TIEXTE(IX,I) containing the results of solving the integral of the birefringence memory function for all possible time intervals and at all positions.

FUNCTION SOC

This routine calculates the strain optical coefficient as a function of temperature (actually position and time) and subsequently divides it by $1 - \nu$. It is used in the calculation of the storage matrix DIMFAC(IX,IT) which contains the result of these calculations

for all possible (IX,IT) pairs. The functional form used for the strain optical coefficient is composed of various expressions depending on the temperature range, as explained in Chapter V. For temperatures lower than T_g the least squares fit calculated by Wust (98) is used, whereas the higher temperature data is simply fit by means of straight lines drawn through the data points (see Figure II.3). The expressions used in the various temperature regions are all defined in terms of the diference $(T - T_g)$; this allows to easily shifting the strain optical coefficient function as a whole, when considering T_gs other than 100°C, bringing into coincidence the "dip" in the fuction with the new T_g.

FUNCTION ALPHA(X,I)

This routine calculates the coefficient of thermal expansion as a function of temperature (position and time). Two levels are provided for this variable, i.e, a rubbery value (above T_g) and a glassy value (below T_g). The transition from one to the other can be made abruptly (step function), or gradually (ramp function), by means of the variables DELTHI and DELTLO. These variables represent the temperature increments on both sides of T_g that constitute the temperature range in which this transition from rubbery to glassy α is made.

```
C ***************************************************************
C *  PROGRAM:  LRW.FOR                                          *
C *                                                             *
C *  RESIDUAL STRESS AND BIREFRINGENCE CALCULATIONS CONSIDERING  *
C *  VISCOELASTIC EFFECTS                                       *
C ***************************************************************
      EXTERNAL TIME,TIME1,STRAIN,P,DELTN,RBAR,RSTAR,CBAR,CSTAR
      EXTERNAL SUMSTR,SUMBIR,RT,RTI,THEDEF,ARGMEM,TEMP,SOC
      COMMON HTCOEF
      COMMON/B1/ITHCL,CLHTIM,IT60CL,CL60TI
      COMMON/B2/ITHX(41),STRESS(41,9)
      COMMON/B3/EPSLON(530)
      COMMON/B4/T0,TAMB
      COMMON/B5/B
      COMMON/B6/ALPTEM(41,530)
      COMMON/B7/NUMXSI
      COMMON/B8/NXSTEP
      COMMON/B9/TG
      COMMON/B10/DELTAX
      COMMON/B11/TIEXTE(41,530)
      COMMON/B12/BIREF(41,9)
      COMMON/B13/DIMFAC(41,530)
      INTEGER HTCOEF,TRIP
C OPEN OUTPUT FILES:
C * PLOTTING FILE FOR TIMES UP TO THE CENTERLINE HARDENING TIME *
C - STRESS PROFILE:
      OPEN (UNIT=24, FILE= 'T120BC.PLT')
C - BIREFRINGENCE PROFILE:
      OPEN (UNIT=22, FILE= 'B120BC.PLT')
C * PLOTTING FILE FOR TIMES AFTER THE CENTERLINE HARDENING TIME *
C - STRESS PROFILE:
      OPEN (UNIT=23, FILE= 'T120BC.GRA')
C - BIREFRINGENCE PROFILE:
      OPEN (UNIT= 21, FILE= 'B120BC.GRA')
C * DATA FILE FOR THE STRAINS *
      OPEN (UNIT=20, FILE= 'FOR20.DAT')
C
C DEFINE EXPERIMENTAL CONDITIONS, THE HEAT TRANSFER PARAMETER,
C THE GLASS TRANSITION TEMPERATURE FOR THE STRESS CALCULATION,
C AND THE SLAB THICKNESS
      T0=120.0
      TAMB=0.0
      TG=100.0
      HTCOEF=1
      B=2.54*0.125
C DEFINE THE TIME VALUES
C * TIME COUNTER VALUE FOR CENTERLINE FREEZE, HUGE DUMMY VALUE
C FOR CENTERLINE FREEZE TIME CALCULATION *
      ITHCL=10000
C * TIME FOR CENTERLINE REACHING 60 DEGREES *
```

```
      CL60TI= 0.3787488
C * TIME FOR CENTERLINE REACHING TAMB+0.1 DEGREES *
      CLAMTI=2.971402
C SPECIFY STEP SIZE FOR X
      NXSTEP=20
      DELTAX=1./FLOAT(NXSTEP)
C THE NUMBER OF X POSITIONS (IX) IS:
      NXSTE1= NXSTEP+1
C SPECIFY NUMBER OF SUBINTERVALS FOR THE SPACE INTEGRALS IN THE
C STRAIN CALCULATION.  NUMXSI NEEDS TO BE AN EVEN NUMBER WITH THE
C ADDITIONAL CONDITION THAT NXSTEP/NUMXSI = INTEGER.  THIS WAY
C THE EVALUATION OF P FOR STRAIN AND STRESS CALCULATIONS CAN BE MADE
C USING THE SAME STORAGE MATRICES ALPTEM AND TIEXTE.
      NUMXSI=20
C DEFINE NUMBER OF PROFILES TO BE OUTPUT
      NSOUT1=0
      NSOUT2=1
C
C CALCULATE THE HARDENING TIME COUNTER VALUE FOR ALL IX POSITIONS
C FIRST CALCULATE THE "TRUE" HARDENING TIME, TIHARD
      TIM=0.0
      DELTIM=0.00001
      IT=1
      IX=NXSTE1
5     X= FLOAT(IX-1)*DELTAX
      TIM= TIM-DELTIM
7     TIM= TIM+DELTIM
      TC1= RT(X,TIM)
      IF(TC1.GE.TG) GO TO 7
      TIMMIN= TIM-DELTIM
      IF(TIMMIN.LT.0.0) TIMMIN=0.0
      TC2= RT(X,TIMMIN)
      FACT= (TC1-TG)/(TC1-TC2)
      TIHARD= TIM-FACT*DELTIM
C
C NOW APPROXIMATE THE TIME COUNTER VALUE TO THE TRUE HARDENING TIME
      IT= IT-1
8     IT= IT+1
      TC= RT(X,TIME(IT))
      IF(TC.GT.TG) GO TO 8
      DELTAT= TIME(IT)-TIME(IT-1)
      IF(ABS(TIME(IT)-TIHARD).LE.DELTAT/2.0) GO TO 22
      ITHARD= IT-1
      GO TO 23
22    ITHARD= IT
23    ITHX(IX)= ITHARD
      WRITE(5,80)IX,ITHX(IX)
80    FORMAT(1X,'ITHX(',I3,')=',I4)
      IX= IX-1
      IF(X.GT.0.0) GO TO 5
```

```
        ITHCL=ITHARD
        CLHTIM=TIME(ITHCL)
        WRITE(5,*)ITHCL,CLHTIM
C
C CALCULATE THE TIME COUNTER VALUE FOR THE CENTERLINE REACHING
C 60 DEGREES.  FIRST INITIALIZE IT60CL TO A HUGE 'DUMMY' VALUE.
        IT60CL= 10000
        IT=ITHCL
        X=0.0
        IT= IT-1
30      IT= IT+1
        TC= RT(X,TIME(IT))
        IF(TC.GT.60.) GO TO 30
        DELTAT= TIME(IT)-TIME(IT-1)
        IF(ABS(TIME(IT)-CL60TI).LE.DELTAT/2.0) GO TO 32
        IT60CL= IT-1
        GO TO 33
32      IT60CL=IT
33      CONTINUE
        CL60TI= TIME(IT60CL)
        WRITE(5,*)IT60CL,CL60TI
C
C NOW CALCULATE THE FINAL TIME COUNTER VALUE (FOR CENTERLINE
C REACHING TAMB+0.1)
        IT= IT60CL
        X=0.0
        IT= IT-1
40      IT= IT+1
        TC= RT(X,TIME(IT))
        IF(TC.GT.(TAMB+0.1)) GO TO 40
        DELTAT= TIME(IT)-TIME(IT-1)
        IF(ABS(TIME(IT)-CLAMTI).LE.DELTAT/2.) GO TO 42
        ITAMB= IT-1
        GO TO 43
42      ITAMB= IT
43      CONTINUE
        WRITE(5,*)ITAMB
C
C ****************************************************************
C STRESS AND BIREFRINGENCE CALCULATION FOR TIMES UP TO THE
C CENTERLINE HARDENING TIME
C ****************************************************************
C
C TRIP IS AN INDICATOR TO TELL WHETHER OR NOT THE STRAINS HAVE BEEN
C CALCULATED FOR THIS STAGE
        TRIP=0
C
C INITIALIZE EPSLON(1)=0.0
        EPSLON(1)=0.0
C
```

```
      DO 500 IX=1,NXSTE1
             IX1=IX
             IOUTCT=1
C EVERY IOUT1 TIME STEPS WILL BE OUTPUT
             IF(NSOUT1.EQ.0) GO TO 65
             IOUT1= ITHCL/NSOUT1
65           CONTINUE
C ITSTR1 IS AN INDICATOR FOR NUMBER OF STRESS (OR BIREFRINGENCE)
C PROFILES ALREADY OUTPUT
             ITSTR1=0
C
             DO 2000 ITIME1= 2,ITHCL
                    IT1=ITIME1
C IF THE STRAINS HAVE ALREADY BEEN CALCULATED FOR THIS STAGE SKIP
C THE CALCULATIONS
                    IF(TRIP.EQ.1) GO TO 20
                    I= IT1-1
                    DO 101 IY=1,NXSTE1
                           IY1=IY
                           ALPTEM(IY1,I)= THEDEF(IY1,I)
                           TIEXTE(IY1,I)=ARGMEM(IY1,I)
                           DIMFAC(IY1,I)=SOC(IY1,I)
101                 CONTINUE
C
C CALCULATE THE STRAINS
                    EPSLON(IT1)=STRAIN(IT1)
                    WRITE(5,44)IT1,EPSLON(IT1)
                    WRITE(20,38)EPSLON(IT1)
44                  FORMAT(1X,'EPSLON(',I4,')=',G15.7)
38                  FORMAT(1X,G15.7)
20                  CONTINUE
C
C EVERY IOUT1 TIMES THE STRESS AND BIREFRINGENCE WILL BE CALCULATED
C FOR THE CURRENT X
                    IOUTCT=IOUTCT+1
                    IF(NSOUT1.EQ.0) GO TO 50
                    IF(ITSTR1.EQ.(NSOUT1-1)) GO TO 14
                    IF(IOUTCT.LT.IOUT1) GO TO 50
                    GO TO 15
14                  IF(ITIME1.NE.ITHCL) GO TO 50
15                  IOUTCT=0
                    ITSTR1=ITSTR1+1
                    STRESS(IX,ITSTR1)=4900.0*(RSTAR(IX1,IT1,IT1-1)
       1                                * EPSLON(IT1)-P(IX1,IT1))
                    BIREF(IX,ITSTR1)= DELTN(IX1,IT1)
                    WRITE(5,2)IX,ITSTR1,STRESS(IX,ITSTR1)
2                   FORMAT(1X,'STRESS(',I3,',',I1,')=',G15.7)
                    WRITE(5,4)IX,ITSTR1,BIREF(IX,ITSTR1)
4                   FORMAT(1X,'BIREF(',I3,',',I1,')=',G15.7)
50                  CONTINUE
```

```
2000            CONTINUE
                TRIP=1
C
C IF NO STRESS AND BIREFRINGENCE PROFILE IS REQUESTED FOR THIS STAGE,
C THERE IS NO NEED TO CONTINUE THE X LOOP
                IF(NSOUT1.EQ.0) GO TO 111
500     CONTINUE
C
C WRITE TO THE PLOT FILES THE NSOUT1 STRESS AND BIREFRINGENCE PROFILES
C
        DO 111 I= 1,NSOUT1
                IT= I*IOUT1
                IF(I.EQ.NSOUT1) IT=ITHCL
                PLTPTS=NXSTEP*2+1
                TIM=TIME(IT)
                TC=RT(1.0,TIM)
                TI=RTI(TIM,TC)
C CALCULATE THE AREA UNDER THE STRESS AND BIREFRINGENCE CURVES FOR
C THIS TIME
                I1=I
                SUMS= SUMSTR(I1)
                SUMB= SUMBIR(I1)
                WRITE(24,5100) PLTPTS,TIM,TI,SUMS
                WRITE(22,5100) PLTPTS,TIM,TI,SUMB
5100            FORMAT('DATA',T15,4G15.7)
C
C WRITE TO THE PLOT FILE THE TOTAL THROUGH-THE-THICKNESS STRESS
C AND BIREFRINGENCE PROFILES FOR THIS TIME, CONSISTING IN THE
CALCULATED
C PROFILE FROM THE CENTERLINE TO THE SURFACE AND ITS MIRROR IMAGE.
        IX= (NXSTEP+2)*(-1)
310     CONTINUE
        IX= IX+1
        IF(IX.GT.(NXSTEP+1)) GO TO 320
        IF(IX.GT.0) GO TO 330
        IF(IX.EQ.0) GO TO 310
        IX=-IX
        X= FLOAT(IX-1)*DELTAX*(-1)
        WRITE(24,5200) X,STRESS(IX,I)
        WRITE(22,5200) X,BIREF(IX,I)
        IX=-IX
        GO TO 310
330     CONTINUE
        IF(IX.EQ.1) GO TO 310
        X= FLOAT(IX-1)*DELTAX
        WRITE(24,5200) X,STRESS(IX,I)
        WRITE(22,5200) X,BIREF(IX,I)
5200    FORMAT(2G15.7)
        GO TO 310
320     CONTINUE
```

```
111     CONTINUE
C
C
C ****************************************************************
C STRESS AND BIREFRINGENCE CALCULATION FOR TIMES AFTER THE
C CENTERLINE HARDENING TIME
C ****************************************************************
C
       TRIP=0
C
       DO 600 IX=1,NXSTE1
              IX2=IX
              IOUTCT=1
              IF(NSOUT2.EQ.0) GO TO 66
              IOUT2= (ITAMB-ITHCL+1)/NSOUT2
66            CONTINUE
              ITSTR2=0
              ITHCL1= ITHCL+1
C
              DO 3000 ITIME2= ITHCL1,ITAMB
                     IT2=ITIME2
C IF THE STRAINS HAVE ALREADY BEEN CALCULATED FOR THIS STAGE SKIP
C THE CALCULATIONS
                     IF(TRIP.EQ.1) GO TO 60
                     I= IT2-1
                     DO 505 IY=1,NXSTE1
                            IY1=IY
                            ALPTEM(IY1,I)= THEDEF(IY1,I)
                            TIEXTE(IY1,I)= ARGMEM(IY1,I)
                            DIMFAC(IY1,I)=SOC(IY1,I)
505                  CONTINUE
C
C CALCULATE THE STRAINS
                     EPSLON(IT2)=STRAIN(IT2)
                     WRITE(5,44)IT2,EPSLON(IT2)
                     WRITE(20,38)EPSLON(IT2)
60                   CONTINUE
C
C EVERY IOUT2 TIMES THE STRESS AND BIREFRINGENCE WILL BE CALCULATED
C FOR THE CURRENT X
                     IOUTCT= IOUTCT+1
                     IF(NSOUT2.EQ.0) GO TO 53
                     IF(ITSTR2.EQ.(NSOUT2-1)) GO TO 16
                     IF(IOUTCT.LT.IOUT2) GO TO 53
                     GO TO 17
16                   IF(ITIME2.NE.ITAMB) GO TO 53
17                   IOUTCT=0
                     ITSTR2= ITSTR2+1
                     STRESS(IX,ITSTR2)= 4900.0*(RSTAR(IX2,IT2,IT2-1)
      1                                 * EPSLON(IT2)-P(IX2,IT2))
```

```
                        BIREF(IX,ITSTR2)= DELTN(IX2,IT2)
                        WRITE(5,2)IX,ITSTR2,STRESS(IX,ITSTR2)
                        WRITE(5,4)IX,ITSTR2,BIREF(IX,ITSTR2)
53                      CONTINUE
3000            CONTINUE
C
C IF NO STRESS AND BIREFRINGENCE PROFILE IS REQUESTED FOR THIS SECOND
C STAGE, CONSIDER THE PROBLEM FINISHED
                IF(NSOUT2.EQ.0) GO TO 333
                TRIP=1
600     CONTINUE
C
C PRINT AND WRITE TO THE PLOT FILE THE NSOUT2 STRESS AND BIREFRINGENCE
C PROFILES
        DO 333 I= 1,NSOUT2
                IT=ITHCL-1+I*IOUT2
                IF(I.EQ.NSOUT2) IT=ITAMB
                PLTPTS= NXSTEP*2+1
                TIM= TIME(IT)
                TC= RT(1.0,TIM)
                TI= RTI(TIM,TC)
C CALCULATE THE AREA UNDER THE STRESS AND BIREFRINGENCE CURVES
                I2=I
                SUMS= SUMSTR(I2)
                SUMB= SUMBIR(I2)
                WRITE(23,5100) PLTPTS,TIM,TI,SUMS
                WRITE(21,5100) PLTPTS,TIM,TI,SUMB
C
C WRITE TO THE PLOT FILE THE TOTAL STRESS AND BIREFRINGENCE PROFILE
C FOR THIS TIME
                IX= (NXSTEP+2)*(-1)
270             CONTINUE
                IX= IX+1
                IF(IX.GT.(NXSTEP+1)) GO TO 280
                IF(IX.GT.0) GO TO 290
                IF(IX.EQ.0) GO TO 270
                IX= -IX
                X= FLOAT(IX-1)*DELTAX*(-1)
                WRITE(23,5200) X,STRESS(IX,I)
                WRITE(21,5200) X,BIREF(IX,I)
                IX= -IX
                GO TO 270
290             CONTINUE
                IF(IX.EQ.1) GO TO 270
                X= FLOAT(IX-1)*DELTAX
                WRITE(23,5200) X,STRESS(IX,I)
                WRITE(21,5200) X,BIREF(IX,I)
                GO TO 270
280             CONTINUE
333     CONTINUE
```

```
C
C
      CLOSE (UNIT=24, FILE= 'T120BC.PLT')
      CLOSE (UNIT=22, FILE= 'B120BC.PLT')
      CLOSE (UNIT=23, FILE= 'T120BC.GRA')
      CLOSE (UNIT=21, FILE= 'B120BC.GRA')
      CLOSE (UNIT=20, FILE= 'FOR20.DAT')
      STOP
      END
C
C
C
      FUNCTION TIME(IT)
      COMMON/B1/ITHCL,CLHTIM,IT60CL,CL60TI
      REAL L
C DEFINE THE PARAMETERS FOR THE EXPANDING TIME SCALE
      M= 20
      L= 4.0
      DELTI1= 0.000016674
      DELTIS= 0.00212
      DELTIF=0.0259265
C FOR TIMES AFTER THE CENTERLINE HARDENING TIME USE ANOTHER
C EXPRESSION FOR TIME
      IF(IT.GT.ITHCL) GO TO 14
C CALCULATE THE NGROUP
      NGROUP= IT/M
C CALCULATE THE CURRENT TIME INCREMENT
      DELTI= DELTI1*(1.0+FLOAT(NGROUP)*L)
C FOR TIMES PRIOR TO THE CENTERLINE HARDENING TIME THE TIME IS:
      TIME= DELTI1*(FLOAT(M)*(1.0+(FLOAT(NGROUP)-1.0)
     1 * (1.0+(L*FLOAT(NGROUP))/2.0))-1.0)
     2 + (FLOAT(IT)-FLOAT(NGROUP)*FLOAT(M))*DELTI
      RETURN
14    CONTINUE
      IF(IT.GT.IT60CL) GO TO 28
      TIME= CLHTIM+FLOAT(IT-ITHCL)*DELTIS
      RETURN
28    CONTINUE
      TIME= CL60TI+FLOAT(IT-IT60CL)*DELTIF
      RETURN
      END
C
C
C
      FUNCTION TIME1(I)
      EXTERNAL TIME
      REAL L
C DEFINE THE PARAMETERS FOR THE TIME SCALE (IDENTICAL TO THOSE OF
C FUNCTION TIME)
      M=20
```

```
      L=4.0
      DELTI1= 0.000016674
C PART DEFINES WHICH INTERMEDIATE VALUE IS TAKEN FOR THE EVALUATION OF
C CBAR IN EACH TIME INCREMENT;  E.G.  PART=0.5 IS MID INTERVAL.
      PART=0.5
C CALCULATE THE NGROUP
      NGROUP= I/M
C CALCULATE THE CURRENT TIME INCREMENT
      DELTI= DELTI1*(1.0+FLOAT(NGROUP)*L)
C CALCULATE THE TIME
      TIME1= TIME(I)+PART*DELTI
      RETURN
      END
C
C
C
      FUNCTION STRAIN(IT)
      EXTERNAL P,RSTAR
      REAL INUM,IDEN
      INTEGER A,B
      COMMON/B7/NUMXSI
      COMMON/B8/NXSTEP
      NRATIO= NXSTEP/NUMXSI
      A=1
      B= NXSTEP+1
      NUMXM2= NUMXSI-2
      H= 1.0/FLOAT(NUMXSI)
      SUMEVN=0.0
      SUMODD= P(A+NRATIO,IT)
      DO 100 I= 2,NUMXM2,2
              IX= NRATIO*I+1
              SUMEVN= SUMEVN+P(IX,IT)
              SUMODD= SUMODD+P(IX+NRATIO,IT)
100   CONTINUE
      INUM= (P(A,IT)+P(B,IT)+4.0*SUMODD+2.0*SUMEVN)*H/3.0
C RESET SUMEVN AND REINITIALIZE SUMODD FOR IDEN CALCULATION
      SUMEVN=0.0
      SUMODD= RSTAR(A+NRATIO,IT,IT-1)
      DO 200 J= 2,NUMXM2,2
              IX= NRATIO*J+1
              SUMEVN= SUMEVN+RSTAR(IX,IT,IT-1)
              SUMODD= SUMODD+RSTAR(IX+NRATIO,IT,IT-1)
200   CONTINUE
      IDEN= (RSTAR(A,IT,IT-1)+RSTAR(B,IT,IT-1)+4.0*SUMODD
     1 +2.0*SUMEVN)*H/3.0
      STRAIN=INUM/IDEN
      RETURN
      END
C
C
```

```
C
      FUNCTION P(IX,IT)
      EXTERNAL RSTAR
      COMMON/B3/EPSLON(530)
      COMMON/B6/ALPTEM(41,530)
      IT1= IT-1
      P1= (EPSLON(IT-1)+ALPTEM(IX,IT1))*RSTAR(IX,IT,IT-1)
      P2= 0.0
      I=1
10    CONTINUE
      IF(I.GT.(IT-2)) GO TO 20
      RSKY= RSTAR(IX,IT,I)
      IF(RSKY.LT.1.0E-30) RSKY= 0.0
      P2= P2+(EPSLON(I+1)-EPSLON(I)-ALPTEM(IX,I))*RSKY
      I= I+1
      GO TO 10
20    CONTINUE
      P= P1-P2
      RETURN
      END
C
C
C
      FUNCTION DELTN(IX,IT)
      COMMON/B3/EPSLON(530)
      COMMON/B6/ALPTEM(41,530)
      COMMON/B13/DIMFAC(41,530)
      EXTERNAL CSTAR
      DELTN0= 0.0
      I=1
10    CONTINUE
      IF(I.GT.(IT-1)) GO TO 20
      CSKY= CSTAR(IX,IT,I)
      IF(CSKY.LT.1.0E-30) CSKY=0.0
      DELTN0= DELTN0+DIMFAC(IX,I)*(EPSLON(I+1)-EPSLON(I)
     1 -ALPTEM(IX,I))*CSKY
      I= I+1
      GO TO 10
20    CONTINUE
      DELTN=DELTN0
      RETURN
      END
C
C
C
      FUNCTION RBAR(IX,IT,I)
      COMMON/B2/ITHX(41),STRESS(41,9)
C FOR TIMES UP TO THE HARDENING TIME
      IF(IT.GT.ITHX(IX)) GO TO 100
      RBAR=0.0
```

```
      RETURN
100   CONTINUE
      IF(I.GT.ITHX(IX)) GO TO 200
      RBAR=0.0
      RETURN
200   CONTINUE
      RBAR=1.0
      RETURN
      END
C
C
C
      FUNCTION RSTAR(IX,IT,I)
      EXTERNAL RBAR
      RSTAR=(RBAR(IX,IT,I)+RBAR(IX,IT,I+1))/2.0
      RETURN
      END
C
C
C
      FUNCTION CBAR(IX,IT,I)
      COMMON/B2/ITHX(41),STRESS(41,9)
      COMMON/B11/TIEXTE(41,530)
      TAU0=60.0
      ITM1= IT-1
      ARG= 0.0
C IF I HAPPENS TO BE EQUAL TO -ITM1- THEN NO SUM IS PERFORMED
      IF(I.EQ.ITM1) GO TO 10
      DO 10 J=I,ITM1
            ARG= ARG+TIEXTE(IX,J)
10    CONTINUE
      POWER= -ARG/TAU0
      IF(POWER.GE.0.0) GO TO 15
      IF(POWER.LT.-80.0) POWER= -80.0
      GO TO 25
15    IF(POWER.GT.88.0) POWER=88.0
25    CONTINUE
      CBAR= EXP(POWER)
      RETURN
      END
C
C
C
      FUNCTION CSTAR(IX,IT,I)
      EXTERNAL CBAR
      CSTAR= (CBAR(IX,IT,I)+CBAR(IX,IT,I+1))/2.0
      RETURN
      END
C
C
```

```
C
      FUNCTION SUMSTR(I)
      COMMON/B2/ITHX(41),STRESS(41,9)
      COMMON/B8/NXSTEP
      COMMON/B10/DELTAX
      INTEGER A,B
      A=1
      B= NXSTEP+1
      NXSM2= NXSTEP-2
      SUMFST=0.0
      SUMSEC= STRESS(A+1,I)
      DO 300 M=2,NXSM2,2
            IX= A+M
            SUMFST= SUMFST+STRESS(IX,I)
            SUMSEC= SUMSEC+STRESS(IX+1,I)
300   CONTINUE
      SUMSTR= (STRESS(A,I)+STRESS(B,I)+4.0*SUMSEC+2.0*SUMFST)
     1 * DELTAX/3.0
      RETURN
      END
C
C
C
      FUNCTION SUMBIR(I)
      COMMON/B12/BIREF(41,9)
      COMMON/B8/NXSTEP
      COMMON/B10/DELTAX
      INTEGER A,B
      A=1
      B= NXSTEP+1
      NXSM2= NXSTEP-2
      SUMFST=0.0
      SUMSEC= BIREF(A+1,I)
      DO 300 M=2,NXSM2,2
            IX= A+M
            SUMFST= SUMFST+BIREF(IX,I)
            SUMSEC= SUMSEC+BIREF(IX+1,I)
300   CONTINUE
      SUMBIR= (BIREF(A,I)+BIREF(B,I)+4.0*SUMSEC+2.0*SUMFST)
     1 * DELTAX/3.0
      RETURN
      END
C
C
C
      FUNCTION RT(X,TIME)
      EXTERNAL TEMP
      COMMON/B4/T0,TAMB
      RT= TEMP(X,TIME)*(T0-TAMB)+TAMB
      RETURN
```

```
      END
C
C
C
      FUNCTION RTI(TIME,TC)
      EXTERNAL THERDF
      COMMON/B5/B
      RTI= TIME*B*B/THERDF(TC)
      RETURN
      END
C
C
C
      FUNCTION THEDEF(IX,I)
      COMMON/B9/ALPHA
      COMMON/B10/DELTAX
      EXTERNAL RT,TIME
      X= FLOAT(IX-1)*DELTAX
      THEDEF= ALPHA*(RT(X,TIME(I+1))-RT(X,TIME(I)))
      RETURN
      END
C
C
C
      FUNCTION ARGMEM(IX,I)
      COMMON/B10/DELTAX
      EXTERNAL RT,TIME,TIME1
      REAL K
      K=0.3126
      X= FLOAT(IX-1)*DELTAX
      POWER= K*(RT(X,TIME1(I))-100.0)
      IF(POWER.GE.0.0) GO TO 10
      IF(POWER.LT.-70.0) POWER= -70.0
      GO TO 11
10    IF(POWER.GT.88.0) POWER=88.0
11    CONTINUE
      ARGMEM= (TIME(I+1)-TIME(I))*EXP(POWER)
      RETURN
      END
C
C
C
      FUNCTION SOC(IX,IT)
C NOTE:  THE STRAIN OPTICAL COEFFICIENT WILL IN GENERAL BE A FUNCTION
C FUNCTION OF THE TEMPERATURE.  HOWEVER, SOC HAS BEEN MADE A FUNCTION
C OF POSITION AND TIME SINCE THESE TWO PARAMETERS DEFINE UNAMBIGOUSLY
C SUCH TEMPERATURE.
C SOC IS ACTUALLY THE RESULT OF DIVIDING THE STRAIN OPTICAL
C COEFFICIENT BY (1 - POISSON'S RATIO)
C
```

```
      EXTERNAL TEMP,TIME
      COMMON/B10/DELTAX
      COMMON/B9/TG
      X= FLOAT(IX-1)*DELTAX
      TC1= RT(X,TIME(IT))
      TC2= RT(X,TIME(IT+1))
      TCAVG= (TC1+TC2)/2.0
C
C THE FOLLOWING STRING OF STATEMENTS DEFINES THE TEMPERATURE DEPENDENCE
C OF THE STRAIN OPTICAL COEFFICIENT FOR THE VARIOUS TEMPERATURE RANGES.
C
      IF(TCAVG.LT.(TG+20.0)) GO TO 10
      SOC= -0.0037/(1.0-0.33)
      RETURN
10    IF(TCAVG.LT.(TG+10.2)) GO TO 20
      SOC= (0.0009898*(TCAVG-TG)-0.02352)/(1.0-0.33)
      RETURN
20    IF(TCAVG.LT.(TG+6.0)) GO TO 30
      SOC= (0.003714*(TCAVG-TG)-0.0513)/(1.0-0.33)
      RETURN
30    IF(TCAVG.LT.TG) GO TO 40
      SOC= (0.04194*(TCAVG-TG)-0.281)/(1.0-0.33)
      RETURN
40    IF(TCAVG.LT.(TG-7.2)) GO TO 50
      SOC= (0.016095*ALOG((TG-TCAVG)/10.0)-0.00183)/(1.0-0.33)
      RETURN
50    SOC= -0.007/(1.0-0.33)
      RETURN
      END
C
C
C
      FUNCTION ALPHA(X,I)
      EXTERNAL RT,TIME
      COMMON/B9/TG
      TC1=RT(X,TIME(I))
      TC2=RT(X,TIME(I+1))
      TCAVG= (TC1+TC2)/2.0
C INITIALIZE DELTHI AND DELTLO.  DELTHI INDICATES THE TEMPERATURE
C INCREMENT WITH RESPECT TO TG AT WHICH ALPHA STARTS TO GRADUALLY
C DECREASE TOWARD ITS VALUE IN THE GLASSY STATE.  DELTLO IS THE
C TEMPERATURE DECREMENT WITH RESPECT TO TG AT WHICH ALPHA ATTAINS
C ITS GLASSY STATE VALUE.  BOTH DELTHI AND DELTLO ARE ALWAYS POSITIVE.
      DELTHI= 5.0
      DELTLO= 10.0
      IF(TCAVG.LE.(TG+DELTHI))GO TO 10
      ALPHA= 0.000586
      RETURN
10    IF(TCAVG.LE.(TG-DELTLO)) GO TO 20
      IF((DELTHI+DELTLO).EQ.0.0) GO TO 20
```

```
      ALPHA= 0.000222+0.000364/(DELTHI+DELTLO)
      1 *(TCAVG-(TG-DELTLO))
      RETURN
20    ALPHA= 0.000222
      RETURN
      END
```

VITA

Javier de la Vega was born in Madrid, Spain on December 14, 1952. He attended elementary and high school there. Upon completion of his basic education he was awarded an A.F.S. (American Field Service International Scholarships) one year scholarship giving him the opportunity to live with an American family in Beloit, Kansas, while attending high school there. Back in Spain, he entered La Escuela Tecnica Superior de Ingenieros Industriales de Madrid, from which he graduated in June 1978 with the Bachelor degree in Mechanical Engineering.

In July of 1978 he participated in the practical training program of the I.A.E.S.T.E. (International Association for the Exchange of Students for Technical Experience), working at the facilities of Norsk Hydro A.S. Aluminum Company at Karmoy (Norway).

Upon completion of his military requirements on December 1979, he joined the engineering firm Andes Ingenieros S.A. of Madrid, where he worked until the summer of 1981. During the 1980-81 scholastic year he attended classes at El Instituto de Plasticos y Caucho in Madrid, from which he received a diploma in June 1981.

In the winter of 1981 he was selected by The Commission for Cultural Exchange Between Spain and USA for a Fulbright Scholarship to pursue higher education in the field of plastic materials. Through this organization he was granted a Graduate Research Assistantship from the Department of Chemical, Metallurgical, and Polymer Engineering of the University of Tennessee. He entered the Graduate School of that

university in September 1981. He recieved the Master of Science degree in Polymer Engineering in December 1983.